Annex 53

Advanced Cooling/Refrigeration Technologies Development

Final Report

Author/s:
Co-Operating Agents
Reinhard Radermacher, University of Maryland, USA
Van Baxter, Oak Ridge National Laboratory, retired, USA.

February 2024
Report no. HPT-AN53-2

HPT-AN53-2
ORNL/SPR-2023/3229

Energy and Transportation Science Division

IEA/HPT Annex 53 Advanced Cooling/Refrigeration Technologies Development – Final Report

Authors and Co-Operating Agents

Reinhard Radermacher
(Minta Martin Professor of Mechanical Engineering
University of Maryland)
Van D. Baxter
(Building Equipment Research Group
Oak Ridge National Laboratory, retired)

Date Published: February 2024

Prepared by
OAK RIDGE NATIONAL LABORATORY
Oak Ridge, TN 37831-6283
managed by
UT-BATTELLE, LLC
for the
US DEPARTMENT OF ENERGY
under contract DE-AC05-00OR22725

Published by Heat Pump Centre
c/o RISE – Research Institutes of Sweden
Box 857, SE-501 15 Borås
Sweden
Phone +46 10 16 53 42
Website https://heatpumpingtechnologies.org

Production Heat Pump Centre, Borås, Sweden

ISBN 978-91-89821-71-2
Report No. HPT-AN53-2

DOI: 10.23697/rfhs-wc33

Preface

This project was carried out within the Technology Collaboration Programme on Heat Pumping Technologies (HPT TCP), which is a Technology Collaboration Programme within the International Energy Agency, IEA.

The IEA

The IEA was established in 1974 within the framework of the Organization for Economic Cooperation and Development (OECD) to implement an International Energy Programme. A basic aim of the IEA is to foster cooperation among the IEA participating countries to increase energy security through energy conservation, development of alternative energy sources, new energy technology and research and development (R&D). This is achieved, in part, through a programme of energy technology and R&D collaboration, currently within the framework of nearly 40 Technology Collaboration Programmes.

The Technology Collaboration Programme on Heat Pumping Technologies (HPT TCP)

The Technology Collaboration Programme on Heat Pumping Technologies (HPT TCP) forms the legal basis for the implementing agreement for a programme of research, development, demonstration and promotion of heat pumping technologies. Signatories of the TCP are either governments or organizations designated by their respective governments to conduct programmes in the field of energy conservation.

Under the TCP, collaborative tasks, or “Annexes”, in the field of heat pumps are undertaken. These tasks are conducted on a cost-sharing and/or task-sharing basis by the participating countries. An Annex is in general coordinated by one country which acts as the Operating Agent (manager). Annexes have specific topics and work plans and operate for a specified period, usually several years. The objectives vary from information exchange to the development and implementation of technology. This report presents the results of one Annex.
The Programme is governed by an Executive Committee, which monitors existing projects and identifies new areas where collaborative effort may be beneficial.

Disclaimer

The HPT TCP is part of a network of autonomous collaborative partnerships focused on a wide range of energy technologies known as Technology Collaboration Programmes or TCPs. The TCPs are organised under the auspices of the International Energy Agency (IEA), but the TCPs are functionally and legally autonomous. Views, findings and publications of the HPT TCP do not necessarily represent the views or policies of the IEA Secretariat or its individual member countries.

The Heat Pump Centre

A central role within the HPT TCP is played by the Heat Pump Centre (HPC).

Consistent with the overall objective of the HPT TCP, the HPC seeks to accelerate the implementation of heat pump technologies and thereby optimise the use of energy resources for the benefit of the environment. This is achieved by offering a worldwide information service to support all those who can play a part in the implementation of heat pumping technology including researchers, engineers, manufacturers, installers, equipment users, and energy policy makers in utilities, government offices and other organisations. Activities of the HPC include the production of a Magazine with an additional newsletter 3 times per year, the HPT TCP webpage, the organization of workshops, an inquiry service and a promotion programme. The HPC also publishes selected results from other Annexes, and this publication is one result of this activity.

For further information about the Technology Collaboration Programme on Heat Pumping Technologies (HPT TCP) and for inquiries on heat pump issues in general contact the Heat Pump Centre at the following address:
Heat Pump Centre
c/o RISE - Research Institutes of Sweden
Box 857, SE-501 15 BORÅS, Sweden
Phone: +46 10 516 53 42
Website: https://heatpumpingtechnologies.org

Co-Operating Agents

Reinhard Radermacher, Minta Martin Professor of Mechanical Engineering, University of Maryland, USA
Van D. Baxter, Distinguished R&D Engineer, Building Equipment Research Group, Oak Ridge National Laboratory, USA, retired

Oak Ridge National Laboratory (ORNL) and Optimized Thermal Systems, Inc. in collaboration with the US Department of Energy, are designated as Co-Operating Agents.

Contact information for the Co-Operating Agents:

Name	Ichiro Takeuchi/Reinhard Radermacher
Affiliation	University of Maryland
Postal address	4298 Campus Dr. University of Maryland, College Park, MD 20742-3035
Telephone number	+1 301 405 5286
E-mail address	takeuchi@umd.edu; raderm@umd.edu

Name	Van D. Baxter/Brian Fricke/Ayyoub Momen
Affiliation	ORNL
Postal address	PO Box 2008, Bldg. 3147, MS - 6070 Oak Ridge, TN 37831 USA
Telephone number	865-574-2104; 865-576-0822; 865-574-4458
E-mail address	vdb@ornl.gov; frickeba@ornl.gov; momena@ornl.gov

Participating countries

China, China Academy of Building Research
Germany, Forschungszentrum Jülich GmbH
Italy, ENEA, Energy Technologies Department
South Korea, The Ministry of Trade, Industry and Energy
United States of America, US Department of Energy

Participants and contributors

Name	Role/Title	Country	Contact information
Oak Ridge National Laboratory PO Box 2008, Bldg. 3147, MS 6070 Oak Ridge, TN 37831 http://web.ornl.gov/sci/buildings/	Co-leader	USA	Van Baxter; 865-574-2104; vdb@ornl.gov Dr. Brian Fricke; 865-576-0822; frickeba@ornl.gov Dr. Ayyoub Momen; 865-574-4458; momena@ornl.gov
Optimized Thermal Systems, Inc. 7040 Virginia Manor Road Beltsville, MD 20705 https://optimizedthermalsystems.com/	Co-leader	USA	Dr. Ichiro Takeuchi; 866-485-8233; takeuchi@umd.edu Dr. Reinhard Radermacher; 866-485-8233 or 301-405-5286; raderm@umd.edu

Ames National Laboratory 128 Spedding Ames, IA 50011	Co-leader	USA	Dr. Julie Slaughter ; 515-294-4720; julies1@ameslab.gov
Korea Institute of Machinery and Materials 156 Gajeongbuk-ro, Yuseong-gu, Daejeon 34103, KOREA https://www.kimm.re.kr/e_main	Co-leader	South Korea	Dr. Seok Ho Yoon; +82-42-868-7064; shyoon@kimm.re.kr
Chung-Ang University 84 Heukseok-ro, Dongjak-gu, Seoul 06974, Korea	Co-leader	South Korea	Dr. Minsung Kim; +82-2-820-5973; minsungk@cau.ac.kr
Fraunhofer Institute for Physical Measurement Techniques (IPM), Deputy Head of Department, Thermal Energy Converters Group Manager, Caloric Systems Georges-Köhler-Allee 30179110 Freiburg, Germany https://www.ipm.fraunhofer.de/en.html	Y	Germany	Dr. Kilian Bartholomé; +49 761 8857-238; kilian.bartholome@ipm.fraunhofer.de
CNR (National Research Council) ITAE (Institute for Advanced Energy Technologies) Via S. Lucia sopra Contesse n. 5 98126 S. Lucia, Messina, Italy	Y	Italy	Dr. Alessio Sapienza; +39 090.624229; alessio.sapienza@itae.cnr.it
Xi'an Jiaotong University Department of Refrigeration and Cryogenic Engineering, School of Energy and Power Engineering, 28 West Xianning Rd, Xi'an, Shaanxi, P.R. China 710049	Co-leader	China	Dr. Suxin Qian; +86 29 82668738; qiansuxin@mail.xjtu.edu.cn
Tsinghua University Beijing 100084, China	Co-leader	China	Dr. Baolong Wang; +86-10-62783461; wangbl@tsinghua.edu.cn
Shanghai Jiao Tong University Mechanical Engineering Institute of Refrigeration and Cryogenics 800 Dongchuan Rd, Mechanical Engineering Building A-434 Shanghai, China, 200240	Co-leader	China	Dr. Xiaoshi Qian; xsqian@sjtu.edu.cn
City University of Hong Kong G5714, 5/F, Yeung Kin Man Academic Building (YEUNG), Tat Chee Avenue, Kowloon, Hong Kong, China	Co-leader	China	Dr. Wei Wu; Tel: +852-55702655, +86-18701691318; weiwu53@cityu.edu.hk

Abstract

This report documents work done under the International Energy Agency (IEA) Heat Pumping Technologies collaborative project IEA Annex 53, *Advanced Cooling/Refrigeration Technologies Development*. Research and development institutes in five Heat Pumping Technologies member countries—Germany, Italy, the People's Republic of China, South Korea, and the United States of America—shared information on a range of advanced, lower-carbon heat pump/air-conditioning (AC) technologies. This annex was launched in response to the anticipated heavy growth in worldwide demand for AC and refrigeration by 2050.

The technical scope of Annex 53 was very broad by design. It is unlikely that there will be only one or even a few so-called *right* solutions to the challenge. Therefore, the participants were free to investigate a wide range of possible technology solutions. Research, development, and demonstration efforts focused on advanced, higher-efficiency technology solutions for future AC and refrigeration systems. Technologies included those based on enhancements of the time-proven vapor compression cycle, electrochemical compression, absorption and adsorption (including compressor-assisted) systems, and others based on nontraditional cycles (including magnetocaloric, elastocaloric, electrocaloric, heat pipe–assisted caloric cycles, and more). Technology readiness levels for the investigated technology options ranged from approximately 2 to about 8 by the end of the annex.

Table of contents

1. Executive Summary

Air-conditioning (AC) and refrigeration systems account for a large share of current global energy consumption, and this demand is expected to increase sharply over the next 50 years unless actions are taken to ameliorate the increase. The adoption of AC in developed countries increased rapidly in the twentieth century, and the twenty-first century is expected to see increased adoption in developing countries—especially those with hotter climates and large, growing populations, such as India, China, Brazil, and Middle Eastern and African nations. The International Energy Agency (IEA) projects that by 2050, AC energy consumption levels will increase by 4.3× over the 2010 levels for non-Organisation for Economic Co-operation and Development (OECD) countries vs. only 1.5× for OECD countries (Figure ES-1) [1].

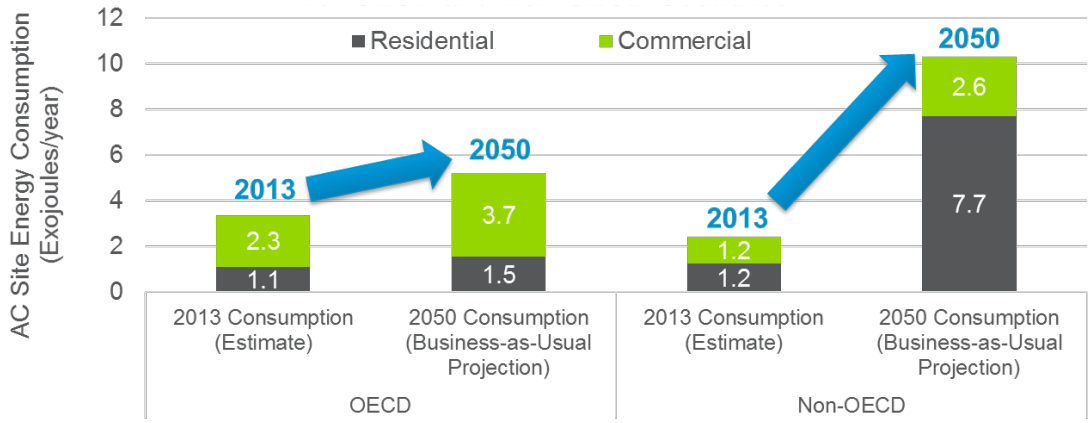

Figure ES-1 Anticipated global AC demand increases (courtesy of Navigant Consulting, Inc.; source: IEA Energy Technology Perspectives 2016)

The demand for refrigeration is expected to increase at similar rates, driven primarily by food preservation and storage needs; food demand is expected to increase 70% by 2050 relative to 2010 [2]. India, for example, has the largest refrigerated warehouse capacity of any country in the world, which is expected to reach approximately 40.7 MMT [3]—almost a 35% increase since 2014 [4]. Moreover, a huge increase in refrigerated transport capacity is also needed to properly serve the warehouse capacity and reduce food wastage. India is estimated to currently have 9,000 refrigerated trucks, but the country needs >600,000 [2]. The need for much cleaner and more efficient refrigeration systems is critical. The United Nations Food and Agriculture Organization (FAO) estimates that approximately one-third of all global food produced is wasted, resulting in huge environmental consequences. FAO estimates that this wastage occupies a land area the size of Mexico, its production consumes 250 km^3/year of water, and it accounts for 3.3 billion t per year of CO_2 emissions.

Global action, both short-term (e.g., increasing the deployment of current best technologies) and long-term (research, development, and demonstration [RD&D] for advanced, higher-efficiency technology solutions), is urgently needed to address this challenge. Annex 53 was initiated in October 2018 to help address the long-term RD&D need. Its main objective is to share information to encourage the development of high-efficiency and low–global warming potential (GWP) AC, refrigeration, and heat pump (HP) technologies. The annex was led by the United States, with participation by research and development (R&D) institutes in the People's Republic of China, Germany, Italy, and South Korea.

This report provides a summary of the current RD&D status of the leading technologies examined by each R&D institute involved in the annex. Technologies of interest follow two distinct paths: those based on the well-known and widely used vapor compression (VC) system and those based on nontraditional cooling approaches that are being increasingly investigated (Figure ES-2). VC could continue to be the system of choice, especially for the near future and possibly for the long-term. To the extent, however, that VC cycle systems continue to use refrigerants with nonzero GWPs—even in small amounts—they will remain vulnerable to further international refrigerant restrictions. Nontraditional technologies (e.g., caloric or other types) generally are not subject to this challenge because they do not rely on

refrigerants in the traditional sense. However, all the nontraditional technologies discussed herein will require additional development before they can significantly affect the market.

Figure ES-2 Two possible future paths for refrigeration and AC systems (courtesy of Navigant Consulting, Inc.; source: US Department of Energy Building Technologies Office, Emerging Technologies Program)

Table ES-1 provides a snapshot summary of each VC-related project investigated by the Annex 53 participants. Nontraditional technologies investigated during the annex are shown in Table ES-2. Capsule descriptions and estimated technology readiness levels (TRLs) are given for each technology option. The tables also include each participant's thoughts about most likely initial end-use applications for the technologies they investigated during Annex 53.

Table ES-1 Advanced VC focus

R&D institute	Technology description	Initial target market/application	TRL estimate
Korea Institute of Machinery and Materials and Chung-Ang University, South Korea	Membrane-based HP	Building AC and dehumidification (DH)	Ranges from about 2 to 5
Tsinghua University, China	1: AC using refrigerant blend with optimized temperature glide in evaporator and condenser 2: hybrid AC; prototype was Global Cooling Prize winner; prototype cost ~2× baseline AC; recent work focusing on reducing cost 3: integrated design method, GraPHsep, for optimized design of HPs and heat exchanger networks	Room AC for 1 and 2; industrial HPs for 3	Ranges from about 7 to 8 >7 ~5
City University of Hong Kong, China	Absorption thermal energy storage	Commercial heating, ventilation, and air-conditioning	Ranges from about 3 to 5
Institute for Advanced Energy Technologies, Italy	Adsorption transformation for cooling (thermal compression)	Integration with renewable energy sources; waste heat recovery in industrial processes; integration in combined cooling, heat, and power; mobile AC/refrigeration	ranges from about 3 or 4 to ≥7
University of Maryland, USA	1: Electrochemical compression (ECC): selective fluid pumping via chemical process (no moving parts) 2: Electrohydrodynamic-enhanced electrochemical DH	Building AC for latent and sensible cooling; evaluating the integration of NH_3 ECC with NH_3 synthesis to produce and store liquid NH_3 for use as internal combustion engine fuel	1: 3 2: 3

R&D institute	Technology description	Initial target market/application	TRL estimate
Oak Ridge National Laboratory, USA	Rotary pressure exchanger for expansion loss recovery in R-744 VC refrigeration systems and HPs	VC refrigeration and HPs, particularly systems using CO_2 as the refrigerant	About 8

Table ES-2 Nontraditional technologies

R&D institute	Technology description	Initial target market/application	TRL estimate
University of Maryland, USA	Elastocaloric (EC) cooling	Initial: small-scale refrigerators (wine coolers, etc.) Eventually: residential refrigerators and small Acs	3
Xi'an Jiao Tong University, China	EC cooling	Initial: portable beverage coolers With further development: residential refrigerator or personal cooling device Thermal-driven EC: solar-thermal AC or refrigerator; waste heat recovery mobile AC	About 4 Ranges from about 2 to 3
Shanghai Jiao Tong University, China	Electrocaloric cooling	Personal cooling devices, electric vehicle battery thermal management or seat coolers, data center on-chip cooling; miniature, portable Acs	Ranges from about 3 to 5
Fraunhofer Institute for Physical Measurement Techniques	Active caloric heat pipe concept	Medical or lab device cooling; mobile AC systems; residential HPs	Ranges from about 3 to 4
Ames National Laboratory, USA	a) High–power density magnetocaloric (MC) systems	Residential refrigerators or AC	Ranges from about 3 to 4
Oak Ridge National Laboratory, USA	Alternative cooling technology using MC materials	Refrigerators; residential or specialty	About 3

1.1. Annex Significant Accomplishments

- **Tsinghua University (TU)/China:** Prototype hybrid AC system developed under partnership between Tsinghua University and Gree Electric Appliances, Inc. of Zuhai, was named one of the two Grand Winners of the Global Cooling Prize competition (2018–2021).
- **TU/China:** Hybrid AC cost reduction efforts have led to potentially 15%–20% lower cost so far.
- **City University of Hong Kong (CUHK)/China:** R&D investigating absorption thermal energy storage system (ATES) cycles achieved maximum energy storage efficiency, energy storage density (ESD), and exergy efficiency values of 1.53, 365.4 kWh/m^3, and 0.61, by a double-effect ATES cycle, a compression-assisted ATES cycle, and the basic ATES cycle, respectively. This work aims to facilitate the rational development of ATES cycles for high-density and high-efficiency thermal energy storage toward carbon neutrality.

- **CUHK/China:** A prototype of a two-stage ATES was successfully developed. Experimental results showed that it can operate under extremely low charging temperatures (~50°C). The two-stage ATES has the advantages of higher ESD and lower charging temperature than the conventional ATES, providing a great option for low-grade renewable energy use.
- **ITAE/Italy:** The team at ITAE showed that employing plastic material could achieve an adsorber mass reduction in the range of 50% to 65% compared to aluminum while still maintaining similar performance.
- **Chung-Ang University (CAU)/South Korea:** To realize active membrane dehumidification, a highly water-selective membrane material will be required.
- **University of Maryland (UoMD)/USA:** Electrochemical NH_3 compressors were shown to have isentropic efficiency that monotonically increases with pressure ratio in contrast with positive displacement mechanical screw compressors, which show a peak in efficiency and then a decrease as pressure ratio continues to rise. Elastocaloric (EC) compressors may, thus, have an advantage for high suction-to-discharge pressure applications.
- **UoMD/USA:** Lab test EC dehumidification prototype achieved dehumidification 175% higher than shown by previous lab systems.
- **UoMD/USA:** A 260 W EC cooling prototype has been developed. This prototype is the largest power caloric system outside of reported magnetocaloric systems and indicates that the EC technology is rapidly maturing.
- **Oak Ridge National Laboratory (ORNL)/USA:** Field tests of a pressure exchanger (PEx) component integrated into the CO_2 transcritical refrigeration system of a supermarket in northern Italy demonstrated coefficient of performance (COP) improvements up to 27% under high–ambient temperature operation.
- **ORNL/USA:** Analytical projections for PEx-equipped HP systems show up to 30% efficiency boost.
- **Xi'an Jiao Tong University (XJTU)/China:** A Ni–Ti EC wine refrigerator design was developed with 100 W cooling power and a projected cost (at volume production) of $270.
- **XJTU/China:** A solar heat–driven EC system design was projected (by simulation) to have a COP >1.0 with a 120°C driving temperature. This COP exceeds that of both a state-of-the-art single-effect LiBr–H_2O absorption chiller and a photovoltaic-driven electric AC unit.
- **Shanghai Jiao Tong University (SJTU)/China:** A proposed electrocaloric HP device operating with a high-entropy polymer achieved a maximum COP of 11.4 (~80% of Carnot) compared with a COP of 1 when operating with a baseline terpolymer.
- **SJTU/China:** The conflict between high thermal conductivity and high electrocaloric effect (ECE) has been demonstrated on the molecular level. Click chemistry has been applied to expand the ordered and disordered structure to achieve both high ECE and large thermal conductivity.
- **SJTU/China:** An interface-regulated nanocomposite exhibited an electrocaloric entropy change of 30.94 J/(kg·K) under 100 MV/m and tripled thermal conductivity of 0.72 W/(m·K). Using a nanocomposite material, the standard model of an electrocaloric refrigerator achieved a 5.23 W/g cooling power density, 6.8× higher than the one operating with a simple material.
- **SJTU/China:** A figure of merit for electrocaloric nanocomposites has been proposed to assess their overall capability in heat-pumping applications.
- **Fraunhofer Institute for Physical Measurement Techniques (IPM)/Germany:** Three heat pipe–coupled caloric technologies—magneto-, elasto-, and electrocalorics—were successfully demonstrated. High cooling power densities of 12.5, 6.25, and 1.50 W/g of MC material were attained for magnetocaloric (MC), EC, and electrocaloric systems, respectively. At this point, an increase in system frequency, and thereby in maximum cooling power density, was hindered by the structure size of the caloric material (MC and EC) or the self-heating owing to dissipative losses in the material (electrocaloric). These

aspects will be addressed in future work, as well as an increase in the temperature lift of the systems by cascading several segments.

- **Ames National Laboratory (ANL)/USA:** An MC device was demonstrated and projected to have approximately 10 W/kg power density at 50 W cooling power (based on total mass of all magnetic material in the device), which is higher than almost all MC devices in similar cooling power ranges.
- **ANL/USA:** Estimates show that power density of similar MC devices can match that of commercially available mechanical compressors up to approximately 500 W. Meeting or exceeding the power density of compressors in given power ranges demonstrates that there is a viable path to cost parity and commercial adoption of the technology.
- **ANL/USA:** The highest estimated power density for MC devices using first-order materials was 162 W/kg at approximately 10 kW.
- **ORNL/USA:** Model results indicate the potential for an MC refrigeration cycle with a 16-stage regenerator to reach 84% of Carnot COP.

1.2. Potential Follow-On Annex Topics

Currently, the main focus in the field of heat pumping technologies is the expedient, effective, and efficient implementation of systems in the field in large numbers. Advancing the technology itself, in the form of more efficient, compact, and lower-cost vapor compression (VC) systems or the development of entirely new technologies that may potentially supplement or replace VC altogether, is taking a back seat. It may be appropriate, therefore, to undertake a follow-up annex or annex-like effort to foster collaboration and the exchange of information among researchers worldwide to expand the cost-effective efficiency envelop of future heat pumping technologies. The objective of such an effort is to promote, enhance, and strengthen research initiatives that help to bring next-generation technologies and approaches for heat pumping to the market, fulfilling a core mission of the IEA Technology Collaboration Programme on Heat Pumping Technologies.

The goal is to enable revolutionary progress of all heat pumping technologies, not incremental advances. All heat pumping (heating, cooling, refrigeration, and dehumidification) technologies would be included in the scope as long as the focus of the work is to go significantly beyond current state-of-the-art approaches and foster novel ideas and concepts. This objective is similar to those of efforts now underway by the International Institute of Refrigeration (IIR) particularly the IIR working group Solid-State Cooling and Heating (https://iifiir.org/en/news/new-iir-working-group-on-solid-state-cooling-and-heating). Therefore, a strong collaboration with the IIR in this proposed follow-up to Annex 53 is strongly encouraged.

This proposed effort is envisioned as a very long-term effort (beyond the duration of typical annexes) and has only one major task: the regular exchange of information among participating researchers to mutually enhance motivation, progress, and creativity. One potential output/deliverable of the work would be to have an annual webinar series where brief updates on specific projects are presented for the wider heat pumping community. These webinars could perhaps be held in conjunction with the ongoing IIR THERMAG events (https://iifiir.org/en/events/11th-iir-conference-on-caloric-cooling-and-applications-of-caloric-materials) or other related conferences when appropriate.

1.3. Specific Future RD&D Topic Suggestions from Annex 53 Participants

- **CAU/South Korea:** Technology development on vacuum membrane dehumidification should be developed further experimentally. Also, the influence by selectivity should be discussed to enhance the system performance. The priority should be set for the development of a high-permeance, high-selectivity membrane.

- **CUHK/China:** Advanced HP technologies for heating should be further investigated. In Annex 53, this work focused on advanced HP technologies for cooling. Because space heating and process heating are also energy-intensive, it is also necessary to investigate some advanced heating technologies. This work is significant for addressing the energy crisis and achieving carbon neutrality.
- **ORNL/USA:** Investigate the application of PEx to high-temperature HPs using CO2 refrigerant.
- **UoMD/USA:** Develop higher-power EC systems. Explore new materials to develop smaller-footprint actuators for implementation as EC system drivers.
- **XJTU/China:** Rate not-in-kind cooling prototypes at target applications' standard rating conditions.
- **SJTU/China:** Continue work on high-entropy ceramics and their multilayer ceramic capacitor (MLCC). If successful, the MLCC would exhibit extended cooling capacity, which is an essential step for fabricating an electrocaloric cooling machine with large cooling power.
- **SJTU/China:** Develop multilayer polymeric capacitors for the wide Tspan of an electrocaloric device.
- **IPM/Germany:** Standardize caloric measurements (e.g., adiabatic temperature change, isothermal entropy change, hysteretic losses of materials, cooling power, temperature lift and efficiency of systems), as well as establishing a standardized nomenclature.
- **ANL/USA:** Demonstrate first-order MC materials and advanced regenerators to achieve power density parity with compressors above approximately 10 kW.
- **ANL/USA:** Investigate additional materials and device concepts that can meet the temperature spans and power (heating or cooling) of additional end-use applications.
- **ANL/USA:** Investigate the potential for both cooling and heating in a single caloric (magneto-, elasto-, electro-, multicaloric) HP.

2. Background and Introduction

Air-conditioning (AC) and refrigeration systems account for a large share of current global energy consumption, and this demand is expected to increase sharply over the next 50 years unless actions are taken to ameliorate the increase. The adoption of AC in developed countries increased rapidly in the twentieth century, and the twenty-first century is expected to see increased adoption in developing countries—especially those with hotter climates and large, growing populations, such as India, China, Brazil, and Middle Eastern and African nations. The International Energy Agency (IEA) projects that by 2050, AC energy consumption levels will increase by 4.3× over the 2010 levels for non-Organisation for Economic Co-operation and Development (OECD) countries vs. only 1.5× for OECD countries (Figure 1) [1].

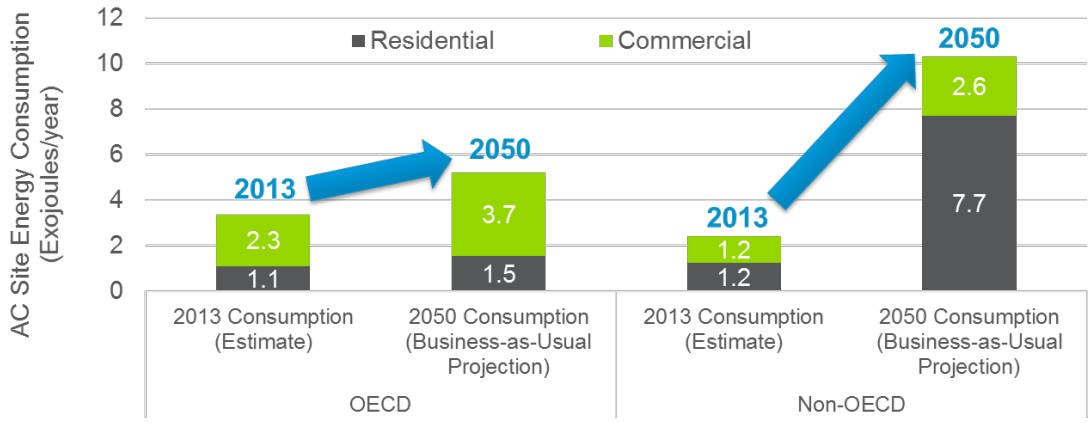

Figure 1 Anticipated global AC demand increases (courtesy of Navigant Consulting, Inc.; source: IEA Energy Technology Perspectives 2016)

The demand for refrigeration is expected to increase at a similar rate as that of the demand for space cooling. Most of the demand for refrigeration is related to food preservation and storage, and the food demand is expected to increase 70% by 2050 relative to 2010 [2]. India, for example, has the largest refrigerated warehouse capacity of any country in the world: >150 million m^3 of space in 2018, which is approximately a 15% increase since 2014 [3]. By 2023, cold storage warehouse capacity in India is expected to reach 40.7 MMT [4] or about 175 million m^3 (converted to cubic meters using the conversion factor of 1 MT = 4.3 m^3 from Salin [4]). Moreover, a huge increase in refrigerated transport capacity also is needed to properly serve the warehouse capacity and reduce food wastage. India is estimated to currently have 9,000 refrigerated trucks, but the country needs >600,000 [3]. The need for much cleaner and more efficient refrigeration systems is critical. The United Nations Food and Agriculture Organization (FAO) estimates that approximately one-third of all global food produced is wasted, resulting in huge environmental consequences. FAO estimates that this wastage occupies a land area the size of Mexico, its production consumes 250 km^3/year of water, and it accounts for 3.3 billion tons per year of CO_2 emissions.

Stationary AC systems alone account for nearly 700 MMT of direct and indirect CO_2-equivalent emissions annually. Indirect emissions from electricity generation account for approximately 74% of this total, direct emissions from hydrofluorocarbon refrigerants account for 7%, and hydrochlorofluorocarbon refrigerants account for 19%. With regard to refrigeration for food preservation, if all the additional food transport trucks needed in India alone were to use current diesel-powered cooling technology, then the impacts from NO_x and other emissions would be enormous. Transitioning to low–global warming potential (GWP) alternative refrigerants could eliminate most direct greenhouse gas emissions from AC and refrigeration, theoretically creating up to a 26% global reduction in annual greenhouse gas emissions related to AC and refrigeration—even without improving system efficiency [2].

Global action, both short-term (e.g., increasing the deployment of current best technologies) and long-term (research, development, and demonstration [RD&D] for advanced, higher-efficiency technology solutions), is urgently needed to address this challenge. Annex 53 was initiated in October 2018 to help address the long-term RD&D need. Its main objective is to share information to encourage the development of high-efficiency and low-GWP AC and refrigeration heat pump (HP) technologies. The annex is led by the United States, and other participating countries include the People's Republic of China, Germany, Italy, and South Korea.

This report provides a summary of the current RD&D status of the leading technologies examined by each research and development (R&D) institute involved in the annex. A brief description of each technology (e.g., current development status, plans for further development, and some indication of performance vs. current systems), along with thoughts about initial target markets and applications, is provided. Future R&D actions are also discussed in some instances, which could be the basis of a future annex (or range of annexes) on advanced lower–global impact alternatives to the current fluorocarbon-based vapor compression (VC) technology systems.

3. Participants' Final Project Summaries

The technical scope of Annex 53 is very broad by design. It is unlikely that there will be only one or even a few so-called *right* solutions to the challenge. Therefore, the participants were free to investigate a wide range of possible technology solutions. Technologies of interest follow two distinct paths: those based on the well-known and widely used VC systems and those based on nontraditional cooling approaches that are being increasingly investigated (Figure 2). VC technology has had decades of RD&D, which is still ongoing. VC could continue to be the system of choice, especially for the near future and possibly for the long term. However, if VC cycle systems continue to use fluorocarbon-based refrigerants with nonzero GWPs—even in small amounts—they will remain vulnerable to further refrigerant restrictions. Nontraditional technologies (e.g., magnetocaloric [MC], elastocaloric [EC] , electrocaloric, electrochemical compression [ECC]) generally are not subject to this challenge because they do not rely on refrigerants in the traditional sense. However, all the nontraditional technologies discussed herein will require additional development before they can significantly affect the market.

Figure 2 Two possible future paths for refrigeration and AC systems (courtesy of Navigant Consulting, Inc.; source: US Department of Energy Building Technologies Office, Emerging Technologies Program)

This section is divided into two parts that deal with the two general future paths described above. VC or other compression-based projects are covered in Section 3.1, and nontraditional technology-based projects are covered in Section 3.2.

3.1. Advanced Vapor Compression–Based Project Descriptions

3.1.1. South Korea, Korea Institute of Machinery and Materials and Chung-Ang University: Membrane Heat Pump

Lead PIs: Dr. Seok Ho Yoon (Korea Institute of Machinery and Materials), Dr. Minsung Kim (Chung-Ang University)

Description

Current active dehumidification methods rely on water vapor condensation, which requires a large amount of cooling energy for latent heat removal. The project's primary purpose is reducing dehumidification energy by removing water vapor in isothermal separation instead of latent heat cooling. The research team considered a water-selective dense membrane under a vacuum environment for this work. The process is called membrane-based vacuum dehumidification (MVD), which is suitable for active and effective dehumidification.

The total heat exchanger (HEx) is a former case of membrane-based moisture transfer. The method has been applied to recover heat and moisture from the ventilated indoor air. Because of its simple structure and ease of manufacturing, either dehumidification/cooling or humidification/heating can be realized easily, but the method has clear limitations of passive function. Considering high–energy saving potentials, the water vapor–discharged MVD (W-

MVD) system and condenser-combined MVD (C-MVD) system were selected and analyzed. Schematic diagrams of both systems are shown in Figure 3.

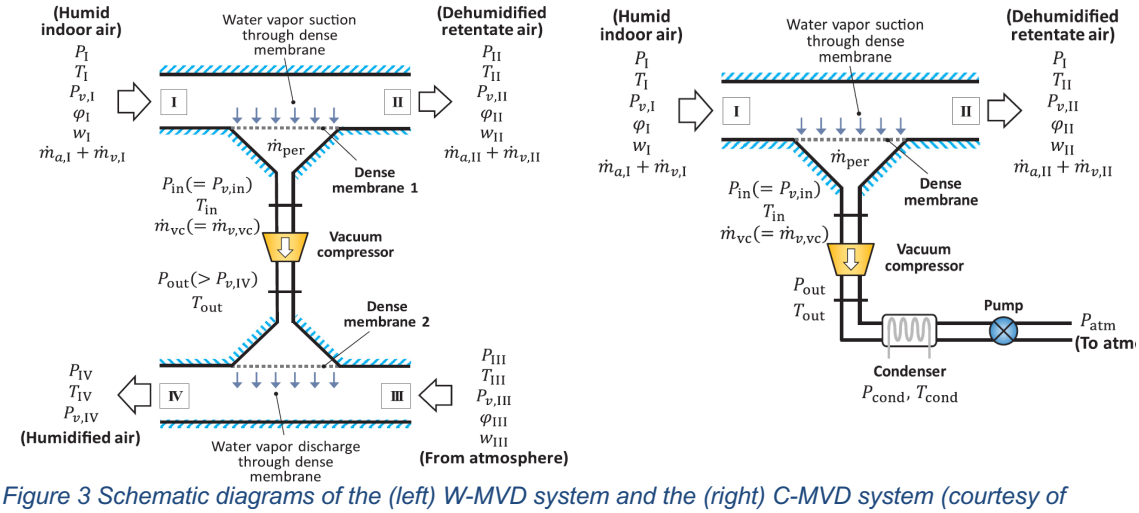

Figure 3 Schematic diagrams of the (left) W-MVD system and the (right) C-MVD system (courtesy of Prof. Minsung Kim; presentation for May 15, 2023, Annex 53 workshop)

Most Significant Accomplishments

Figure 4 shows the coefficient of performance (COP) comparison between the W-MVD and C-MVD systems. As the ambient temperature increases, all the COPs are decreased owing to the temperature difference between the high and low heat sources.

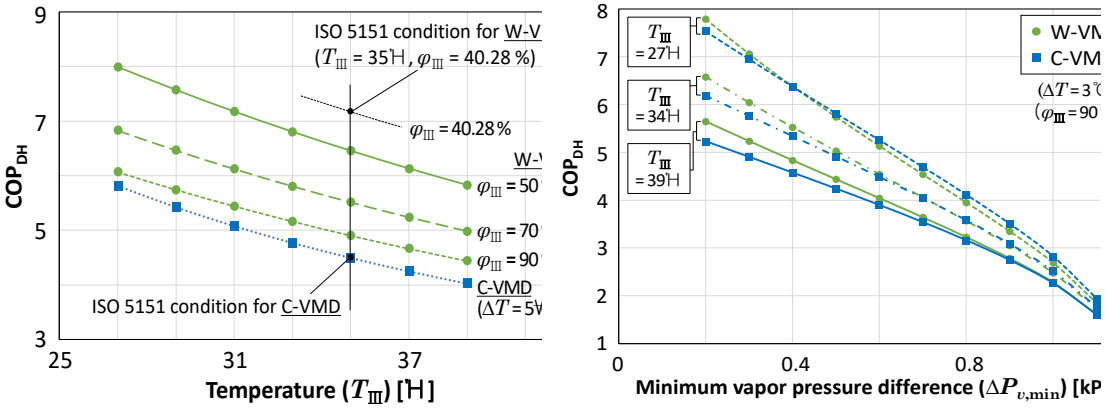

Figure 4 COP comparison between W-MVD and C-MVD system. (a) Influence of relative humidity (φ_{III}) on W-MVD system. (b) Influence of ambient temperature(T_{III}) on C-MVD system. Schematic diagrams of (left) W-MVD system and (right) C-MVD system (courtesy of Prof. Minsung Kim; presentation for May 15, 2023, Annex 53 workshop)

Figure 5 shows the seasonal performance comparison of membrane heat pumps (MHPs) based on W-MVD and C-MVD mechanisms based on the climate of Seoul, South Korea, in 2019. The W-MVD HP system shows a higher COP compared with the C-MVD system. The cooling seasonal performance factor of the W-MVD HP system is 8.08, and that of the C-MVD HP system is calculated as 6.90. Figure 6 shows that MHP performance improves as the minimum vapor pressure difference, $\Delta P_{v,min}$, decreases.

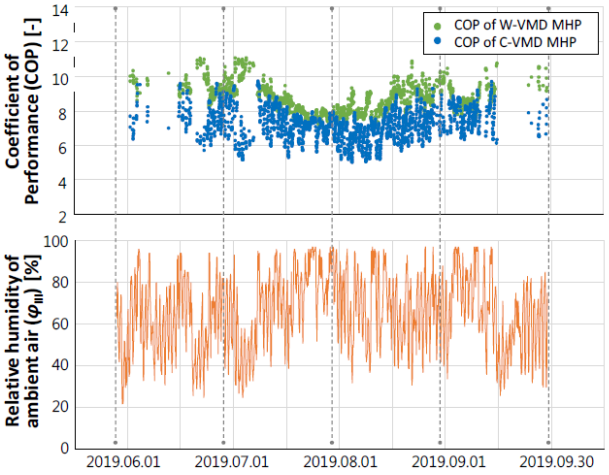

Figure 5 Simulation of the seasonal performance of the MVD systems (courtesy of Prof. Minsung Kim; presentation for May 15, 2023, Annex 53 workshop)

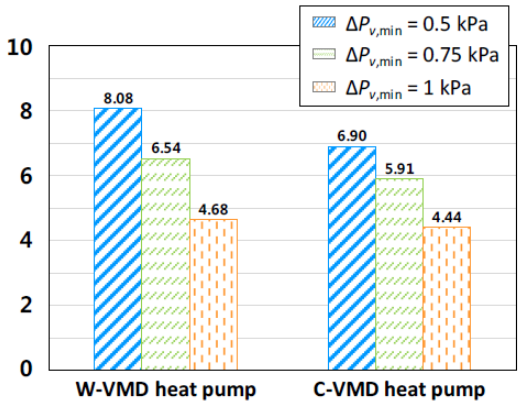

Figure 6 MHP performance by minimum vapor pressure difference (courtesy of Prof. Minsung Kim; presentation for May 15, 2023, Annex 53 workshop)

The former studies assumed that membranes have infinite selectivity. However, the selectivity of air and water vapor should be finite, and air will inevitably pass through the membrane. In this case, periodic evacuation is necessary to remove air infiltration. A modified structure of W-MVD is suggested in Figure 7.

The average COP per cycle changed according to the vacuum compressor operation time, as depicted in Figure 8. If the marginal compression ratio is set to the maximum compression ratio of the compressor, the average dehumidification efficiency may decrease. The smaller a membrane's selectivity, the greater the optimal compression ratio; thus, the use of a compressor with higher compression performance is required. To realize active membrane dehumidification, a highly water-selective membrane is necessary.

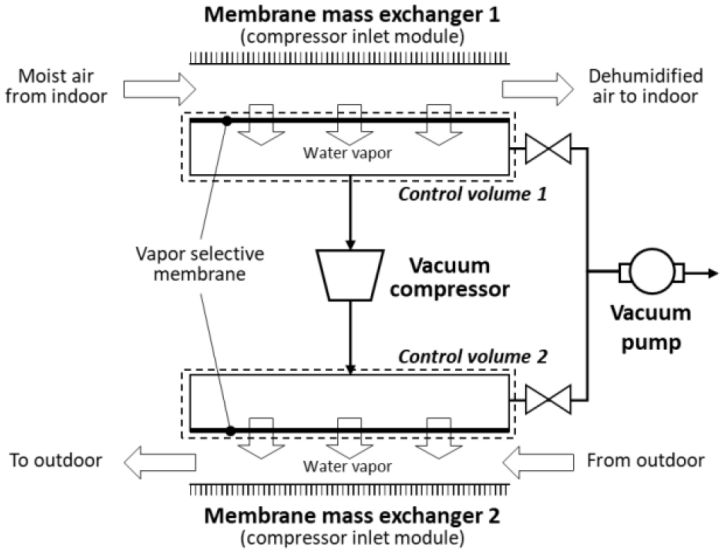

Figure 7 Revised MVD with a finite selectivity membrane by a vacuum pump for dry air discharge (courtesy of Prof. Minsung Kim; presentation for May 15, 2023, Annex 53 workshop)

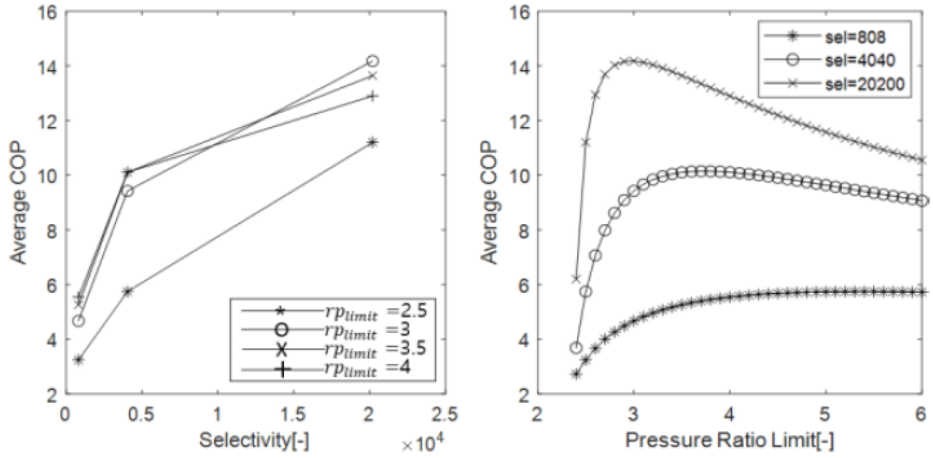

Figure 8 Average COP per cycle changed according to the vacuum compressor operation time (courtesy of Prof. Minsung Kim; presentation for May 15, 2023, Annex 53 workshop)

Follow-On Work Priorities

Technology development on vacuum membrane dehumidification should be developed further experimentally. Also, the influence by selectivity should be discussed to enhance the system performance. The priority should be set for the development of a high-permeance, high-selectivity membrane.

Relevant Publications

Lim, H., S. Choi, Y. Cho, S. Kim, and M. Kim. 2020. “Comparative thermodynamic analysis of membrane-based vacuum air dehumidification systems.” *Applied Thermal Engineering* 179, no. 115676: 1–13.

Lim, H., J. Lee, S. Choi, S. Kim, M. Jung, J. Lim, and M. Kim. 2020. “Performance simulation of membrane heat pumps based on vacuum membrane dehumidification system.” *Journal of Mechanical Science and Technology* 34, no. 2: 941–948.

Ku, D., S. Bae, S. Kim, M. Jung, S. Jeong, G. Seo, and M. Kim. 2023. “Cyclic operation of a membrane-based vacuum dehumidification system by finite selectivity of the membrane.” *Journal of Mechanical Science and Technology* 37: 2087–2094.

3.1.2. China, Tsinghua University: Advanced VC Systems Development

Lead PI: Dr. Baolong Wang

Three different projects have been investigated and are briefly summarized in this section.

Develop Refrigerant VC Cycles for Room AC and/or Chiller Applications

This project aims to develop refrigerant VC cycles for room AC/chiller applications with the temperature matching in the evaporator and condenser. By using blend refrigerants with proper temperature glide for the evaporator and condenser HExs and the optimum system configuration with a two-section or relay evaporator and a two-cylinder compressor, the exergy loss in the HExs of these small–compression ratio systems can be largely decreased. Figure 9 illustrates the basic two-stage cycle, and Figure 10 shows a modification with a recuperator HEx (on L-evaporator exit line) and economizer HEx (on M-evaporator exit line). The advantages of the proposed systems have been confirmed by simulations and lab tests. Figure 11 illustrates test results showing that the economizer and recuperator (ERHX-REC) cycle had the highest COP among all the relay evaporation cycle variants tested—3.4% to 6.6% better than a basic two-stage cycle with a single evaporator (light blue line in the figure). The ERHX-REC cycle COPs were approximately 14% to 21% better than that of a single-stage cycle (gray line in the figure).

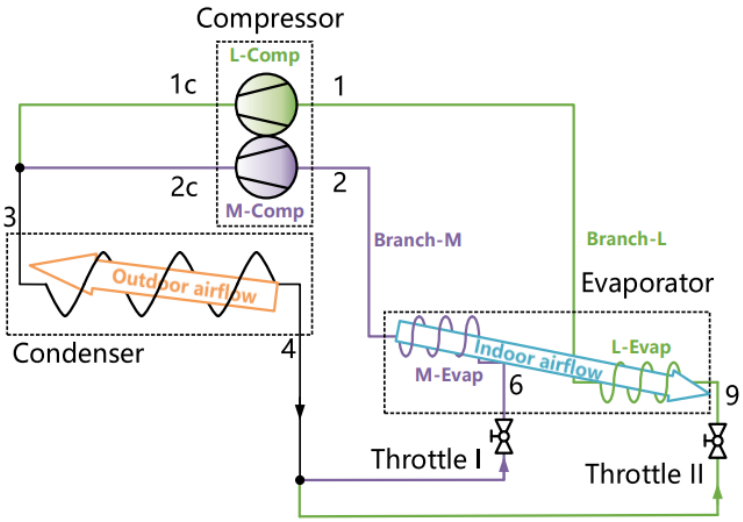

Figure 9 Basic two-stage VC cycle for refrigerant mixtures with two-section evaporator (courtesy Prof. Baolong Wang; presentation for February 2, 2023, Annex 53 meeting)

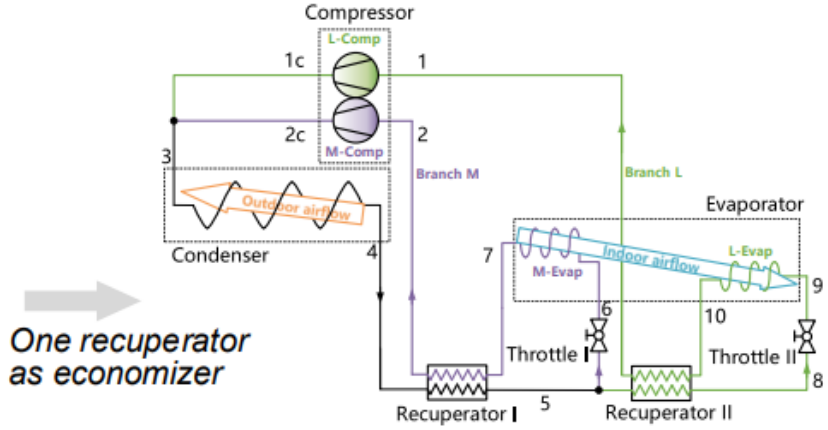

Figure 10. Modification of basic two-stage VC cycle with ERHX-REC (courtesy Prof. Baolong Wang; presentation for February 2, 2023, Annex 53 meeting)

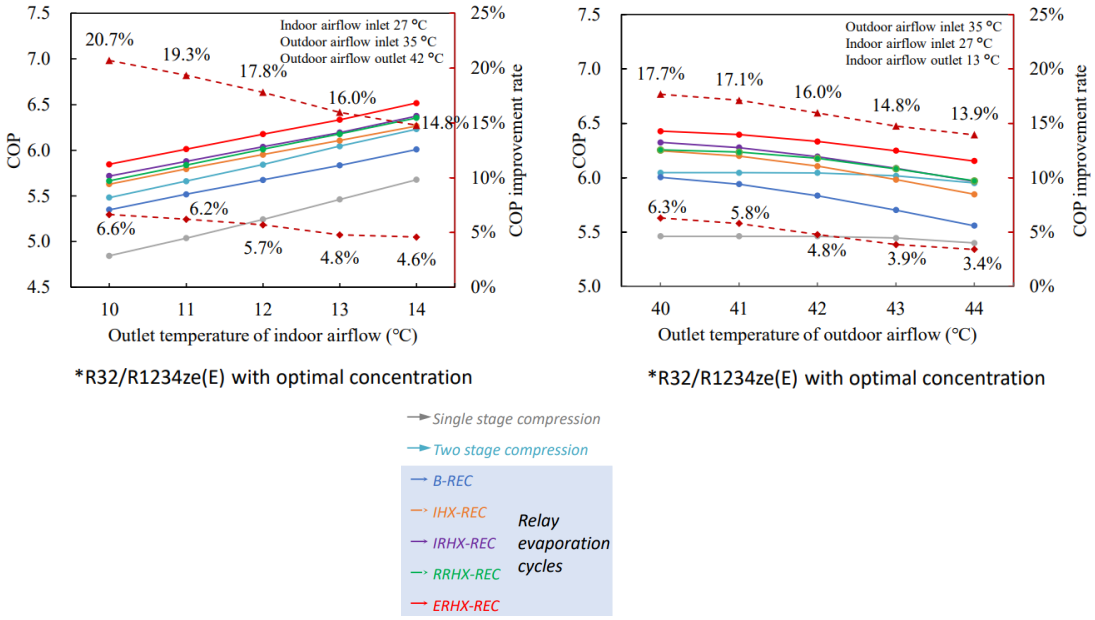

Figure 11: Two-stage evaporator cycle COP results vs. single-stage and two-stage cycles (courtesy Prof. Baolong Wang; presentation for February 2, 2023, Annex 53 meeting)

Develop a Hybrid Superhigh-Efficiency AC

The hybrid AC earned the Grand Winner Award of the Global Cooling Prize (GCP). It can decrease climate impacts by 85.7% compared with the GCP baseline AC product. The GCP prototype system integrates solar photovoltaic and evaporative cooling with a VC AC system. The prototype cost was estimated at approximately $1,000 or about twice that of the baseline AC used in the GCP competition. Cost reduction efforts have been underway since then, with a goal to bring the price down to approximately $800–$850. Figure 12 illustrates a schematic of a simpler, less costly version of the GCP prototype, still suitable for hot, dry, underdeveloped areas.

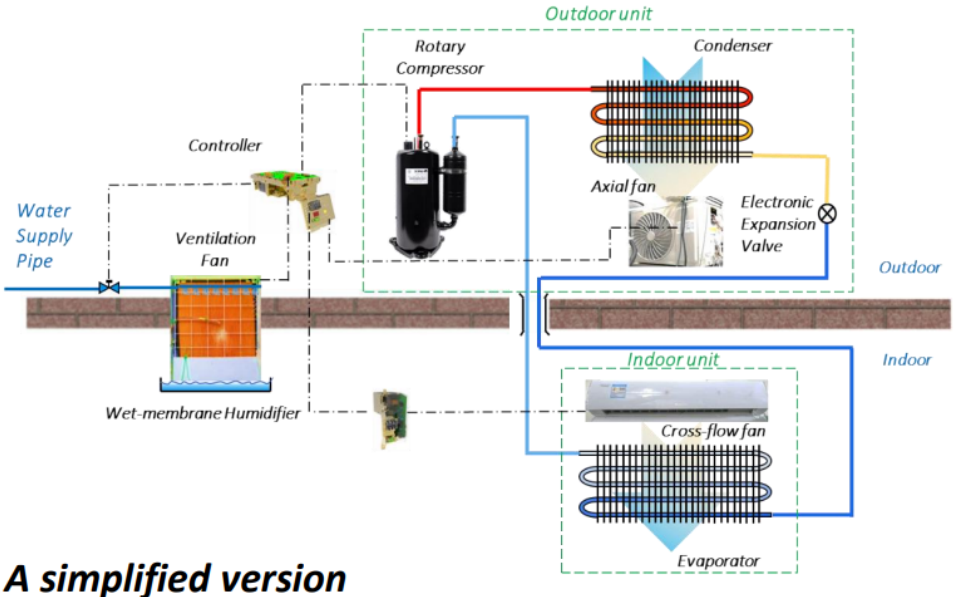

Figure 12 Schematic of lower-cost hybrid AC design (courtesy of Prof. Baolong Wang; presentation for February 2, 2023, Annex 53 meeting)

Figure 13 shows simulated energy savings rates for the simplified hybrid AC system vs. a standard AC unit for different climate zones in China. Laboratory tests to emulate a typical day's operation showed an approximately 38% energy efficiency ratio enhancement in the

Beijing area (semiwet climate) and approximately 280% energy efficiency ratio enhancement in the Lanzhou area (semidry/dry climate).

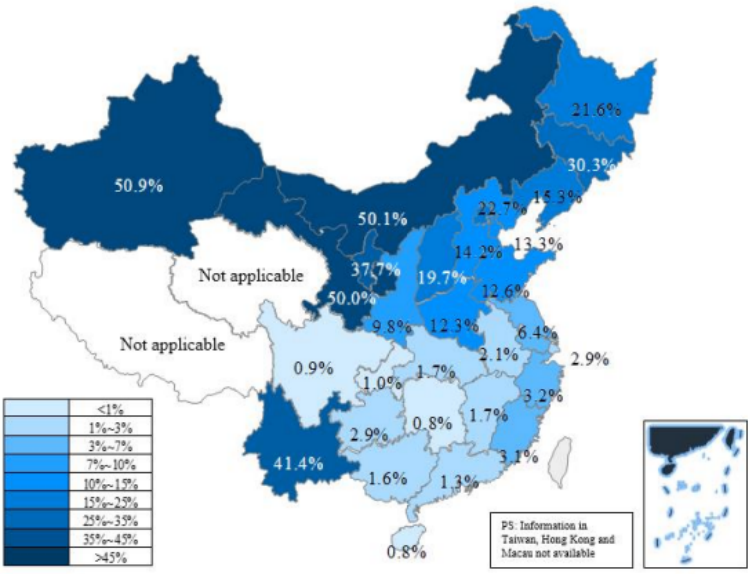

Of

Figure 13 Simulated hybrid AC energy savings vs. baseline AC product (courtesy Prof. Baolong Wang; presentation for February 2, 2023 Annex 53 meeting)

Develop a General Construction Method for Efficient VC Systems

An integrated construction method of a VC cycle and HEx network, named GraPHsep, was developed to automatically realize selecting the refrigerant, constructing the refrigeration cycle, and constructing the medium HEx network. It could be an artificial intelligence tool for the optimization design of thermal systems with multiple heat sources and heat sinks. The estimated technology readiness level (TRL) is approximately 5 or a bit higher. Possible applications include an industry HP.

Most Significant Accomplishments

- Prototype hybrid AC system, developed under partnership between Tsinghua University and Gree Electric Appliances, Inc. of Zuhai, was named a Grand Winner of the Global Cooling Prize competition (2018–2021).

- Hybrid AC cost reduction efforts led to potentially 15%–20% lower cost.

Recent Publications Related to the Annex 53 Work

Cui, Mengdi, Baolong Wang, Cuiling Wang, Falin Wei, and Wenxing Shi. 2023. “GraPHsep: An integrated construction method of vapor compression cycle and heat exchanger network.” *Energy Conversion and Management* 277: 116576.

Chen, Wei, Xianting Li, Tiancheng Li, Wenxing Shi, Baolong Wang, and Yang Cao. 2023. “Design method of general heat exchanger networks with heat pumps based on thermal energy discretization and matching.” *Journal of Cleaner Production* 384: 135620.

Yang, Zixu, Youlin Zhang, Hansong Xiao, Rong Zhuang, Xiangfei Liang, Mengdi Cui, Xin Li, Jiaan Zhao, Qi Yuan, Ruiqi Yang, Baolong Wang, and Wenxing Shi. 2022. “Comprehensive test of ultra-efficient air conditioner with smart evaporative cooling ventilation and photovoltaic.” *Energy Conversion and Management* 254: 115267.

Cui, Mengdi, Baolong Wang, Falin Wei, and Wenxing Shi. 2022. “Novel zeotropic refrigeration cycles for air cooling with large temperature decrease.” *Energy and Buildings* 274: 112450.

Cui, Mengdi, Zuo Cheng, Baolong Wang, Falin Wei, and Wenxing Shi. 2023. “Experimental investigation on an auto-cascade quasi two-stage compression heat pump system.”

Applied Thermal Engineering 219, (Part A): 119498.
Liu, Qiulin, Falin Wei, Guodong Li, Zongxiang Kan, Jiawei Yang, Hangtian Zhu, Baolong Wang, and Huaizhou Zhao. 2022. "Highly efficient thermoelectric air conditioner with kilowatt capacity realized by ground source heat-exchanging system." *iScience*, 25, no. 5: 104296.
Cui, Mengdi, Baolong Wang, Falin Wei, and Wenxing Shi. 2022. "A modified exergy analysis method for vapor compression systems: Splitting refrigerant exergy destruction." *Applied Thermal Engineering* 201, no. 25 (Part A): 117728.

3.1.3. China, City University of Hong Kong: Absorption Thermal Energy Storage

Lead PI: Dr. Wei Wu

Absorption Thermal Energy Storage (ATES)

ATES plays a significant role in balancing the mismatch between renewable/waste energy supply and building energy demand. Working fluids are critical to the high performance and reliability of ATES, but conventional salt-based mixtures suffer from crystallization risks, and the popular ionic liquid–based mixtures are quite expensive. This work explored crystallization-free and low-cost deep eutectic solvents (DESs) to achieve reliable and affordable ATES. A comprehensive comparison between the emerging DES-based and traditional working fluids was conducted. For a basic ATES with inferior operating conditions, NH_3/glyceline yielded the highest energy storage efficiency (ESE) and exergy efficiency, outperforming the traditional refrigerant/salts. A compression-assisted ATES was further adopted, enabling NH_3/DESs to use ultralow-grade heat as low as 40°C. The compression-assisted ATES using NH_3/glyceline is promising for large-scale applications in terms of cost per kilowatt [Figure 14 (c) and (d)].

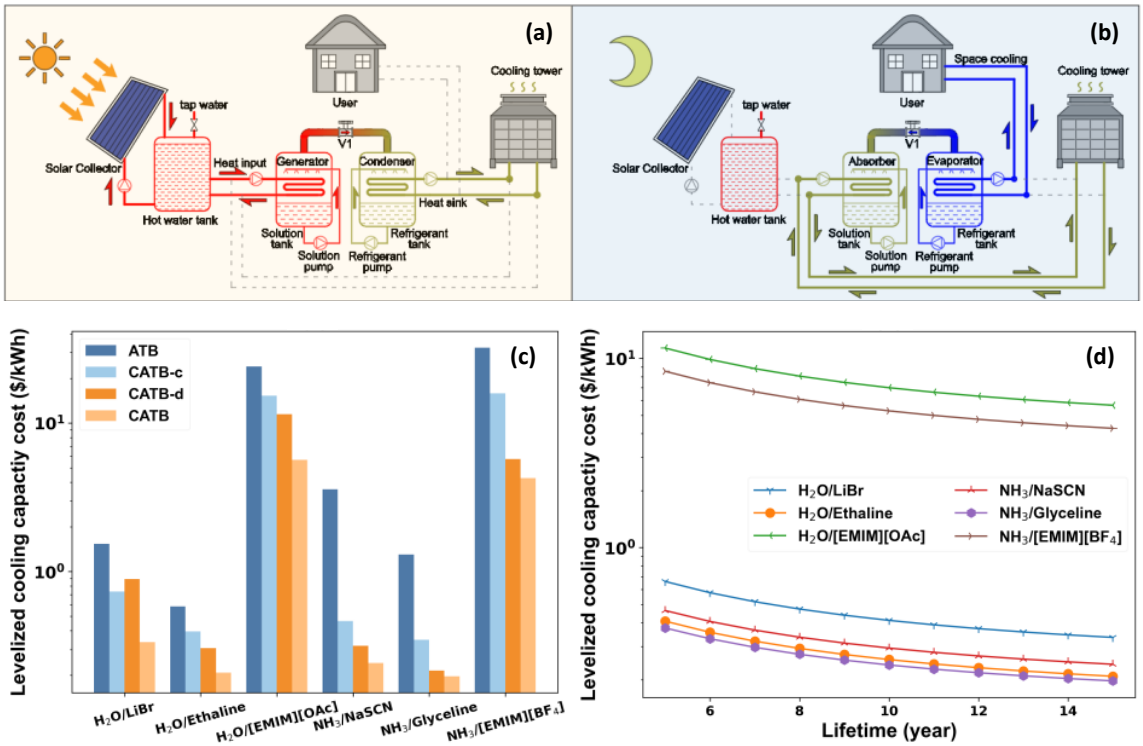

*Figure 14 Configuration and fluids of solar ATES. (a) Charging process, (b) discharging process, (c) levelized cooling capacity cost (LCC) comparison between different fluids for different cycles, and (d) LCC comparison between different fluids with varying lifetimes. (*ATB *stands for* absorption thermal battery*, which is equivalent to ATES)*

Furthermore, this work investigated a solar ATES in a building for space cooling. The annual dynamic performance was compared in four representative cities by simulation using an

experimentally validated model considering transient supply–demand matching. Also, parametric studies were conducted for the solar ATES designed with different solar collector sizes and solution charges. The highest cooling met ratio of 0.95 was obtained in Singapore, with an ESE of 0.66, an overall solar-to-cooling efficiency of 0.24, and an energy storage density (ESD) of 125.8 kWh/m^3. The highest ESD of 157.1 kWh/m^3 was achieved, which was much higher than the sensible and latent thermal energy storage for space cooling. This study can facilitate the promotion and development of ATES technology.

Relevant Publications

Ding, Z., Y. Sui, C. Zhai, Z. Sui, H. Lin, F. Li, and W. Wu. 2023. "Transient supply–demand matching and numerical parametric study of solar absorption thermal battery for space cooling." *Energy Conversion and Management* 288: 117177.

Sui, Y., Z. Ding, C. Zhai, H. Lin, and W. Wu. 2023. "Crystallization-free and low-cost deep eutectic solvents for absorption thermal battery utilizing ultra-low-grade energy." *Energy Conversion and Management* 284: 116984.

Ding, Z., and W. Wu. 2023. "Dynamic discharging characteristics of absorption thermal battery under different capacity regulation strategies." *Energy and Built Environment* 4, no. 3: 341–353.

Ding, Z., W. Wu, S.-M. Huang, H. Huang, Y. Bai, and Z. He. 2023. "A novel compression-assisted energy storage heat transformer for low-grade renewable energy utilization." *Energy* 263, no. A: 125681.

Ding, Z., W. Wu, W., and M. K. Leung. 2022. "On the rational development of advanced thermochemical thermal batteries for short-term and long-term energy storage." *Renewable and Sustainable Energy Reviews* 164: 112557.

Ding, Z., and W. Wu. 2022. "Type II absorption thermal battery for temperature upgrading: Energy storage heat transformer." *Applied Energy* 324: 119748.

Ding, Z., and W. Wu. 2022. "A novel double-effect compression-assisted absorption thermal battery with high storage performance for thermal energy storage." *Renewable Energy* 191: 902–918.

Ding, Z., W. Wu, and M. Leung. 2021. "Advanced/hybrid thermal energy storage technology: Material, cycle, system and perspective." *Renewable and Sustainable Energy Reviews* 145: 111088.

Ding, Z., and W. Wu. 2021. "A hybrid compression-assisted absorption thermal battery with high energy storage density/efficiency and low charging temperature." *Applied Energy* 282: 116068.

Wu, W., Z. Ding, Y. Sui, and M. Leung. 2021. "Comparative dynamic performance of hybrid absorption thermal batteries using H_2O/1,3-dimethylimidazolium dimethylphosphate." *Energy Conversion and Management* 228: 113690.

Ding, Z., W. Wu, Y. Chen, and M. Leung. 2020. "Dynamic characteristics and performance improvement of a high-efficiency double-effect thermal battery for cooling and heating." *Applied Energy* 264: 114768.

Wu, W., Y. Bai, H. Huang, Z. Ding, and L. Deng. 2019. "Charging and discharging characteristics of absorption thermal energy storage using ionic-liquid-based working fluids." *Energy* 189: 116126.

Significant Accomplishments

This study conducted comparative investigations among different ATES cycles from a multicriteria perspective, including ESE, ESD, exergy efficiency, charging temperature, and initial cost (Figure 15). Different cycles, including the basic cycle, compression-assisted cycle, double-stage cycle, double-effect cycle, and double-effect compression-assisted cycle, were included to cover a wide range of design options. The effects of charging/discharging/cooling temperatures on the storage performance were analyzed in three scenarios (i.e., short-term cold storage, short-term heat storage, and long-term heat storage). Results indicated that the compression-assisted cycle and the double-stage cycle could improve the ESD and lower the charging temperatures (e.g., below 70°C), the double-effect cycle could enhance the ESE, and the double-effect compression-assisted cycle could achieve improvements in ESE and ESD simultaneously, with a maximum ESE above 1.30 and ESD over 300 kWh/m^3, and bridged the temperature gap (i.e., 100°C–140°C) between the single-effect and double-effect

cycles. The maximum ESE, ESD, and exergy efficiency are 1.53, 365.4 kWh/m^3, and 0.61, respectively, achieved by the double-effect cycle, the compression-assisted cycle, and the basic cycle, respectively [Figure 15(b)]. This work aims to facilitate the rational development of ATES cycles for high-density and high-efficiency thermal energy storage toward carbon neutrality.

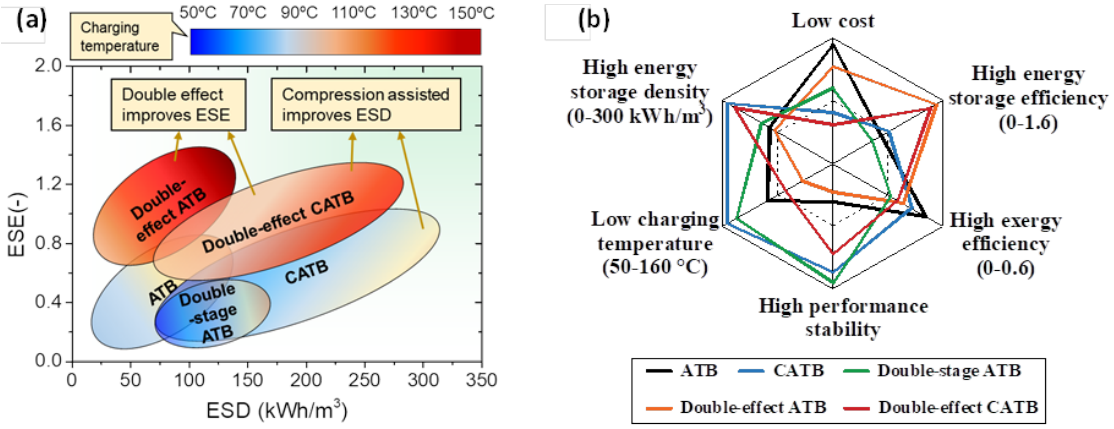

*Figure 15 Systematic evaluation of energy storage characteristics of various ATB cycles. (a) Comparison of the ESE, ESD, and charging temperature and (b) comprehensive comparison of various aspects. (*ATB *stands for* absorption thermal battery*, which is equivalent to ATES)*

End-Use Applications

The most relevant end-use application of the ATES technology is commercial heating, ventilation, and air-conditioning (HVAC). In summer, the ATES stores excessive solar energy and then discharges it for space cooling. In winter, the ATES stores excessive solar energy and then discharges it for space heating. Therefore, the ATES technology is a promising solar cooling/heating solution toward carbon neutrality.

Follow-On Work Priorities

Advanced HP technologies for heating is one priority for follow-on work. In Annex 53, this study focused on advanced HP technologies for cooling. Because space heating and process heating are also energy-intensive, it is also necessary to investigate some advanced heating technologies. This work is significant for addressing the energy crisis and achieving carbon neutrality.

3.1.4. Italy, Institute for Advanced Energy Technologies: Thermally Driven Adsorption Transformations for Cooling

Lead PI: Dr. Alessio Sapienza

Thermally Driven Adsorption Heat Transformation (AHT) Processes

Technologies and systems based on AHT processes currently represent a fascinating option to meet the growing worldwide demand of cooling, refrigeration, and space heating and the severe regulations on the environmental impact of HVAC technologies. In fact, the progressive disposal of high-GWP/ozone depletion potential refrigerants and the planned phasing out of hydrochlorofluorocarbons is boosting the search for possible alternatives capable of replacing the traditionally used fluids and cooling technologies. Among the so-called *natural refrigerants*, H_2O (R-718) emerges as a promising candidate for its wide availability at low cost and the high phase change enthalpy. Cooling technologies based on natural refrigerant adsorption systems represent an interesting alternative to traditional HVAC technologies for different applications.

The operation of an adsorption cooling machine is based on the reversible ad-/desorption of a refrigerant fluid (e.g., H_2O, NH_3, ethanol) on/from a porous material (e.g., zeolites, silica gel,

active carbons) realized in the so-called *thermal compressor* or *adsorber* consisting of the adsorbent material integrated in a HEx. The cooling cycle is realized by a system layout composed, in its basic configuration, of one adsorber, one evaporator, and one condenser. Figure 16 depicts the typical thermodynamic transformations of an adsorption cooling/refrigeration/heating cycle plotted on the isosteric chart of a generic working pair (refrigerant + adsorbent). A typical cycle consists of two isosters and two isobars, as presented on the Clapeyron diagram ln(P) vs. (−1/T) (Figure 16). The heat supplied from an external heat source at temperature T_H is used for isosteric heating of the adsorbent (stage 1–2) and removing adsorbed vapor (regeneration stage 2–3) at constant vapor pressure P_M. Commonly, the regeneration temperature is in the range of 60°C–90°C. The heat Q_{des} is supplied for desorption. During desorption process 2–3, the valve between the adsorber and condenser is opened, and the desorbed vapor is collected in the condenser, where the heat of condensation Q_{con} is released. The regenerated adsorbent is cooled by a heat carrier (cooling fluid) at temperature T_M. The cooling is first performed at constant uptake w_1 (isoster 3–4) and then at constant pressure P_L (isobar 4–1). During adsorption process 4–1, the valve between the adsorber and the evaporator is opened. Here, the cooling effect is produced. The heat of adsorption Q_{ads} transfers to the cooling fluid and can be supplied to a consumer for space heating. During isosteric stages, the valve between the adsorber and condenser/evaporator is closed.

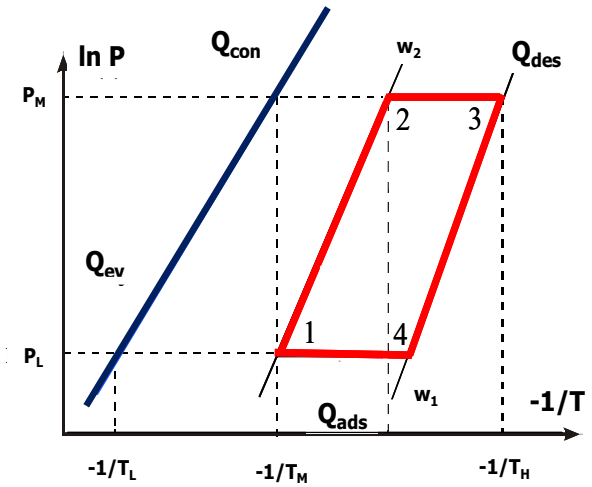

Figure 16 Typical thermally driven cooling/refrigeration/heating adsorption cycle on the pressure–temperature diagram.

Project Description: Current Development Status

Despite the interesting features of these technologies, considerable efforts must still be made to enhance their performance to aim at competing with commonly used mechanical vapor compression or absorption machines. In fact, the current state of the art indicates rather low specific cooling power, which means bulky and heavy machines. Subsequently, these technologies could be still inadequate, especially for those specific applications that impose very strict constraints in terms of lightness, compactness, and efficiency (e.g., automotive AC). Also, the capital cost of the few market-available sorption cooling machines is still an open issue.

Further Development Plans/Approach

To increase the overall performance and the economic feasibility of an adsorption cooling machine, an intelligent design of all components should be created. In particular, the adsorber's design should be deeply investigated. The first step is a convenient choice of the adsorbent material by a comprehensive analysis that takes into account both the thermodynamic and dynamic aspects. Although the thermodynamic properties of the AHT cycle were comprehensively studied, the dynamic optimization of AHT adsorbers is still an open issue. The AHT dynamics are a complex process that regard all main components of a sorption machine (i.e., the adsorber, evaporator/condenser) whose performance are affected

by the HEx's design (geometry, material), adsorbent configuration (loose grains or coating), grain size, layer thickness, and other main variables such as the heat carrier's flow rates, condenser/evaporator efficiency, and more. The study on the adsorber's design should take into account all design parameters: the sorbent nature and configuration (e.g., grains, coating, foams), the geometry, and the material used for HExs' manufacturing (e.g., plastic, aluminum).

The main goal of this activity reported here was the optimization of the adsorber's design. In particular, this work studied the technical potential of plastic-based adsorbers and how all main parameters affect the performance of the adsorbers.

Potential Target Applications/Markets

Potential target applications of the thermally driven adsorption cooling machines are the integration with renewable energy sources (e.g., solar cooling/refrigeration systems), waste heat recovery from industrial processes, and integration in combined cooling, heating, and power systems or mobile AC.

Increasing cooling power density can make this technology very competitive for the mobile sector (mobile HVAC), and the phasing out of hydrofluorocarbons could open a wide potential market for an adsorption machine employing H_2O as the refrigerant.

Key Results: Development of Plastic Adsorbers for Adsorption Chillers

The activity evaluated the feasibility of plastic adsorbent HExs (HEx + sorbent material) for adsorption cooling applications. The development of new sorbents, innovative geometry, or new adsorbent reactors with enhanced thermophysical properties, low production cost, and reduced weight is a trendy issue in this research area. Adsorption chiller production involves a number of manufacturing processes that negatively affect the production cost and, thus, the technology acceptance. In comparison, 3D printing is a rapidly spreading and simple method of manufacturing that allows the production of parts directly from a computerized virtual model. Promotion, commercialization, and market penetration of adsorption-based systems can be facilitated by the 3D printing technique.

In particular, the National Research Council (CNR) Institute for Advanced Energy Technologies studied the possible replacement of aluminum or steel-based HExs for adsorbers with 3D printed components. Three different potential plastic materials were identified—acrylonitrile butadiene styrene (ABS), polylactic acid (PLA), and nylon. Microscale, flat-type HExs were realized by a 3D printer, integrated with the sorbent AQSOA FAM Z02, and experimentally tested to measure the dynamic performance of plastic adsorbers in terms of the specific cooling power (SCP). Furthermore, a thermodynamic analysis was addressed to evaluate how the plastic material affects the cooling COP under different operating conditions. From a thermodynamic point of view, a mathematical model was used considering two operating conditions typical for adsorption AC—T_{ev} = 7°C and T_{con} = 40°C, and T_{ev} = 10°C and T_{con} = 30°C—while the desorption temperature was varied from 50°C to 95°C.

Employing plastic material is possible to get a relevant reduction of the HEx's mass (respect to the aluminum HEx) ranging from 62% (ABS) to 54% (PLA). In terms of cooling COP, Figure 17 shows that the performance of different supporting materials (i.e., aluminum, steel, plastic materials) is quite similar. This result means that higher values of the specific heat for the plastic materials are compensated by the HEx's mass reduction. Such analysis demonstrates that it is possible to employ plastic exchangers without negatively affecting the thermodynamic properties of the adsorber.

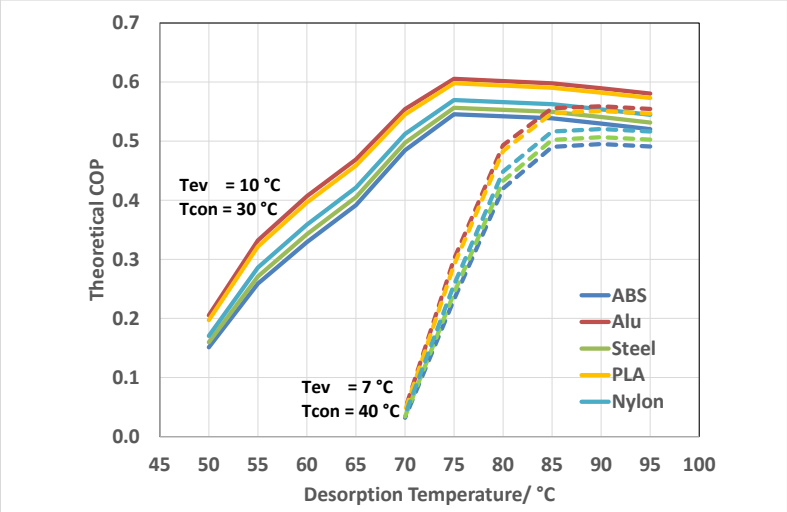

Figure 17 Cooling COP for different materials [5]

The dynamic performance of the plastic adsorbers were experimentally measured by the gravimetric version of the Large Temperature Jump method. This method is commonly considered to be the most appropriate methodology to evaluate the adsorption dynamic for temperature-initiated adsorption heat transformations. Details about the method and the gravimetric version of the Large Temperature Jump method experimental apparatus are reported in the references.

For the cooling boundaries T_e = 10°C, T_c = 30°C, and T_h = 90°C, the plastic adsorbers were able to deliver a maximum specific cooling power of 1.88–2.40 kW/kg of dry sorbent, and the metallic adsorber reached 2.34 kW/kg. Results are also confirmed at different percentages of saturation of the sorbent (63%/80%/90%). This result means that for the tested adsorber configurations, the plastic and metallic HExs were able to deliver an equal SCP, meaning that the overall heat transfer properties of the adsorber are not affected by the lower value of the thermal conductivity of plastic respect to metal (see Table 1).

Table 1 SCP values obtained for all tested HExs' configurations at T_e = 10°C, T_c =30°C, and T_h = 90°C [5]

	SCP max ($k_{80\%}$) (kW/kg)	**SCP 90% (kW/kg)**	**SCP 80% (kW/kg)**	**SCP 63% (kW/kg)**
Aluminum	2.34	0.87	1.24	1.47
ABS	1.88	0.89	1.02	1.46
PLA	2.40	0.93	1.25	1.54

Results showed that both in terms of thermodynamic and dynamic performance, the plastic adsorbers are competitive with metallic ones with a relevant mass reduction and the possibility to manufacture complex geometries by the 3D printing technology (Figure 18). The potential application of plastic material and 3D printing manufacturing will affect the technical and economic feasibility of this cooling technology.

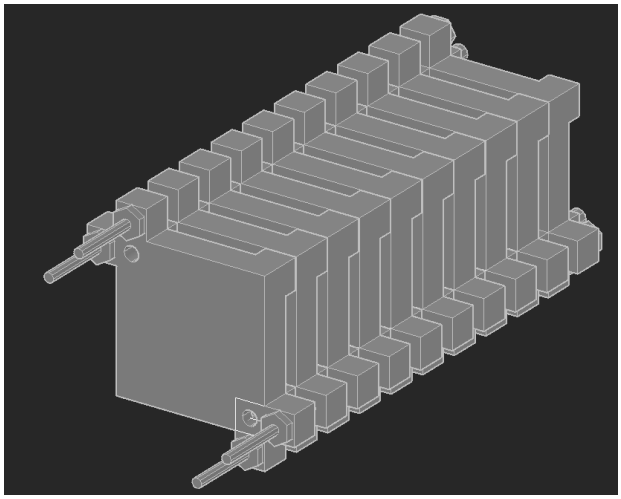

Figure 18 A potential modular complex layout for plastic adsorbers [5]

Key Results: Optimization of the Adsorber's Layout

The aim of the activity was the optimization of several design parameters:

- The HEx's geometry optimization
- Sorbent configuration optimization
- Comparison of different sorbents

Different small-scale adsorber configurations (see Figure 19) have been realized and tested in a lab-scale adsorption chiller (1 kW cooling potential), and their performances were evaluated in terms of specific (SCP) and volumetric cooling power. The following parameters of the design were studied:

- FAM Z02 vs. silica gel
- 3 HExs' geometries
- Coated adsorbers
- Granular adsorbers
- Hybrid adsorbers (coating + grains)

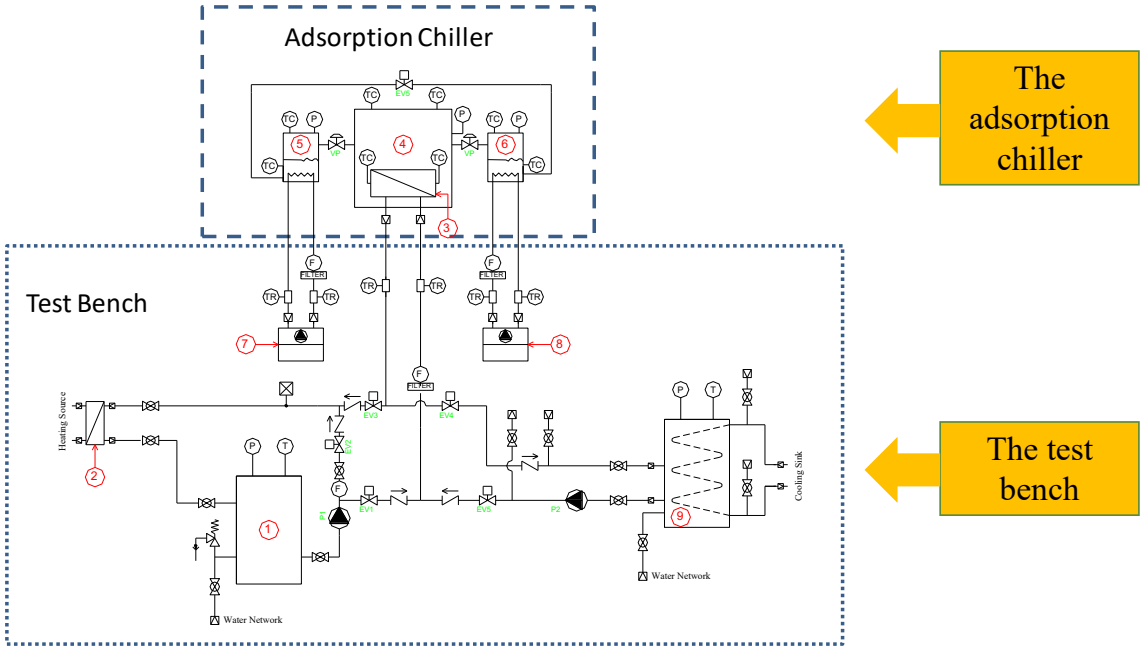

Figure 19 1 kW, single-bed, lab-scale adsorption chiller connected to a test bench

Figure 20 summarizes the main results achieved. In particular, the following conclusions were drawn:

- FAM Z02 is the best sorbent material.
- The coating configuration has a high SCP but low volumetric cooling power.
- The hybrid configuration is the best-performing one.

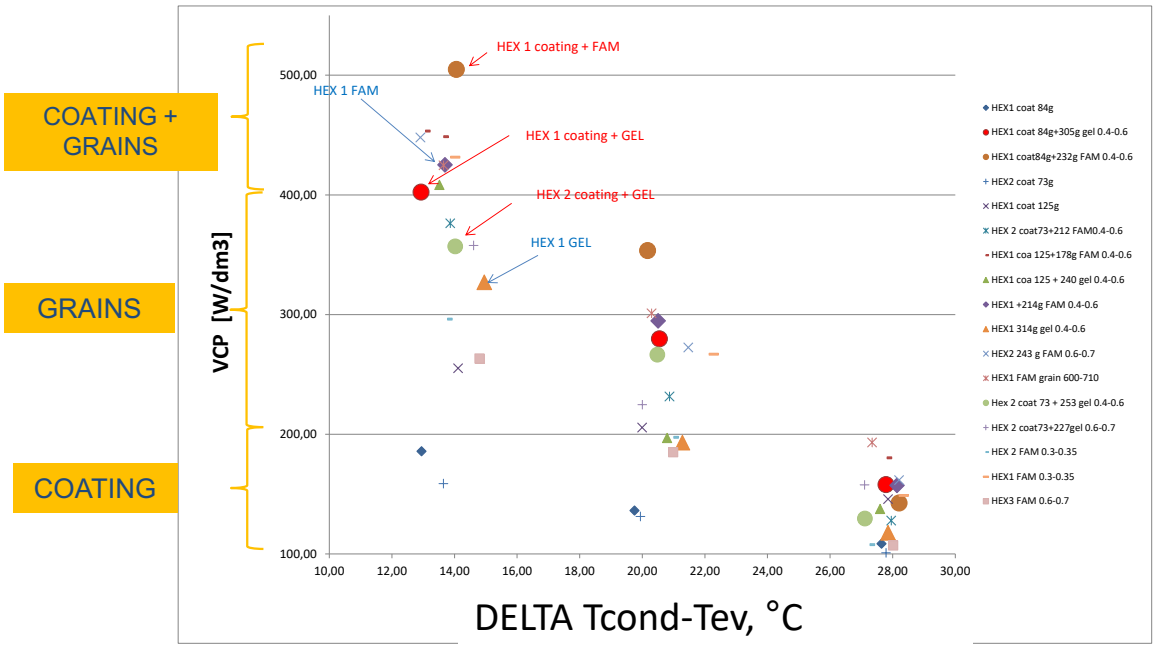

Figure 20 Results of different adsorbent configuration comparison

Relevant Publications

Sapienza, Alessio, Vincenza Brancato, Yuri Aristov, and Salvatore Vasta. 2021. "Plastic heat exchangers for adsorption cooling: thermodynamic and dynamic performance." *Applied Thermal Engineering* 188: 116622.

3.1.5. USA, University of Maryland: Electrochemical Compression (ECC) and Dehumidification (DH)

Lead PIs: Dr. Chunsheng Wang, Dr. Yunho Hwang, and Dr. Reinhard Radermacher

Description

An electrochemical compressor (ECC) is a mass transport device capable of selectively pumping fluids via an electrochemical process without moving mechanical parts. The ECC uses the same ion exchange membranes found in hydrogen fuel cells. However, although fuel cells consume gas to generate electrical potential, the ECC consumes electricity to increase the pressure by moving the working fluid across the membrane without creating any net chemical changes in the working fluid.

Development Status and Plans

The University of Maryland has two ongoing projects related to ECC: electrochemical NH_3 compression and electrohydrodynamic (EHD)-enabled electrochemical dehumidification (DH) (Figure 21).

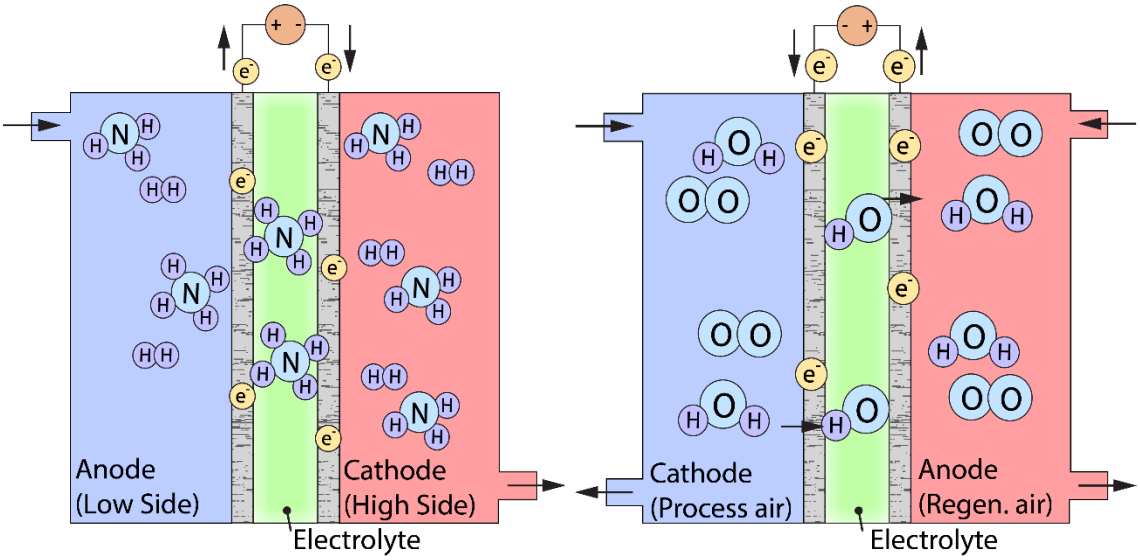

Figure 21 Schematic diagram of (left) NH_3 ECC and (right) EHD-enabled DH processes (courtesy of the University of Maryland)

NH_3 Compression Project

As the world transitions away from fossil fuel energy sources, ECC emerges as a promising low-CO_2 technique for synthesizing NH_3 for energy storage—specifically, energy stored in the form of pressurized NH_3. Liquified NH_3 can also serve as a carbon-free fuel for internal combustion engines. The performance of an NH_3 ECC stack has been experimentally investigated under steady-state operating conditions to demonstrate the technology's utility in such applications. Figure 22 is a photo of the test apparatus used.

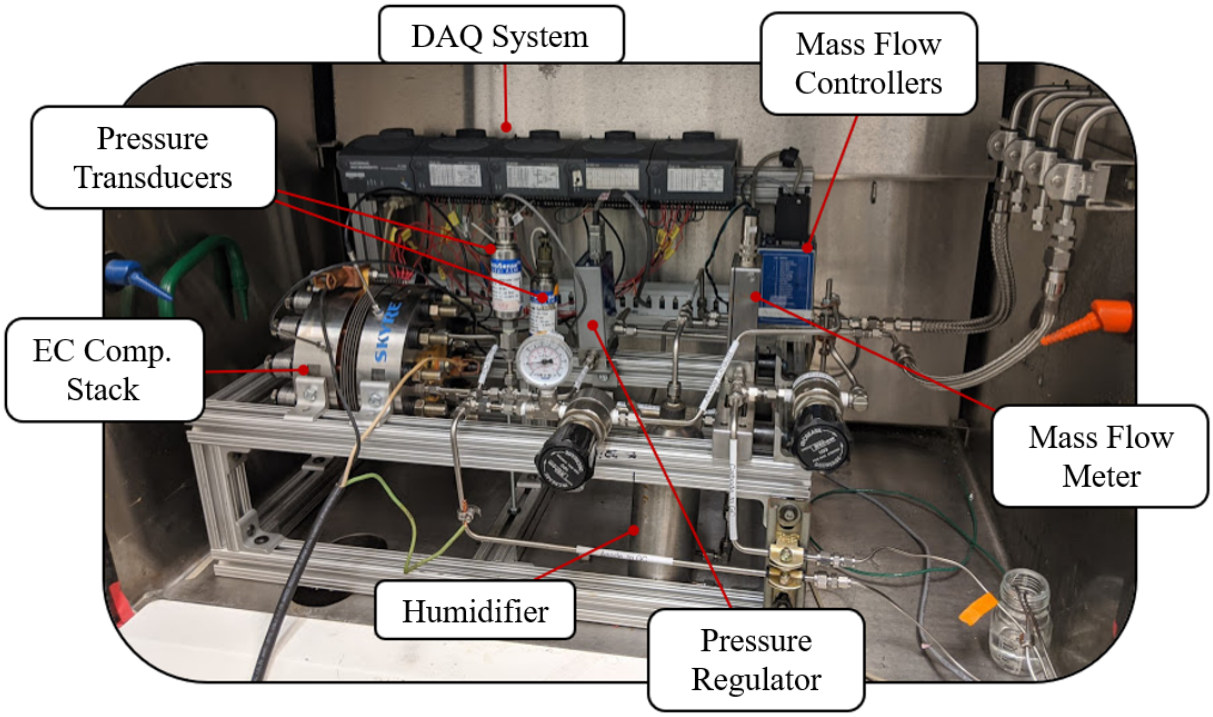

Figure 22 Photograph of the ECC stack test facility (courtesy of the University of Maryland). NOTE: DAQ means data acquisition; and EC means electrochemical in this figure

Using hydrogen as a carrier gas, the effects of pressure and current on the operation of an ECC NH_3 compressor stack were examined. The total voltage increased significantly with increasing current but increased marginally with increasing pressure. Although the lab test device provided useful compression work in all observed cases, back-diffusion of NH_3 hampered the performance, reducing the flow rate of the effluent fluid by as much as 67%. The maximum observed single-cell efficiency was 40% with respect to ideal isentropic compression (Figure 23). Cell efficiency in this work is computed as the electrochemical efficiency of a single cell in the stack as the ratio of the ideal stack voltage to the real voltage. The ohmic losses associated with high current and the back-diffusion effect are likely responsible for the low cell efficiency.

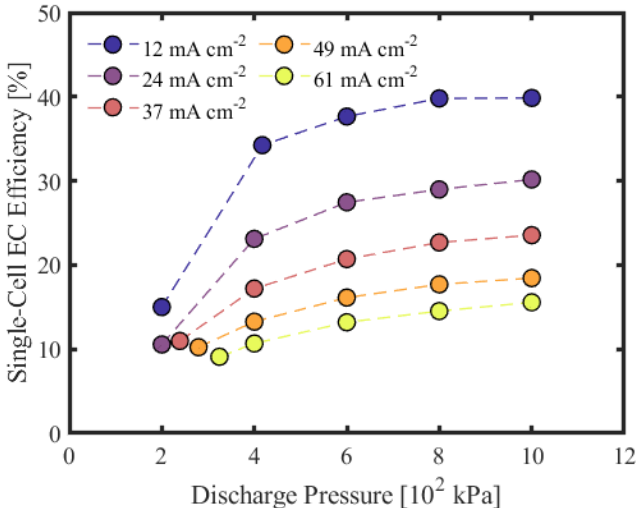

Figure 23 Variation of single-cell ECC efficiency with pressure and current (courtesy of the University of Maryland)

One particular finding concerning isentropic efficiency characteristics of the ECC is illustrated in Figure 24, which compares the isentropic efficiency of the ECC with a commercially available mechanical screw compressor.

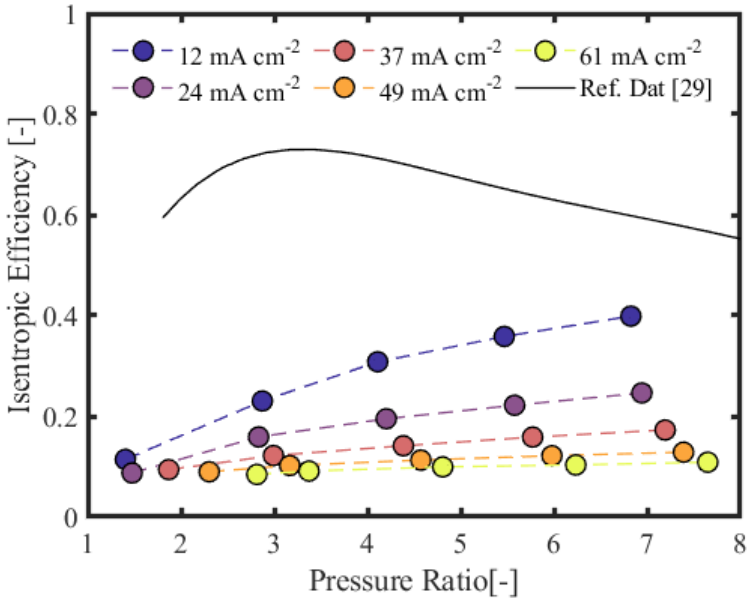

Figure 24 ECC isentropic efficiency (courtesy of the University of Maryland)

Although the ECC efficiency was significantly lower than that of the mechanical compressor, an advantage of the ECC becomes apparent. The ECC's efficiency increased with increasing pressure ratio, and the mechanical compressor's efficiency peaked with a pressure ratio between three and four before then decreasing. Consequently, the ECC may be advantageous for very high-pressure ratios. Conversely, however, the ECC efficiency decreased with increasing current densities because of the higher overpotentials. Because the flow rate is dependent on the current density, the ECC may be less advantageous for high–flow rate applications. A greater membrane area could improve the efficiency for a given flow rate but would increase the cost of the system.

EHD DH Project

Electrochemical DHs and alkaline fuel cells have similar reactions and mass transport mechanisms, so both cells can use the same hydroxide conducting membrane—namely, the anion exchange membrane. This study developed the membrane electrode assembly (MEA) material in-house, built an MEA prototype, and constructed a performance evaluation facility to measure its performance in the lab. The MEA prototype had an active area of 5 cm^2. Figure 25 is a photo of the test bench used.

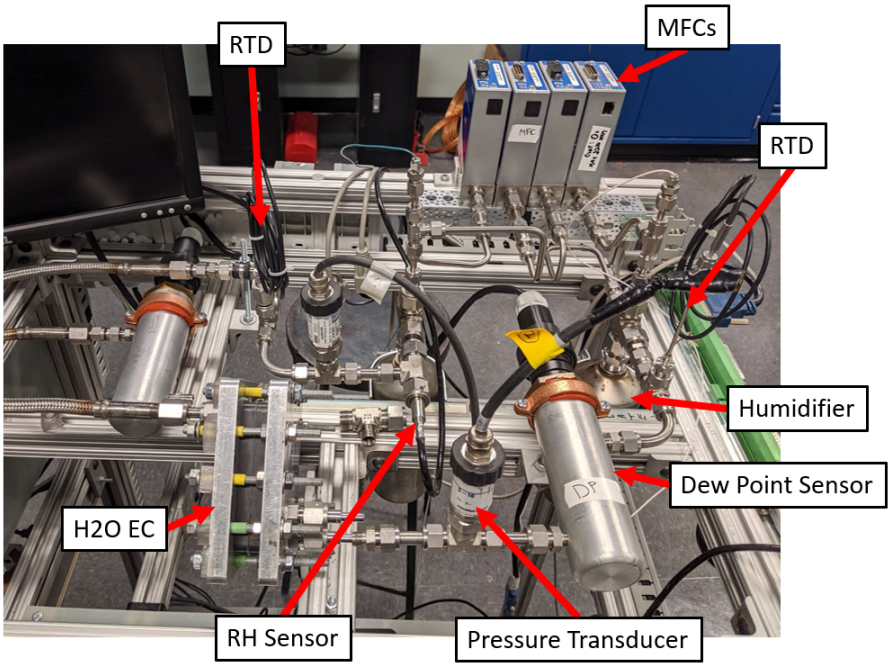

Figure 25 Photograph of the EHD DH facility. EC is electrochemical, RTD is resistance temperature device, and RH is relative humidity. (courtesy of the University of Maryland)

Test results are given in Table 2 comparing results from tests 1–6 [6] and 7–9 [7] with the recent 2022 University of Maryland work (tests 10–12).

Table 2. Comparison of electrochemical DH performance

No.	Electric field (V)	Air inlet of anode side				Air inlet of cathode side				Water removal (g/[day·m^2])	DH efficiency (g/[J·m^2])
		m_a (g/s)	V_a (mL/min)	T (°C)	HR (g/kg)	m_a (g/s)	V_a (mL/min)	T (°C)	HR (g/kg)		
1	3	0.0324	1,502	21.5	14.7	0.0324	1,502	21.5	10.7	4,020	0.0225
2	3	0.0111	516	21.5	14.7	0.0111	516	21.5	10.7	2,539	0.0195
3	3	0.0270	1,251	22.6	13.2	0.0270	1,251	22.9	12.6	2,610	0.0150
4	3	0.0111	516	22.6	13.2	0.0111	516	22.9	12.6	1,975	0.0155
5	3	0.0323	1,497	21.9	11.3	0.0323	1,497	22.3	11.6	2,116	0.0140
6	3	0.0111	516	21.9	11.3	0.0111	516	22.3	11.6	1,622	0.0150
7	3	0.0163	755	19.5	13.4	0.0163	755	19.3	8.6	2,821	0.0190
8	3	0.0113	524	17.7	12.1	0.0113	524	17.4	8.0	2,328	0.0190
9	3	0.0054	250	16.6	11.3	0.0054	250	16.5	8.0	1,693	0.0155
10	3	0.0143	600	20	7.2	0.0143	600	20	8.7	9,700	0.0417
11	2	0.0143	600	20	7.2	0.0143	600	20	8.7	6,900	0.0307
12	2	0.0190	800	20	7.2	0.0190	800	20	8.5	9,300	0.0619

NOTE: HR is humidity ratio

In the tests, the team investigated the role of oxygen flow rate at 600 to 800 mL/min on DH performance while both the cathode and anode relative humidities were maintained at around 50% with the applied potential of 2 V (tests 11 and 12). Test results show that the DH's water removal performance was increased from 6,900 g/(day·m^2) to 9,300 g/(day·m^2) when the dry oxygen flow rate was increased by the enhanced water mass transfer kinetics. The highest electrochemical DH efficiency was achieved in test 12 at 0.0619 g/(J·m^2), which is 175% higher than the previous work. Researchers are planning to scale up the membrane size in future work.

Most Significant Accomplishments

- Electrochemical NH3 compressors are shown to have isentropic efficiency that monotonically increases with discharge in contrast with positive displacement mechanical screw compressors, which show a peak in efficiency and then decrease as discharge pressure continues to increase. Electrochemical compressors may, thus, have an advantage for high–discharge pressure applications.
- The lab test electrochemical DH prototype achieved DH efficiency 175% higher than that shown by previous lab systems.

Most Relevant End-Use Application Areas

- Low-CO_2 technique for synthesizing NH_3 for energy storage and liquid fuel applications

Relevant Publications

Tao, Y., Y. Hwang, R. Radermacher, and C. Wang. 2019. "Experimental study on electrochemical compression of ammonia and carbon dioxide for vapor compression refrigeration system." *International Journal of Refrigeration* 104: 180–188.

Baker, J., L. Cao, C. Wang, Y. Hwang, and R. Radermacher. 2023. "Performance investigation of an electrochemical ammonia compressor stack." *International Journal of Refrigeration* 153: 67–77.

Cao, L., J. Baker, Y. Hwang, R. Radermacher, and C. Wang. 2023. "Development of an electrochemical membrane dehumidifier." *Proceedings of the 2023 International Congress of Refrigeration*.

3.1.6. USA, Oak Ridge National Laboratory: Expansion Loss Reduction Using Rotary Pressure Exchanger

Lead PI: Dr. Brian Fricke

Description

A pressure exchanger (PEx) consists of a cylindrical rotor with an array of channels arranged around the rotor's axis. The rotor spins between two stationary end plates, each of which contains ports for controlling the fluid flow into and out of the rotor channels. Through rotation, the channel ends are periodically exposed to different port pressures, initiating compression and expansion within the rotor channels. Thus, the pressure of a high-pressure stream can be transferred to a low-pressure stream to raise the pressure of the low-pressure stream and reduce the pressure of the high-pressure stream. A cutaway view of a PEx and a rotor are shown in Figure 26.

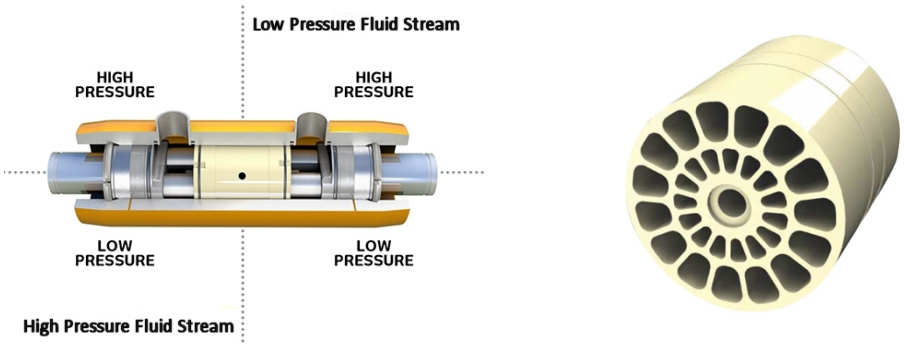

Figure 26 PEx: (a) cutaway view of the PEx, showing (center) the rotor and the inlets and outlets for low-pressure and high-pressure flows, and (b) detail of rotor (courtesy of Energy Recovery Inc., 2017)

PExs have been successfully used in reverse osmosis water desalination applications to provide energy recovery and reduce pumping requirements. This project investigated the application of the technology to VC refrigeration applications and evaluated its potential to enhance efficiency.

Current Development Status and Summary Results

The proposed PEx technology has fundamental resemblance to a HEx. HExs transfer heat energy between two fluid streams, whereas the PEx transfers work energy. PEx performance was initially modeled and simulated using computational fluid dynamics.

Work under this project focused on developing a PEx analytical model and refining the computational fluid dynamics modeling, working with a manufacturer (Energy Recovery Inc. [ERI]) to design and fabricate a prototype PEx suitable for CO_2 refrigeration applications, lab testing the prototype in a laboratory test rig, and finally field testing a PEx in a full-size supermarket in Italy.

Figure 27 illustrates the principal reasons that adding a PEx to a transcritical CO_2 (R-744) system improves its performance. When the PEx refrigerant flow through the compressor is reduced, the total compressor work is also reduced. Additionally, the enthalpy entering the evaporator is decreased, thus increasing the total enthalpy change in the evaporator. Both these effects are amplified at higher ambient heat rejection temperatures.

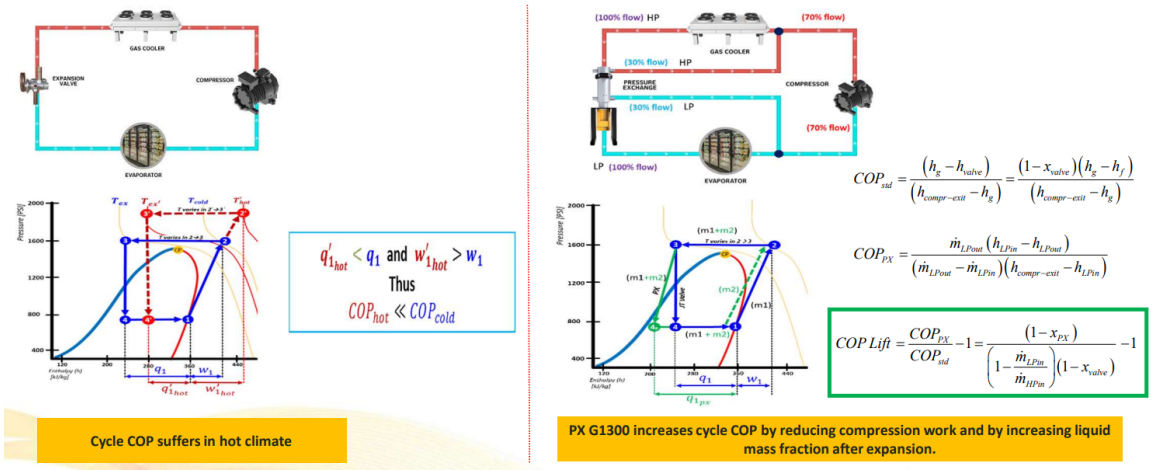

Figure 27 Transcritical CO_2 cycle schematics (right) with and (left) without a PEx component, illustrating reasons for cycle enhancement with the PEx (courtesy of ERI and Oak Ridge National Laboratory from a presentation for May 15, 2023, Annex 53 workshop at the 2023 IEA Heat Pump Conference)

A supermarket system with a 120 kW medium-temperature refrigeration load and 30 kW low-temperature load illustrates the potential benefit of adding a PEx to the system. Figure 28 shows potential energy savings for the PEx-equipped system increasing from approximately 2–3 kW at 10°C gas cooler exit temperature to approximately 75 kW at about 48°C, with the savings

accelerating rapidly as the gas cooler exit temperature reaches 40°C and higher.

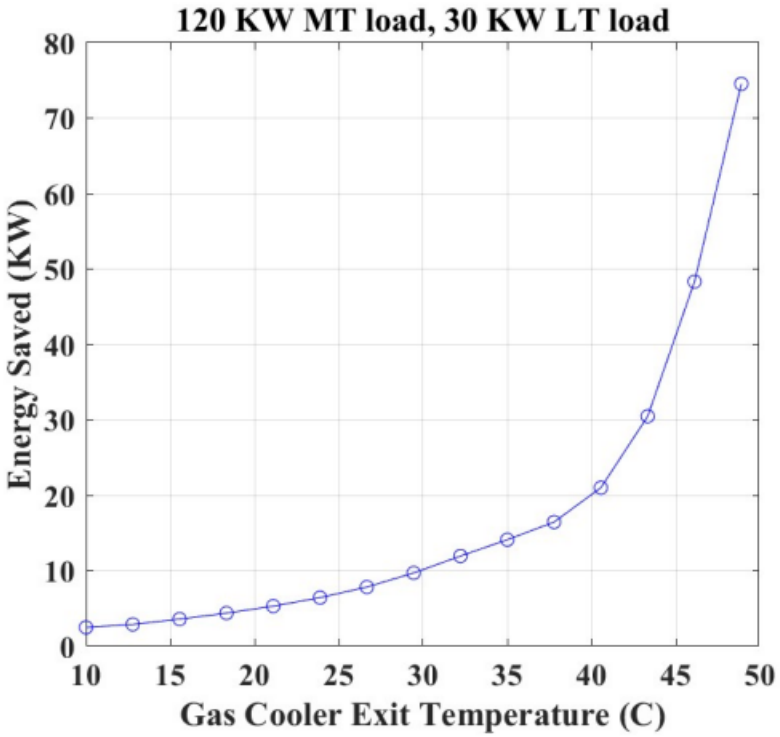

Figure 28 Analytically projected energy savings vs. gas cooler exit temperature for PEx-equipped transcritical CO_2 supermarket refrigeration system over a simple four-component system (courtesy of ERI and Oak Ridge National Laboratory from a presentation for May 15, 2023, Annex 53 workshop at the 2023 IEA Heat Pump Conference)

ERI fabricated a prototype PEx for R-744 application and performed a series of tests in collaboration with Oak Ridge National Laboratory (ORNL) in their laboratory. Figure 29 is a photo of the high- and low-pressure sections of the test loop used with the PEx component installed in the high-pressure section. Note that the loop only included a medium-temperature evaporator load.

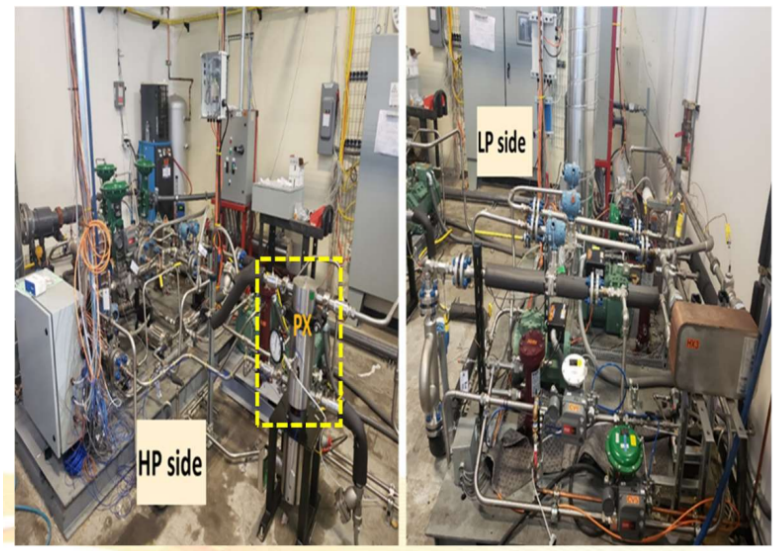

Figure 29 Photo of ERI's test loop with (yellow box) PEx component integrated. HP is high pressure, and LP is low pressure (courtesy of ERI and ORNL from a presentation for May 15, 2023, Annex 53 workshop at the 2023 IEA Heat Pump Conference)

Under a 120 kW medium-temperature load, the PEx-equipped system showed a compressor work reduction of approximately 10 kW, which led to COP increases up to 18% relative to that of a standard baseline transcritical booster refrigeration system (Figure 30). The PEx drive motor power was added to that of the compressor in computing the COP of the PEx-equipped system.COP improvement from the PEx system was damped slightly because of the PEx motor power (estimated at approximately 1%–2% of the compressor motor power).

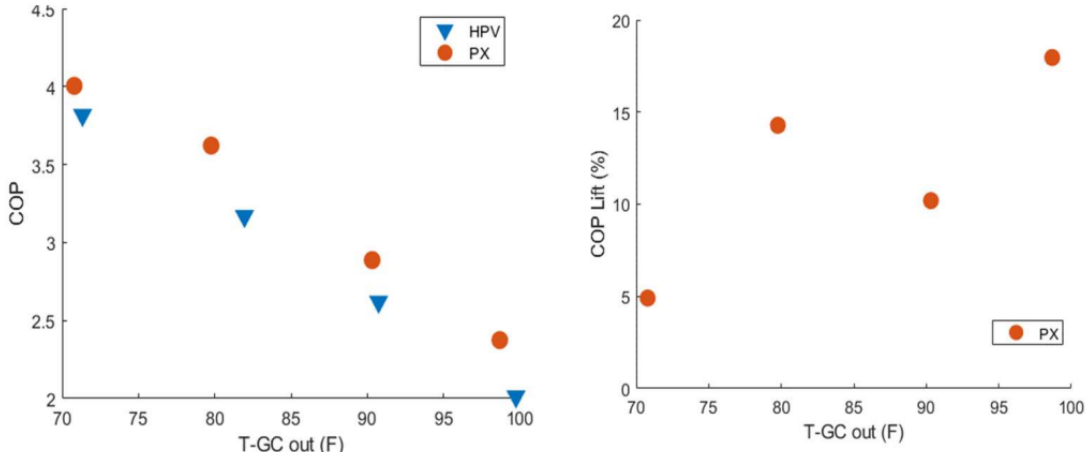

Figure 30 Comparison of measured performance of PEx-equipped transcritical booster CO_2 system with standard baseline booster system (courtesy of ERI and ORNL from a presentation for May 15, 2023, Annex 53 workshop at the 2023 IEA Heat Pump Conference)

Subsequent to the lab evaluations, a PEx component was integrated into in the CO_2 refrigeration system of a 1,500 m^2 supermarket located in northern Italy. The system had 135 kW of medium-temperature refrigeration load and 30 kW of low-temperature load. Performance measurements, presented in Figure 31, showed a 27% COP boost (including the effect of the PEx component drive motor).

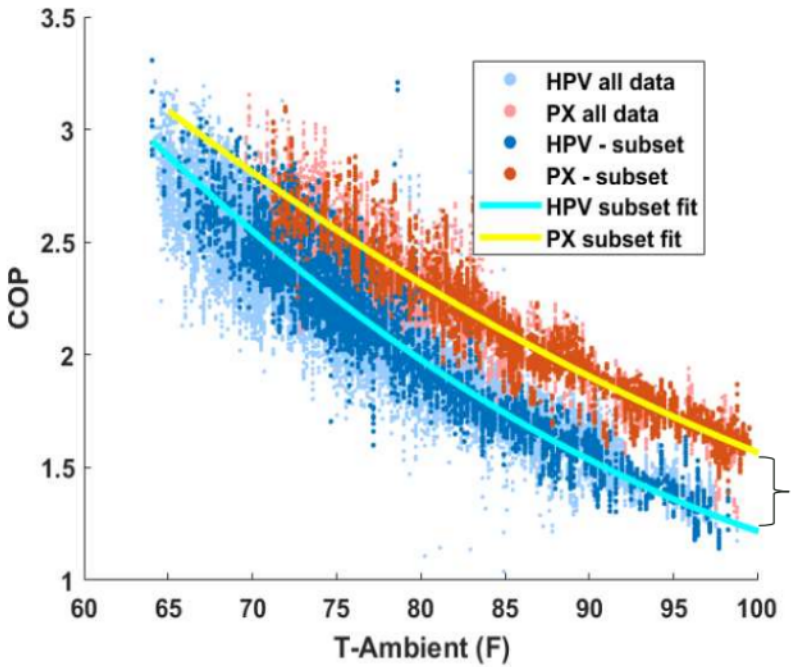

Figure 31 COP vs. ambient temperature results from PEx system field test in northern Italy (courtesy of Azam Thatte, ERI, and Brian Fricke, ORNL, from a presentation for May 15, 2023, Annex 53 workshop at the 2023 IEA Heat Pump Conference)

Most Significant Accomplishments

- Field tests of a PEx component integrated into the CO2 transcritical refrigeration system of a supermarket in northern Italy demonstrated COP improvements up to 27% under high–ambient temperature operation.
- Analytical projections for PEx-equipped HP systems show up to 30% efficiency boost.

Most Relevant End-Use Application Areas

- Supermarket refrigeration and industrial or space conditioning HPs
- Other potential applications include the following:
  - Thermal energy storage for renewable generation systems
  - Thermal energy storage for waste heat recovery and temperature boost
  - Reducing levelized cost of energy of geothermal power generation

Follow-On Work Priorities

- Investigate application of PEx to high-temperature HPs using CO_2 refrigerant

Relevant Publications

Sarawate, N., A. Thatte, and O. Samudrala. 2023. "Novel architectures for transcritical CO_2 refrigeration cycle using rotary pressure exchanger." *Proceedings of the ASME Turbo Expo 2023: Turbomachinery Technical Conference and Exposition* 5: Cycle Innovations, June 26–30, 2023, Boston, Massachusetts.

Thatte, A., and B. A. Fricke. 2022. "New types of low global warming, energy efficient refrigeration architectures using a trans-critical rotary pressure exchanger." *ASHRAE Transactions* 128, no. Part 2: 360–368.

Saeed, M. Z., A. Hafner, A. Thatte, and C. H. Gabrielli. 2022. "Simultaneous implementation of rotary pressure exchanger and ejectors for CO_2 refrigeration system." 15th IIR-Gustav Lorentzen Conference on Natural Refrigerants, June 13–15, 2022, Trondheim, Norway.

Elatar, A., B. Fricke, V. Sharm, and K. Nawaz. 2021. "Pressure exchanger for energy recovery in trans-critical CO_2 refrigeration system." *Energies* 14, no. 6.

Fricke, B., K. Nawaz, A. Elatar, and V. Sharma. 2019. "Increasing the efficiency of a carbon dioxide refrigeration system using a pressure exchanger." International Congress of Refrigeration, August 24–30, 2019, Montréal, Canada.

Elatar, A., B, Fricke, K. Nawaz, and V. Sharma. 2019. "Modeling of Pressure Exchanger for Energy Recovery on Trans-Critical CO_2 Refrigeration Cycle." International Mechanical Engineering Congress and Exposition, November 11–14, 2019, Salt Lake City, Utah.

3.2. Nontraditional Technology-Based Project Descriptions

3.2.1. USA, University of Maryland: Multi-Mode Elastocaloric (EC) Cooling

Lead PIs: Dr. Ichiro Takeuchi, Dr. Yunho Hwang, and Dr. Reinhard Radermacher

Among zero-GWP, nonflammable, and nontoxic alternatives to vapor compression, caloric cooling (and heating), which uses field-driven phase transitions in solids, has emerged as a potential frontrunner because of its intrinsically high energy conversion efficiency. Caloric materials include magnetocaloric (MC), electrocaloric, and mechanocaloric materials. MC materials and devices have been explored for almost 50 years, and refrigeration systems with kilowatt-range cooling power have been demonstrated. Their high magnetic field requirement (>1 T) has, however, hampered commercialization of MC cooling technology.

Mechanocaloric cooling is driven by mechanical stress, and reflecting the diversity of ways in which materials can be subjected to stress, it can be induced by uniaxial stress (EC), torsional stress (twistocaloric), bending stress (flexocaloric), or hydrostatic pressure (barocaloric). Owing to the large intrinsic material temperature lifts of EC materials, EC cooling devices represent some of the most promising caloric technologies. Figure 32 illustrates a typical EC material cycle between loading and unloading the material. The total temperature span in this example is approximately 16 K.

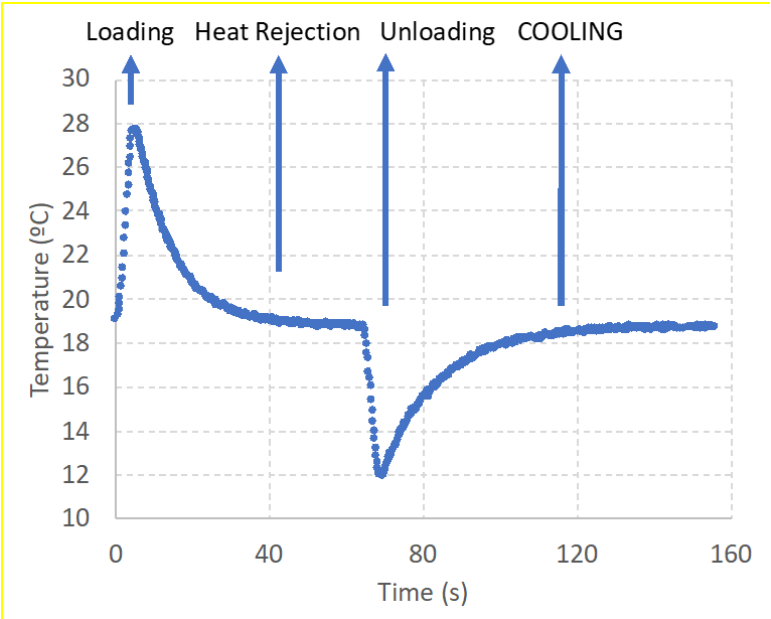

Figure 32 Temperature variation during Nitinol loading and unloading

Compared with MC and electrocaloric counterparts, which usually require large fields, practical actuators can be implemented for driving EC devices. Most EC devices are based on superelastic (SE) shape memory alloys (SMA), but prototypes using polymers have also been reported. To date, the largest adiabatic temperature lifts ($\Delta T_{adiabatic}$) recorded from direct measurements on *any* caloric material under a practical range of fields are from EC materials, including Ni–Mn–Ti and Ni–Ti, which displayed material $\Delta T_{adiabatic}$ of 31.5 K and 38.5 K, respectively.

Some of the successful caloric cooling prototypes are based on active regeneration schemes, which are used to boost the temperature span across the devices from limited adiabatic temperature changes of caloric materials—in particular, MC and electrocaloric materials. Because the adiabatic temperature change of EC materials can exceed 20 K, non-regenerative, single-stage EC systems are viable for applications such as ACs or refrigerators. Single-stage operation is characterized by a uniform temperature inside materials at any stage of each cycle, which is facilitated by a large utilization factor (percentage of heat exchange medium, which is displaced during each cycle), allowing the majority of the caloric effect to be

directly transferred from the refrigerant materials to the heat sink and heat source. Examples of single-stage EC systems are tensile prototypes using Ti–Ni sheets or wires based on a solid-to-solid contact heat exchange mechanism, compressive prototypes using Ni–Ti tubes incorporating various heat transfer fluid schemes, and the biaxial stretching prototype using rubber membranes.

To enhance the temperature span of EC prototypes, cascading multiple single-stage schemes has been experimentally demonstrated in a four-stage device with a 27 K temperature span and a three-stage, fluid-based device using Ni–Ti wires. Active regeneration has also recently been successfully implemented for EC cooling with a temperature span close to 20 K and 31.3 K with 60 W cooling power. Unlike single-stage operation, active regeneration is characterized by a large temperature gradient across the caloric material at any phase of each cycle, where a small utilization factor is essential to maintain the enhanced temperature gradient. Nonetheless, the enhanced temperature span in active regenerators comes at a cost of a significant portion of the sensible heat remaining inside the regenerator to establish and sustain the temperature span.

To capture the best aspects of the active regeneration cycle, as well as the large utilization operation, in a single practical prototype, this work has developed a multimode EC cooling system leveraging the large temperature span of the active regeneration mode [Figure 33(A)] and the efficient cooling of the maximum utilization mode [Figure 33(B)]. In the prototype, the two modes can be easily switched from one to the other by controlling the operation sequences of valves in the heat exchange fluid network.

The deviatoric stress state associated with the phase transformation in EC materials needs to be taken into account to design the field actuation and the cycle lifetime in EC systems. This work used the uniaxial stress—the simplest deviatoric stress state—realized by the compressive or tensile actuation to implement in EC cooling prototypes. Although compressive and tensile loadings can give rise to similar EC effects, the compressive actuation can hinder the advancing of cracks, significantly extending the lifetime of the materials. There have been reports of EC materials enduring over 10 million cycles in compression modes. With 0.1 Hz operation for a usage modality of 12 h/day and 180 days/year, 10 million cycles corresponds to 12.8 years, which is beyond an accepted lifetime of a commercial appliance. Thus, this study enlisted compressive actuation in the multimode EC cooling systems. The ideal geometry of the EC materials not only exhibits robust mechanical integrity under cyclic compression but is also conducive to heat exchange between the material and the heat-transfer fluid. To this end, this study has designed these systems around readily available Ni–Ti tubes, which can be configured into a bundle for relative ease of compression, as well as for flowing heat-exchange fluid in the uniaxial direction. This EC system consisting of four bundles of Ni–Ti tubes can deliver up to 260 W in delivered useful cooling (measured against heat load) operating in the maximum utilization mode, the largest reported cooling power for EC devices to date, and a temperature span of 22.5 K in the active regeneration mode. With such high-performance characteristics, this EC system rivals some of the best reported MC systems.

Nineteen Ni–Ti tubes are packed in a hexagonal bundle configuration and surrounded by a layer of stainless steel tubes, which prevent the Ni–Ti tubes from coming in direct contact with a bundle holder sleeve. The holder is necessary to circumvent buckling of the tubes, and the stainless steel tubes work to minimize the friction that the outer Ni–Ti tubes experience during compression [Figure 33(C)]. Each Ni–Ti tube bundle is compressed in the axial direction by two loading heads. The loading heads also serve as a fluid manifold to evenly disperse the heat exchange fluid into the 19 Ni-Ti tubes, and the profile of the flow channel inside the loading heads has been optimized based on the simulated streamline. To enhance the heat exchange efficiency between the fluid and the Ni–Ti tubes, triangle polymer inserts are placed inside each Ni–Ti tube to block 40% of the cross-sectional area.

The current multimode EC cooling system consists of two sets of two (paired) bundles of Ni–Ti tubes. For simplicity, this report only shows one pair of tube bundles in Figure 33(A) and 33(B), denoted as *Bundle 1* and *Bundle 2*. The two paired bundles are operated at a half-cycle out of phase with each other to achieve work recovery, where compression of one bundle is always assisted by the unloading force of the other, to achieve high-efficiency operation.

In the active regeneration mode and the maximum utilization mode, the two paired bundles of Ni–Ti tubes are cycled in four major steps: (1) the actuator compresses one bundle and unloads the other bundle adiabatically without flowing any fluid, (2) the first bundle rejects heat to the heat exchange fluid while the second bundle absorbs heat from the fluid and provides cooling, (3) the actuator unloads the first bundle and compresses the second bundle adiabatically, and finally (4) the first bundle cools the heat exchange fluid while the second bundle rejects heat to the fluid.

The major difference between the two modes is in the details of the heat exchange processes. When a large temperature span is desired (for instance, for air DH or for HP applications), the heat exchange fluid network is operated in such a way that each bundle of Ni–Ti tubes is simultaneously connected to the heat sink and the heat source, to which cooling is delivered [Figure 33(A)]. This process is the active regeneration mode, where a unidirectional fluid network is implemented to minimize dead fluid volume. In this mode, the displaced fluid volume is less than the fluid volume inside the Ni–Ti tubes, and only a portion of the latent heat from the Ni–Ti tubes is pumped to the heat sink and the heat source. The majority of the latent heat remains inside the Ni–Ti tubes to accumulate the fluid temperature before the fluid exits the Ni–Ti tubes during heat rejection and lowers the fluid temperature during the cooling process. A temperature gradient along the flow direction can be sustained to establish a large temperature span, as has been applied in MC cooling systems for decades.

Maximum utilization mode can be implemented when a relatively large cooling power is required (e.g., during the initial turn-on process for an AC or a refrigerator). The maximum utilization mode features at least a tenfold increase in displaced fluid volume compared with the active regenerator mode, leading to a homogeneous temperature distribution inside the Ni–Ti tubes, and most of the latent heat could be extracted and used in the heat sink and the heat source. To fully displace the remnant fluid inside the Ni–Ti tubes, the valves are switched so that the first bundle is only connected to the heat source when the Ni–Ti tubes are unloaded, while the second bundle is connected to the heat sink after it is loaded [Figure 33(B)]. In the maximum utilization mode, heat recovery by exchanging heat between the two paired bundles can be applied to precool the first bundle before unloading and preheat the second bundle before loading, which adds an additional two steps to the cycle.

Any refrigeration device has a trade-off between the cooling power and the temperature span. This trade-off exists because the total sum of the cooling power and the cooling effect that sustains the temperature span remains constant according to the first law of thermodynamics. Such a trade-off is captured in the Pareto front curve on the power–ΔT diagram. In this multimode EC cooling system, the maximum utilization mode has delivered 260 W at 1.9 K at one end and ΔT of 8 K at the other end of the performance Pareto front [Figure 34(A)]. The 260 W result is the largest delivered cooling power (measured against real heat load) of any reported EC cooling systems to date, and in future systems, this value can be boosted by simply increasing the amount of Ni–Ti material or implementing a different material with a larger latent heat.

On the other hand, in the active regenerator mode, ΔT as large as 22.5 K was achieved [Figure 34(B)]. The 22.5 K temperature span is larger than the material's adiabatic temperature change of 11 K at the strain level of 3.5%, resulting in a regeneration factor of 1.8 that illustrates the effectiveness of active regeneration. By combining the maximum utilization mode and the active regeneration mode, an *integrated* Pareto front can be attained, which expands the performance domain in the power–ΔT diagram, superseding the Pareto front of each respective mode alone.

The key controlling factor that bridges the two modes is the utilization factor, which determines the percentage of heat exchange fluid that is displaced during each cycle. The optimum

utilization factor controls the competition between the latent heat to be extracted from the Ni–Ti tubes and the EC effect that maintains the temperature gradient in the active regeneration and the passive regenerator (in the maximum utilization mode) [Figure 34(C)]. Such strong dependence of the overall performance of these devices on the utilization factor is consistent with previous reports on EC and MC active regenerators. This multimode EC cooling system has successfully extended the range of the optimum utilization factor from less than one in the active regeneration mode to more than six in the maximum utilization mode, adding flexibility in operations and, thus, applications of the EC cooling system.

Several measures can be introduced to further improve the performance of the current system. One measure is to further reduce the fluid-to-solid thermal mass ratio inside the Ni–Ti tubes by varying the geometries of the inserts. Improved heat transfer is expected in Ni–Ti tubes with an increased blocked area because the heat transfer in the boundary layer becomes more efficient and the thermal inertia of the fluid is reduced. The numerical model in this study shows that compared with the current triangle-shaped inserts, by going to circular-rod inserts with 82% blockage of the flow channel in each Ni–Ti tube, a 65% increase can be expected in cooling power at a zero temperature span in the maximum utilization mode [Figure 34(D)]. Also, increasing the cycle frequency of the active regeneration mode can directly enhance the cooling power. For instance, by going from the current frequency of 0.071 Hz to 0.125 Hz, the power can be enhanced by a factor of 1.2.

The multimode EC cooling concept demonstrated here can be further extended to cascading multiple bundles of Ni–Ti tubes so that variations in the modes can be implemented. For instance, cascading two bundles at active regeneration mode or maximum utilization mode, which is expected to help fill the performance gap in Figure 34(A), can realize a smooth transition between the two modes. Operating and switching multiple bundles of Ni–Ti tubes to operate in different modes can facilitate high-efficiency performance in a wide range of working conditions. This work suggests that such versatility is the key to the successful commercialization of this zero-GWP technology. In the future, the researchers also expect to be able to implement copper-based EC materials, which require much smaller stress compared with Ni–Ti, enabling higher-efficiency system operation with smaller actuators.

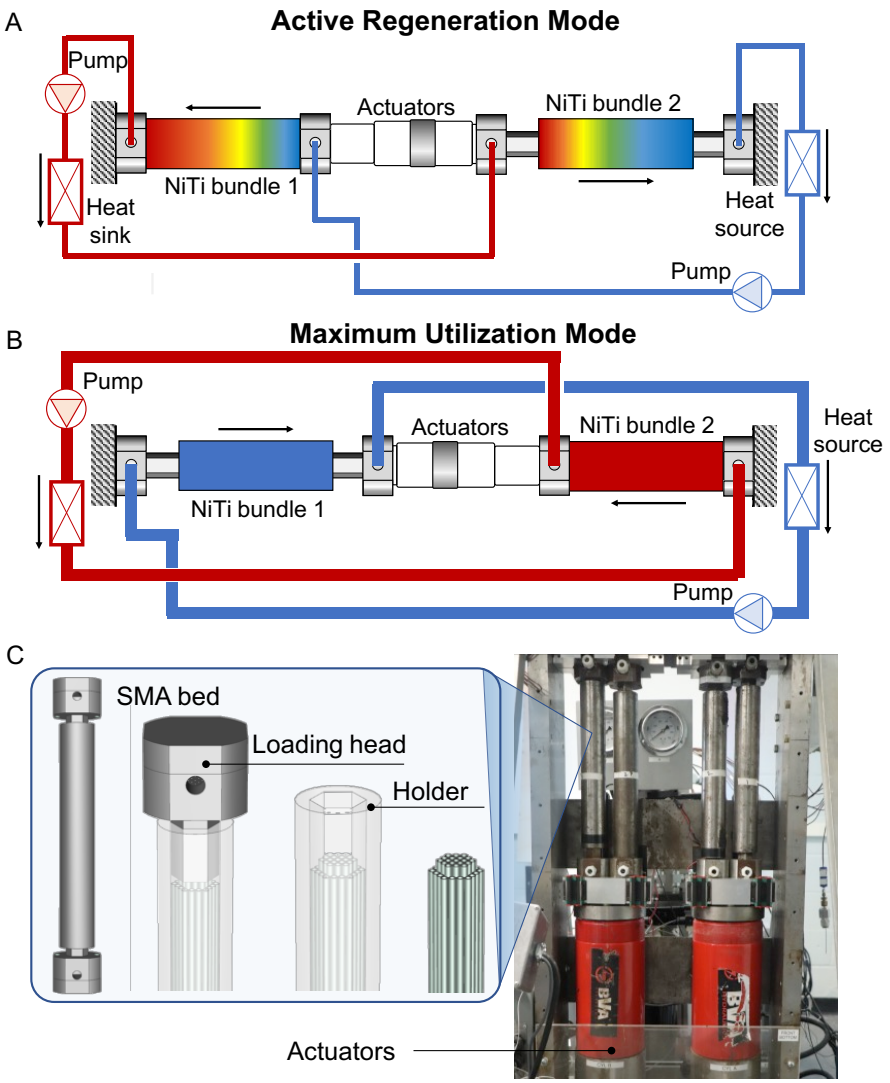

Figure 33 System design schematics and operating principles of the multimode EC cooling system. (A) Active regeneration mode for achieving a large temperature span, which develops across each Ni–Ti bundle located inside a tube assembly. The snapshot represents the phase of the cycle where Bundle 1 is being compressed, and heat exchange fluid flows from the cold end of the bundle toward the hot end, while at the same time, Bundle 2 is being unloaded, and fluid flows from the hot end of the bundle to the cold end. (B) Maximum utilization mode (which provides enhanced cooling power as indicated by the complete extraction of EC effect in both bundles with uniform temperature) is at the phase of the cycle when Bundle 2 is being compressed, and the bundle is connected to the heat sink fluid circuit, while the other bundle is unloaded and connected to the heat source fluid circuit. Note that for both modes, compression work done to one bundle by an actuator in the middle is always assisted by synchronized unloading in the other bundle, achieving work recovery. (C) Photo of the central part of the multimode EC cooling system, which stands at 0.3 × 0.8 m with 1.3 m in height, with detailed schematics of the Ni–Ti tube assembly. From left to right: completed assembly with loading heads on both ends; loading head compresses on Ni–Ti tubes; complete bundle inside the holder; 19 Ni–Ti tubes in a bundle are surrounded by 18 shorter and flexible stainless tubes, shielding Ni–Ti from coming in direct contact with holder wall. Heat exchange fluid flows inside each Ni–Ti tube.

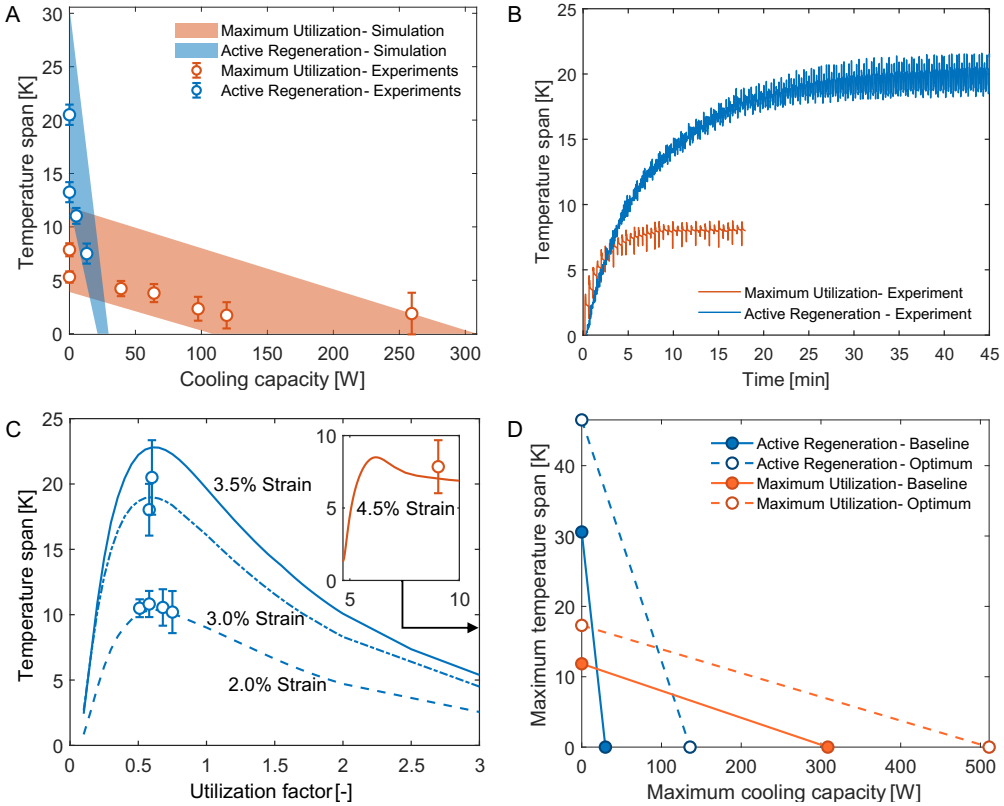

Figure 34 Performance of the multimode EC cooling system. (A) Temperature span vs. cooling power for the (blue colored data) active regenerator mode and the (orange colored data) maximum utilization mode. The data points are experimentally measured values (error bars represent the measured range within one cycle plus the equipment uncertainty), and the shaded regions are ranges observed in simulations taking into account various heat leak coefficients. For the active regeneration mode and maximum utilization model, the Ni–Ti tubes are compressed to 3.5% and 4.5%, respectively, for loading. (B) The evolution of the temperature span occurs as a function of time. For the maximum utilization mode, the saturation temperature span of 8 K is reached after 10 min and 20 cycles. The active regenerator mode takes longer to saturate, but the final temperature span is much larger, and it is approximately 22.5 K. (C) Temperature span as a function of the utilization factor. The blue curves are simulation data at three different strains for the active regenerator mode, where the temperature span peaks sharply for all three tested strains where the utilization factor is 0.6, accompanied by the experimental data points. The orange curve (simulation) and the experimental data point are for the maximum utilization mode. (D) Expected performance enhancement upon implementing various inserts inside Ni–Ti tubes for promoting heat exchange. Blue solid line and dashed line are the performance of active regeneration mode with baseline insertion and optimized insertion, respectively. Orange solid line and dashed line are the performance of maximum utilization mode with baseline insertion and optimized insertion, respectively.

Most Significant Accomplishments

A 260 W EC cooling prototype has been developed. This prototype is the largest-power caloric system outside of reported MC systems and indicates that the EC technology is rapidly maturing.

Most Relevant End Use Application Areas

Because 100 W scale cooling is still modest in delivered wattage, initial applications will be small-scale refrigerators such as wine coolers. As more prototypes are successfully built, the plan is to move on to larger-scale and other applications, including regular-size residential refrigerators and small AC units.

Follow-On Work Priorities

The goal is to develop higher-power EC systems. This work is also exploring new materials so that smaller-footprint actuators can be implemented as drivers.

Relevant Publications

Emaikwu, N., D. Catalini, J. Muehlbauer, I. Takeuchi, R. Radermacher, and Y. Hwang. 2019. "Development of a cascade active elastocaloric regenerator." American Society of Mechanical Engineers 2019 ES 13th International Conference on Energy Sustainability Co-Located with the Summer Heat Transfer Conference.

Qian, Suxin, David Catalini, Jan Muehlbauer, Boyang Liu, Het Kiritbhai Mevada, Huilong Hou, Jun Cui, Yunho Hwang, Reinhard Radermacher, and Ichiro Takeuchi. 2023. "High-performance multi-mode elastocaloric cooling systems." *Science* 370: 722–727.

3.2.2. China, Xi'an Jiao Tong University: Elastocaloric (EC) Cooling

Lead PI: Dr. Suxin Qian

Accomplishments

EC cooling uses the temperature change when applying uniaxial stress to a solid material. In SMAs, sufficient stress leads to the martensitic phase transition that releases significant latent heat for cooling. EC cooling prototypes have been developed for almost 10 years since their invention at the University of Maryland. This project explored the potential performance of EC prototypes for two applications: compact refrigerators for wine and beverages and solar heat–driven AC.

Mechanical-Driven EC Refrigerator

This work developed an EC refrigerator prototype using Nitinol (Ni–Ti) wires as the refrigerant. As shown in Figure 35, 18 0.7 mm $Ni_{38.8}$–$Ti_{61.2}$ wires were pulled by a single linear actuator at an inclined angle, such that when the actuator pulls the Ni–Ti wires, the wires transform to martensite and reject the latent heat to the heat sink on the left, and when the actuator releases the force, the wires transform back to austenite and absorb heat from the refrigerated cabinet on the right. The single motor was specifically tuned to operate at large torque and slow speed (less than 600 rpm) so that no gearbox was needed. Although the Ni–Ti wires were horizontally mounted in the initial design, the second-generation design changed it to the vertical arrangement to minimize the effects of gravity, and the system could operate more smoothly.

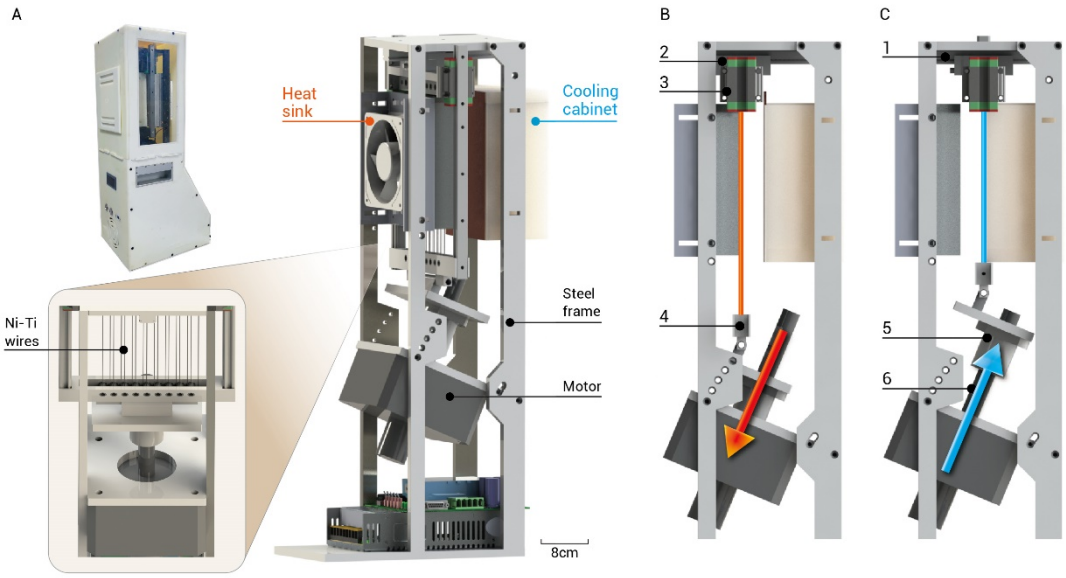

Figure 35 Illustration of the EC refrigerator prototype (second generation). (A) Photo of the refrigerator. (B) Illustration of the Ni–Ti wires releasing heat to the heat sink. (C) Illustration of the Ni–Ti wires cooling the heat source

In Figure 36, at 4.8% strain (8.0% for full transformation), the second-generation prototype achieved an optimum frequency in terms of a temperature span at 0.152 Hz (2.5 s for heat exchange with the hot-side radiator and cold-side radiator and 0.8 s for loading and unloading). At this optimum frequency, when the fan on the heat sink was turned off, the system reached a 9.2 K temperature span after 170 cycles. This temperature span was close to the theoretical limit because the adiabatic temperature change of the Ni–Ti wire was 7.8 K upon loading and 6.6 K upon unloading. When the fan on the heat sink was turned on, the temperature of the cold-side HEx (to transfer heat from the refrigerated cabinet to Ni–Ti wires) became 5.8 K lower than the ambient temperature. The cooling power at the cold-side HEx was measured by an electric heater. The system achieved the maximum 3.1 W cooling power when the temperature span was zero.

The system performance was less than expected because of the insufficient heat exchange area of the Ni–Ti wires when they touch the hot-side and cold-side HExs. To increase the contact heat transfer area, this work developed a third-generation prototype using Ni–Ti plates instead of Ni–Ti wires. Using the experimentally validated numerical model, this study numerically demonstrated that the prototype could operate at 0.36 Hz as the optimum frequency when using a 0.1 mm Ni–Ti plate, which resulted in the maximum cooling power of 14.4 W using the same linear actuator as the driver. Once the prototype magnetic SMA Ni–Mn–Ti–B becomes available in large quantities in the future, this work predicts a maximum of 11.7 W cooling power and a maximum of 24 K system temperature span, as well as a system COP of 1.9 when the ambient temperature is 32°C and the refrigerated temperature is 12.8°C. This performance already surpassed thermoelectric wine refrigerators, where a typical wine refrigerator's COP was approximately 0.3–0.5 (tested in the lab). The COP of a high-efficiency, VC-based, commercially available wine refrigerator was measured to be 1.5 to 1.8. Thus, the EC refrigerator has a potentially higher efficiency than current VC-based refrigerators, as well.

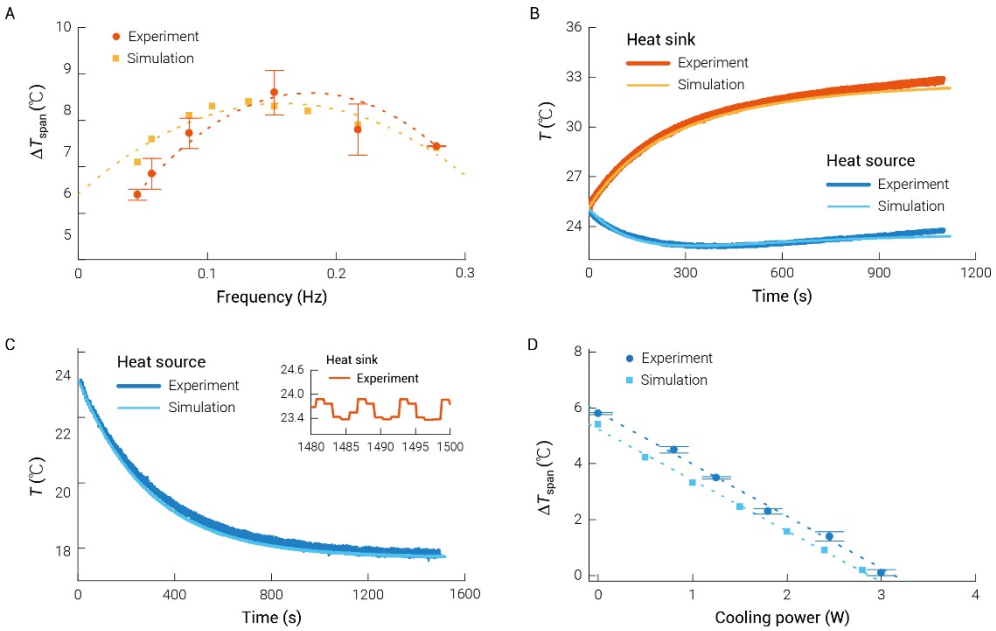

Figure 36 Measured performance of the EC refrigerator. (A) Temperature span ΔT_{span} at different frequencies when both HExs are adiabatic. (B) Temperature evolution of the hot-side radiator (heat sink) and cold-side radiator (heat source). (C) Temperature evolution of the cold-side radiator when the hot-side radiator (heat sink) is actively cooled and the cold-side radiator is adiabatic. (D) Performance map of the EC refrigerator

The third-generation prototype was based on the two-stage cascade configuration (Figure 37). In the configuration shown in Figure 37, the two Ni–Ti plates are synchronized, and another antagonistic design was also under development to achieve work recovery. In Figure 37, the Ni–Ti plate on the left is the low-temperature stage, which cools the refrigerated cabinet and rejects heat to the intermediate HEx. The high-temperature stage absorbs heat from the intermediate HEx and rejects heat to a higher temperature (i.e., ambient). The two-stage, third-generation prototype facilitates a higher temperature span. This work measured a 15.4 K, adiabatic, no-load temperature span in the two-stage configuration, or alternatively, the refrigerated cabinet can be cooled 12 K below the ambient temperature. These numbers represent a more than 70% improvement compared with the single-stage prototype, indicating good functionality of the cascading design. The performance is not optimized yet, and researchers are still conducting more comprehensive tests.

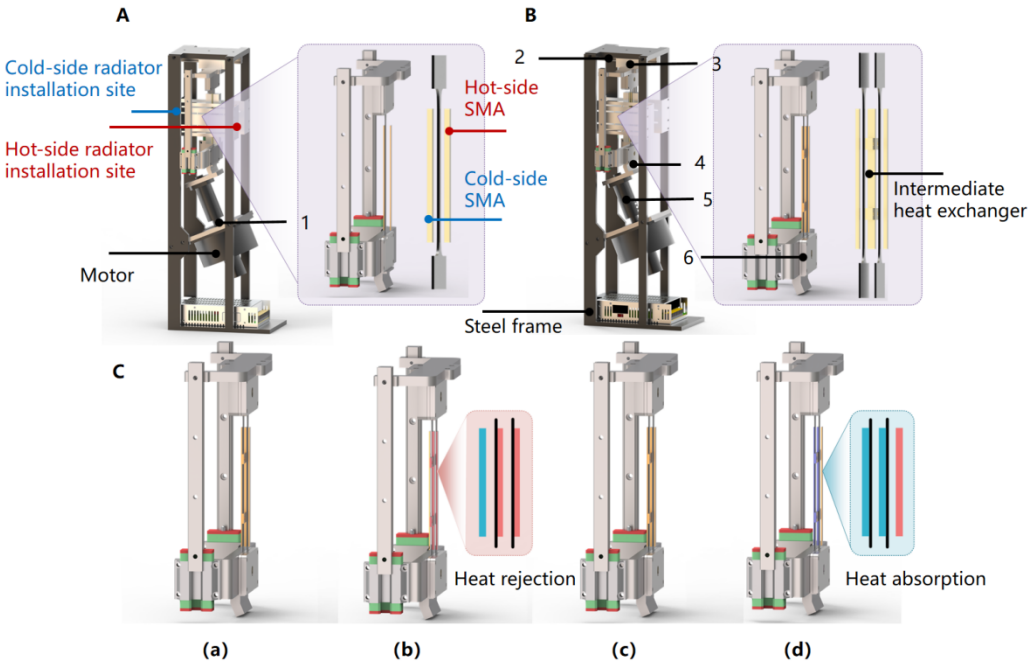

Figure 37 Illustration of the third-generation EC refrigerator. (A) Side view of the single-stage EC device using Ni–Ti plate. (B) Side view of the two-stage EC device using two Ni–Ti plates cascaded by an intermediate HEx. (C) Operating principle with four steps.

Six prototypes were developed and have been extensively tested by the study's researchers and collaborators at another institute. The Ni–Ti wires and Ni–Ti plates were obtained from a commercial supplier (retail price is still too high at this moment—approximately $300/kg, equivalent to $1.5/W based on measured SCP). The customized linear actuators (four were ordered) were $20–$50 each, which is anticipated because actuators with similar power are widely available on the market. The customized steel frames in the prototype were $700 each, and if manufactured in large quantities, at least 10× reduction (to $70 each) is possible. Thus, the projected cost of a Ni–Ti EC wine refrigerator with 100 W cooling power would be $270.

Only a 0.9 L refrigerated cabinet was implemented in this prototype. The evaluation of the TRL would be 4 (lab validation), and researchers will continue to work to scale up the prototype with real loads and improve its performance under real standard rating conditions while reducing its cost.

Heat-Driven EC Cooling

This study developed the concept of a heat-driven EC cooling system, and its target application is solar-thermal AC. In Figure 38, the concept system consists of an SMA actuator made of Ni–Ti wires with a transition temperature at 70°C, which functions as a linear actuator that drives the SE refrigerant (Ni–Ti parallel plate regenerator, in this case). When flowing hot water from the solar thermal collector (SHEX in Figure 38) to the SMA actuator above its transition temperature, the Ni–Ti wires shrink and provide tensile force to load the Ni–Ti plates. The Ni–Ti plates release heat to the ambient (HHEX in Figure 38). The SMA actuator wires are then cooled by fluid at ambient temperature (HHEX), and they transform back to their original length and thus unload the Ni–Ti plates. The Ni–Ti plates absorb the latent heat and provide refrigeration to the cooling heat exchanger (CHEX).

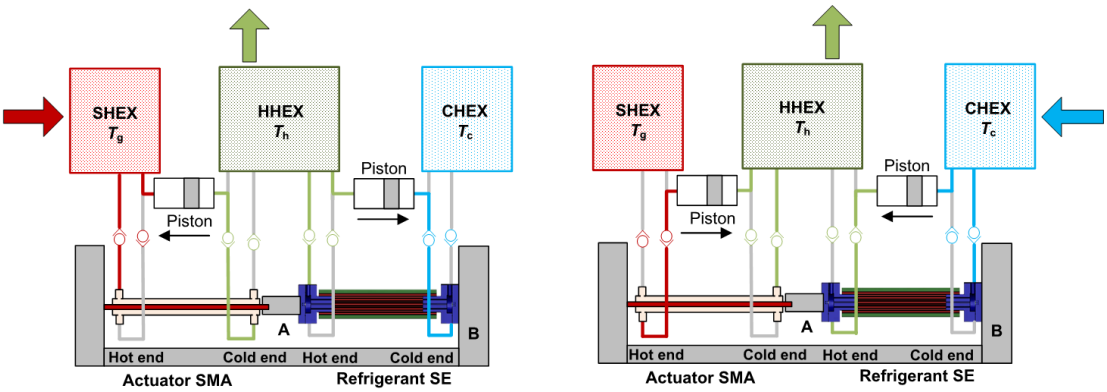

Figure 38 Schematic of the heat-driven EC cooling system. (A) Heating SMA actuator and loading SE refrigerant. (B) Cooling SMA actuator and unloading SE refrigerant

A prototype single-wire SMA actuator was fabricated and tested, which demonstrated 3.75% and 3.5% strain variation when heated above 120°C and 100°C, respectively. These values agreed well with simulation data because the maximum uncertainty was less than 9.9%. This work numerically showed that the SMA actuator should have a linear transition temperature gradient to efficiently use the input heat from the solar thermal collector. When the source temperature, ambient temperature, and refrigeration temperature are 100°C, 30°C, and 20°C, respectively, the simulated system COP was 0.8, which is higher than the state-of-the-art single-effect LiBr–H_2O absorption chillers. At 120°C driving temperature, the system COP could reach above 1.0, demonstrating a novel approach to sufficiently use solar thermal energy. Taking a photovoltaic-driven VC AC unit as a reference, assuming 15% electricity generation efficiency and a COP of 4.5 of the VC AC, the overall solar-to-cooling efficiency is 0.675, which is approximately 15% less than the predicted COP of the heat-driven EC cooling system.

A heat-driven prototype was improved over the past 3 years to fix a series of technical challenges, including sealing the fluid-based SMA actuator, minimizing the dead volume inside the actuator, and minimizing the dead actuator mass that would otherwise consume the actuating displacement. Extensive tests were conducted in 2023, where researchers could measure a stable strain of approximately 3% for a single 0.7 mm refrigerant wire. A solid-state heat source and heat sink were applied, which were controlled by a separate motor. At a cycling duration of 10 s—4 s for heating the actuator and 6 s for cooling the actuator—an approximately 1 K temperature span can be obtained between the heat sink and heat source after 2–3 min.

The evaluation of the TRL of this technology would be between 2 and 3 (concept numerically validated and partial experimental validation on the system level). Researchers are currently working with a major AC company in China to continue developing this technology.

Potential Applications

Wine refrigerator. Wine refrigerators require delivering a few dozen watts of cooling at a 20 K temperature span (already achievable using current EC technology). Because EC cooling can be driven by an actuator with a much lower speed than VC compressors, low noise and low vibration are the unique advantages. Thus, minimizing the footprint of the EC refrigerator while further increasing its efficiency is important for developing commercial-level EC wine refrigerator prototypes in the future.

Off-grid solar refrigerator. The heat-driven SMA actuator-driven EC system can greatly facilitate off-grid cooling applications (e.g., a vaccine refrigerator in off-grid regions). The photovoltaic/photothermal collector provides power for a controller and circulating pump, and one unit of input thermal energy at 110°C translates to 0.8 units of cooling at a zero temperature span or 0.14 units of cooling at a 38 K temperature span. When providing 200 W cooling to a vaccine refrigerator with a glass door (approximately 300–500 L storage volume), a photovoltaic/photothermal collector with 1.5 m^2 area is needed in addition to 0.85 kg of SMA for the actuator and refrigerant.

Thermal energy storage. SMA materials are not only refrigerants but also good candidates for thermal energy storage. This dual functionality of SMAs is superior to conventional VC refrigerants, where a dedicated thermal energy storage material is needed, such as ice or paraffin wax. For specific applications where cooling (or heating) is only occasionally needed, EC cooling integrated with the thermal energy storage concept is a better solution, where the actuator with a much smaller capacity can gradually load multiple EC materials slowly (isothermally) while maintaining their loaded state. When cooling is needed, all EC materials discharge their cooling capacity instantly.

Significant Accomplishments

- A Ni–Ti EC wine refrigerator design was developed with 100 W cooling power and a projected cost (at volume production) of $270.
- A solar heat driven EC system design was projected (by simulation) to have a COP > 1.0 with a 120°C driving temperature. This COP exceeds that of both a state-of-the-art single-effect LiBr–H2O absorption chiller and a photovoltaic-driven electric AC unit.

Potential Tasks for a Follow-Up Annex

- Rating not-in-kind cooling prototypes at target applications' standard rating conditions

Main Publications

Chen, Y., Y. Wang, W. Sun, S. Qian, and J. Liu. 2022. "A compact elastocaloric refrigerator." *Innovations* 3: 100205.

Lu, Y., S. Qian, and J. Shen. 2022. "A fully solid-state cold thermal energy storage device for car seats using shape-memory alloys." *Frontiers in Energy*.

Qian, S., Y. Wang, S. Xu, Y. Chen, L. Yuan, and J. Yu. 2021. "Cascade utilization of low-grade thermal energy by coupled elastocaloric power and cooling cycle." *Applied Energy* 298: 117269.

Qian, S., Y. Wang, L. Yuan, and J. Yu. 2019. "A heat driven elastocaloric cooling system." *Energy* 182: 881–899.

Qian, S., S. Yao, Y. Wang, L. Yuan, and J. Yu. 2022. "Harvesting low-grade heat by coupling regenerative shape-memory actuator and piezoelectric generator." *Applied Energy* 322: 119462.

Tan, J., Y. Wang, S. Xu, H. Liu, and S. Qian. 2020. "Thermodynamic cycle analysis of heat driven elastocaloric cooling system." *Energy* 197: 117261.

Wu, Y., Y. Liu, and S. Qian. 2023. "Numerical simulation of a foam regenerator for elastocaloric cooling." *Applied Thermal Engineering* 221: 119819.

Yuan, L., Y. Wang, J. Yu, A. Greco, C. Masselli, and S. Qian. 2023. "Numerical study of a double-effect elastocaloric cooling system powered by low-grade heat." *Applied Thermal Engineering* 218: 119302.

3.2.3. China, Shanghai Jiao Tong University: Cooling Systems Based on the Electrocaloric Effect (ECE)

Lead PI: Dr. Xiaoshi Qian

Description

The electrocaloric effect (ECE) links two dipolar entropy states by applying and removing electric fields to a condensed matter. Since the giant ECE in dielectrics was discovered more than 12 years ago, electrocaloric cooling technology (Figure 39) has quickly gained attention in both academia and industry. Electric field–polarization coupling effects, which underpin the ECE and electrocaloric cooling cycles, are one of the most efficient forms of energy conversion, approaching 90% efficiency. Electrocaloric solid-state cooling represents a zero-GWP technology, making it a highly efficient refrigeration alternative.

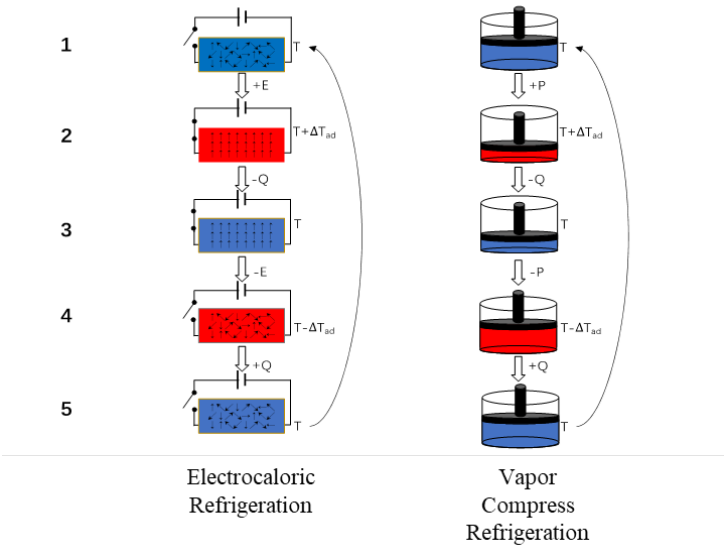

Figure 39 Schematics of electrocaloric and VC refrigeration processes

The Discovery of Polar High-Entropy Polymers for Giant ECE

In this century, the prediction and, later, the direct observation of the giant ECE rejuvenated the research field [8, 9]. The 5–10 K of temperature change induced by electrical charging/discharging the condensed matter suddenly made ECE possible in many potential applications.

Electrocaloric cooling has been directly demonstrated in many ferroelectrics, including inorganics and organics, such as lead-based ceramics [10], lead-free ceramics [11], and single crystals [12], as well as poly(vinylidene fluoride)-based polymers [13]. Owing to the high demand of the energy reversibility, it is generally recognized in the field that electrocaloric materials should be designed as relaxor ferroelectrics [14], in which dipoles are in a more randomized (or relaxed) state rather than forming an ordered, bulky ferroelectric domain. Because of the large pool of the inorganic ferroelectrics, the inorganic electrocaloric materials were perovskites ranging from $PbTiO_3$-based, $BaTiO_3$-based, $SrTiO_3$-based, and $KNbO_3$-based ceramics, single crystals, solid solutions, and several 2D inorganic materials, as well as others. A recent breakthrough has been reported in the multilayer ceramic capacitor (MLCC) of $PbSc_{0.5}Ta_{0.5}O_3$, in which large ECE was directly recorded in bulk material that can be manufactured by current industrial processes [15].

Challenges remain to widespread implementation of electrocaloric-based cooling. So, its current TRL is estimated at 3–5. Prioritization of electrocaloric material properties during manufacturing processes is essential to ensure long-term quality performance of electrocaloric-based systems. State-of-the-art electrocaloric ceramics and polymers require giant electric fields to induce the required drops (T > 5 K). However, these large fields reduce the dielectric stability and restrict the lifetime of the electrocaloric material.

This work developed a series of modified electrocaloric polymers, which exhibited a giant electric field under low electric fields [16]. Figure 40 shows that for fields under 50 MV/m, the entropy change of the polymer is enhanced by 300% compared with the state-of-the-art electrocaloric polymers [base terpolymer P(VDF-TrFE-CFE)].

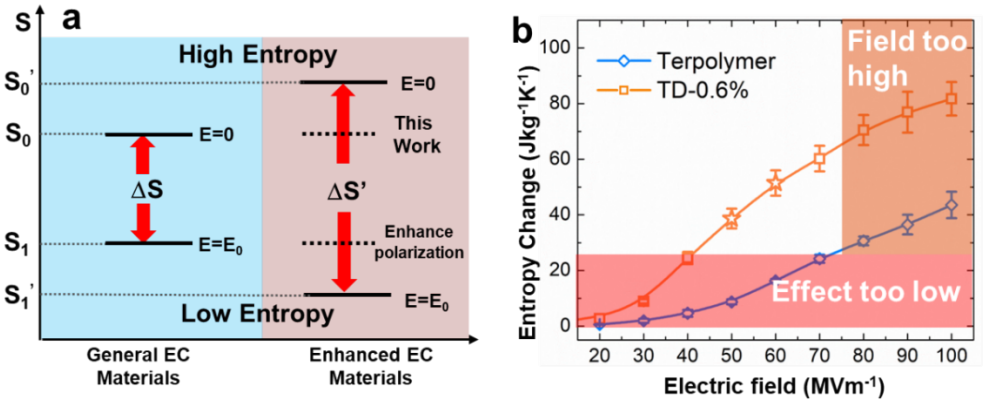

Figure 40 (a) Schematics of achieving giant ECE under low field via designing a high-entropy material. (b) Directly measured ECE of the high-entropy polymer (TD-0.6%) and the state-of-the-art polymer P(VDF-TrFE-CFE) (noted as Terpolymer*). In this figure, EC is electrocaloric.*

Detailed structural analyses (Figure 41) revealed that the newly developed electrocaloric polymer contains a greatly increased number of polar entities, which significantly enhanced the zero-field polar entropy of the material system. Therefore, this study suggests that it is a polar, high-entropy polymer. Additionally, in situ x-ray diffraction results (Figure 41) indicated that the high-entropy polymer was quite responsive under the low electric field. The α–β phase transition was markedly enhanced in the high-entropy polymer (noted as TD-0.6%).

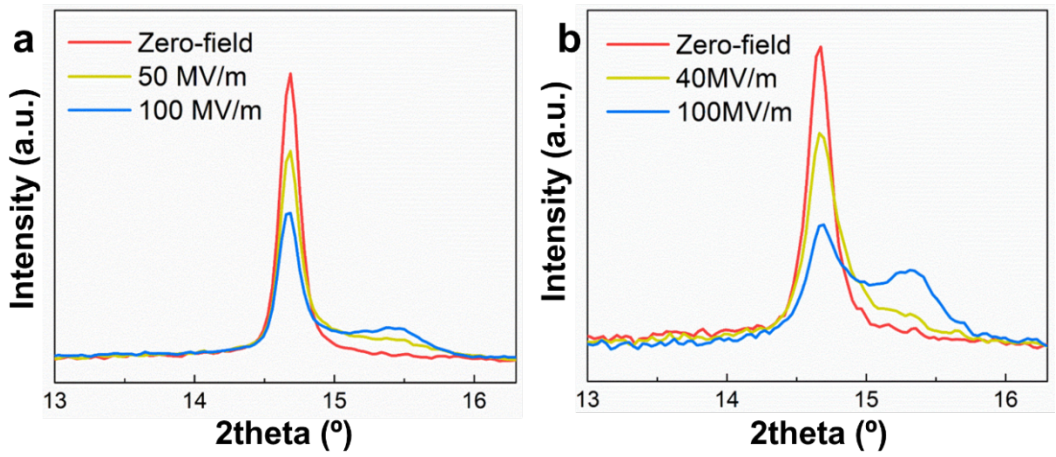

Figure 41 In situ x-ray diffraction indicated a stronger phase transition in the (b) high-entropy polymer compared with (a) that in the base terpolymer.

To evaluate the effect that the high-entropy polymer has on the device from its point of view, this study designed a model of an electrocaloric HP employing the active electrocaloric regeneration based on a previous report [17]. The polymeric material working element cycles back and forth between the two ends of the regenerator and maintains good thermal contact with its surface. During the movement, the electric field applied on the material changes periodically, and the working element absorbs heat from one end and ejects heat to the other. The simulation compares the performances of devices operating different polymers discussed in this work (the base terpolymer and the TD-0.6%) in terms of COP, the cooling power density, and the maximum temperature span (T_{span}). The properties of each working body were assessed based on the material properties and the specific configurations.

Figure 42 shows the detailed properties of the electrocaloric HP device operating with both the base terpolymer and the TD-0.6%. Thanks to the exceptional electrocaloric effect of the TD-0.6% material, the device achieved a cooling power density of 5.2 kW/kg at a zero T_{span} and a T_{span} of 63 K under 50 MV/m at zero-power conditions, compared with 1.4 kW/kg and 14 K for operation with the base terpolymer. The large T_{span} should be achievable in a practical experiment because the large ECE of TD-0.6% under low fields (≤50 MV/m) persists over a wide temperature window from 10°C to 70°C. Owing to the significantly reduced losses in the

high-entropy TD-0.6%, the device operating with this polymer achieved the highest COP of 11.4 (80% of Carnot) compared with a COP of 1 when operating with the base terpolymer, representing a 1,000% enhancement in efficiency.

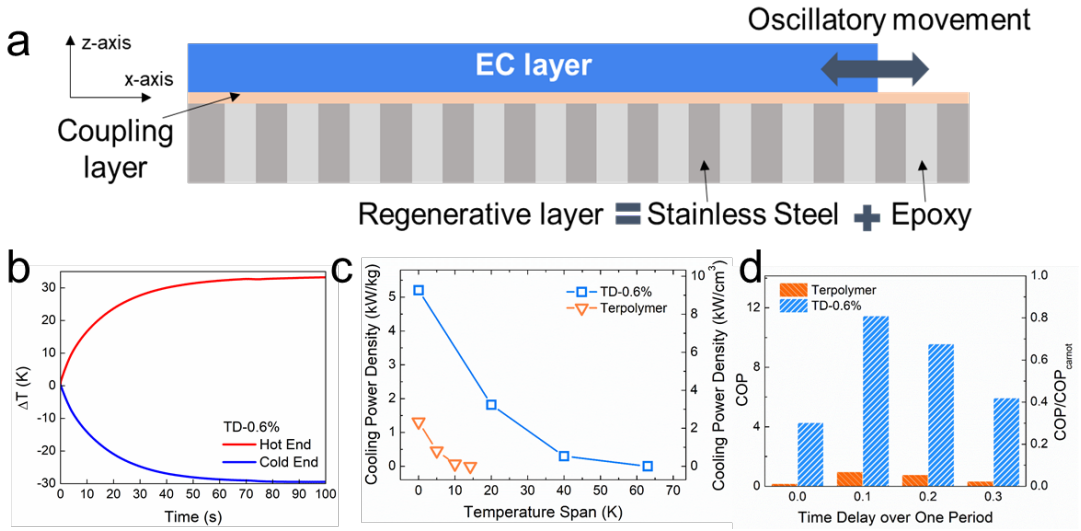

Figure 42 (A) Schematics of the proposed electrocaloric HP device. (B) Simulated temperature evolution on the hot and cold ends of the device. Simulated (C) cooling power density and (D) COP of the high-entropy polymer TD-0.6% compared with the base terpolymer P(VDF-TrFE-CFE)

With a large ECE, the polymer would still require high thermal conductivity to efficiently exchange heat with external sources/sinks. However, this study demonstrated that a general conflict exists between the structural ordering required by high thermal conductivity and the polar disordering required by the large ECE. For example, this work showed that a simple mixture of the BN nanosheet (BNNS), known for its impressive high thermal conductivity, and the state-of-art terpolymer (TD-0.6%) would result in a dramatic deterioration of the ECE, albeit with an enhanced thermal conductivity in the nanocomposite mixture. The results indicated that the degree of freedom of the dipoles in the polymer has been significantly hindered by the existence of the atomically ordered BNNS close by [Figure 43(a)].

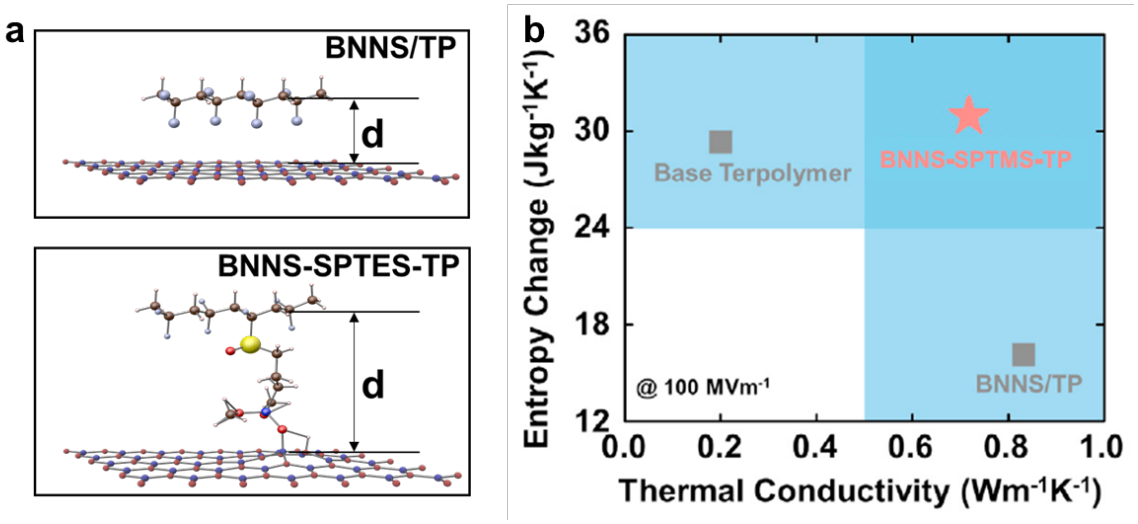

Figure 43 (a) Molecular structures of (bottom) BNNS–3-sulfurouspropyltrimethoxysilane (SPTMS)–terpolymer (TP) and (upper) BNNS/TP schematically show the different distances between polymer chains and BNNSs. (b) Electrocaloric entropy change under the electric field of 100 MV/m and thermal conductivity in the base terpolymer, BNNS/TP, and BNNS–SPTMS–TP

To release the degree of freedom of dipole orientation, this study applied click chemistry and introduced 3-sulfurouspropyltrimethoxysilane (SPTMS) to covalently graft BNNS on the

electrocaloric polymer [18]. This study opened up the space between the BNNS and the polymer chains and concurrently achieved large ECE and high thermal conductivity (i.e., a facile order-disorder synergy) [Figure 43(b)]. The interface-regulated nanocomposite exhibited the electrocaloric entropy change of 30.94 J/(kg·K) under 100 MV/m and tripled thermal conductivity of 0.72 W/(m·K). As the result, the rates of the heat exchange from the polymer to the heat sink and source were doubled, as was the cooling power of the electrostatic force–driven electrocaloric device (Figure 44).

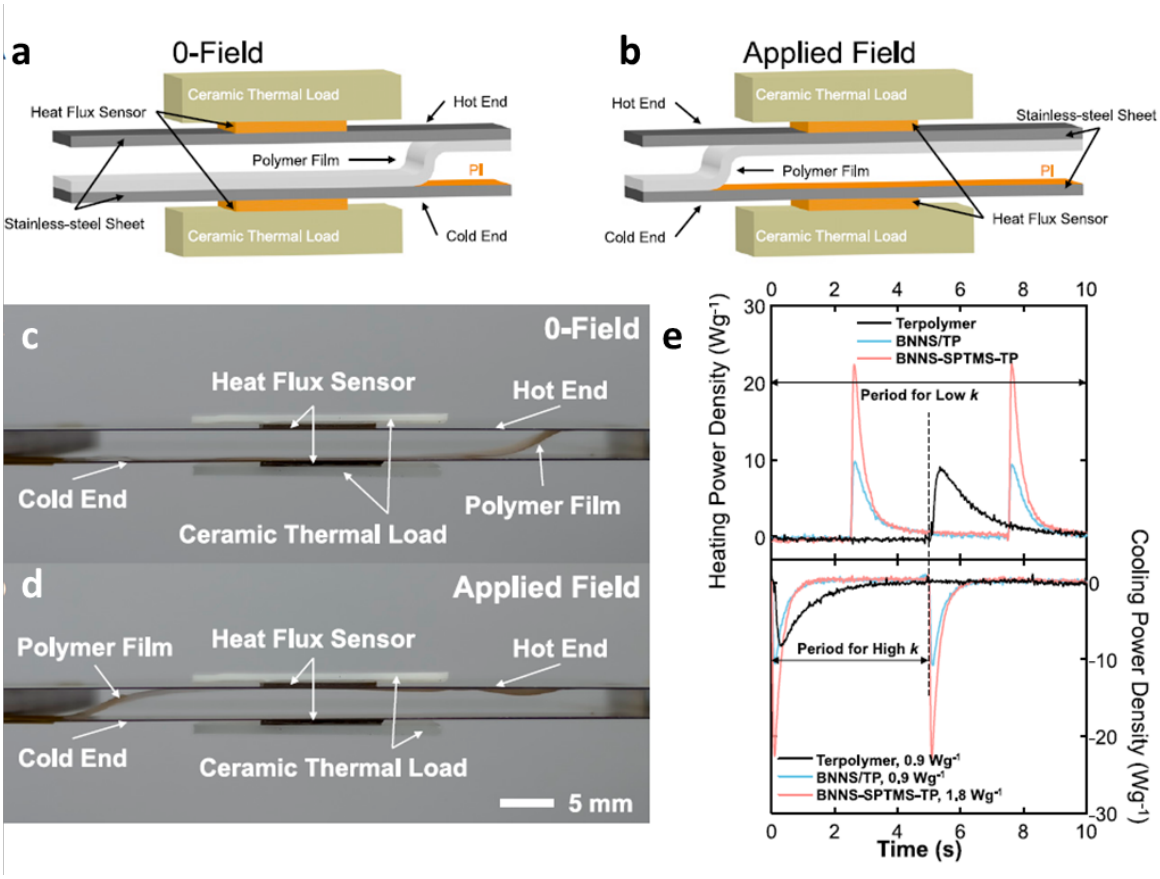

Figure 44 Experimental analysis for heat flux signals of the electrocaloric devices operating different polymers. (a, b) Schematic structures of the film-like electrocaloric device for heat flux testing under (a) 0-field and (b) applied field.(c, d) Geometry of the device operating in an oscillating cycle in which the electrocaloric polymer film is attaching to (c) the cold end and (d) the hot end from the side view. (e) Heating and cooling power densities recorded at the hot and cold ends of the device. TP stands for terpolymer

Using the nanocomposite material mixture containing SPTMS, a standard model of an electrocaloric refrigerator achieved a 5.23 W/g cooling power density, which is 6.8× higher than the one operating with the simple mixture. A figure of merit (FOM) for electrocaloric nanocomposite materials has been proposed to assess their overall capability in the heat-pumping applications [18].

Most Relevant End Use Application Areas

As this work focuses on reducing the required voltage for generating large ECEs, the advances in the high-entropy electrocaloric polymers would enable technologies such as wearable cooling devices and miniature, portable AC.

Follow-On Work Priorities

This team is currently working on high-entropy ceramics and their MLCC. If successful, the MLCC would exhibit extended cooling capacity. This capacity is essential for fabricating an electrocaloric cooling machine with large cooling power. Additionally, in a follow-on annex, this team will work on the multilayer polymeric capacitors for the wide T_{span} of an electrocaloric device.

Most Significant Accomplishments

- A proposed electrocaloric HP device operating with a high-entropy polymer achieved a maximum COP of 11.4 (~80% of Carnot) compared with a COP of 1 when operating with a baseline terpolymer.
- The conflict between high thermal conductivity and high ECE has been demonstrated on the molecular level. Click chemistry has been applied to expand the ordered and disordered structure to achieve both high ECE and large thermal conductivity.
- Interface-regulated nanocomposite materials exhibited an electrocaloric entropy change of 30.94 J/(kg·K) under 100 MV/m and a tripled thermal conductivity of 0.72 W/(m·K). Using the nanocomposite material, a standard model of an electrocaloric refrigerator achieved a 5.23 W/g cooling power density, which is 6.8× higher than one operating with a simple material mixture.
- A FOM for electrocaloric nanocomposite materials has been proposed to assess their overall capability in the heat-pumping applications.

Recent Publications Related to Annex 53

Han, D., et al. 2023. "Molecular interface regulation enables order-disorder synergy in electrocaloric nanocomposites." *Joule* 7: 1–17.

Kang, Liqi, Donglin Han, Liang Hong, Lirong Zheng, and Xiaoshi Qian. 2023. "Statistical mechanical model of the giant electrocaloric effect in ferroelectric polymers." *ACS Macro Letters* 12, no. 7: 848–853.

Qian, X., X. Chen, L. Zhu, and Q. M. Zhang. 2023. "Fluoropolymer ferroelectrics: Multifunctional platform for polar-structured energy conversion." *Science* 380, no. 6645: eadg0902.

Du, F., Z. Song, Y. Xu, D. Han, Q. Li, S. Zheng, J. Shen, and X. Qian. 2023. "Multi-element B-site substituted perovskite ferroelectrics exhibit enhanced electrocaloric effect." *Science China Technological Science* 66: 1119–1128.

Cai, Yu, et al. 2023. "Polymeric nanocomposites for electrocaloric refrigeration." *Frontiers in Energy* 17: 450–462.

Qian, Xiaoshi. 2022. "Pumping into a cool future: Electrocaloric materials for zero-carbon refrigeration." *Frontiers in Energy* 16: 19–22.

Presentations

Qian, Xiaoshi. 2023. "Nano-Scale Manipulation of Polar Entropy in Ferroelectric Polymers Generates Giant Electrocaloric Effect for Cooling." 2023 IEEE International Symposium on Applications of Ferroelectrics, International Symposium on Integrated Functionalities, and Piezoresponse Force Microscopy Workshop Joint Conference, oral presentation.

Qian, Xiaoshi. 2023. "Giant and Durable Electrocaloric Effect in Polar High-Entropy Polymers." Materials Research Society Spring Meeting 2023, invited virtual talk.

Qian, Xiaoshi. 2022. "Giant Electrocaloric effect at Ultralow fields." 9th International Institute of Refrigeration International Conference on Caloric Cooling and Applications of Caloric Materials (THERMAG), invited.

Qian, Xiaoshi. 2022. "Giant electrocaloric effect in relaxor ferroelectric polymers with high polar entropy." International Symposium on Ferroelectric Material and Applications (ISFMA), invited.

Qian, Xiaoshi. 2021. “Electrocaloric Cooling: from Ferroelectrics to Refrigeration.” Asian Symposium on Computational Heat Transfer and Fluid Flow 2021, Qingdao, China, invited talk.

Qian, Xiaoshi. 2021. “Achieving Polar High-Entropy Polymer for Fatigue-Resistant Electrocaloric Cooler.” 18th International Workshop on Piezoelectric Materials and Applications in Actuators (IWPMA 2021), Pennsylvania State University.

3.2.4. Germany, Fraunhofer Institute for Physical Measurement Techniques: Active Heat Pipe Concept Applied to Caloric Cooling Systems

Lead PI: Dr. Kilian Bartholomé

Project Description

Phenomenological material model for first-order electrocaloric material [19]. Electrocaloric cooling systems use a phase transformation from the paraelectric to the ferroelectric state by applying or removing an electric field to pump heat. Lead scandium tantalate (PST) materials show a first-order phase transition and are one of the most promising candidates for electrocaloric cooling. To model caloric cooling systems, accurate and thermodynamically consistent material models are required. In this study, a phenomenological model based on an analytical equation for the specific heat capacity is used to describe the material behavior of bulk PST material. This model is fitted to the experimental data, showing very good agreement (Figure 45). Based on this model, essential material properties such as the adiabatic temperature change and isothermal entropy change of this material can be calculated.

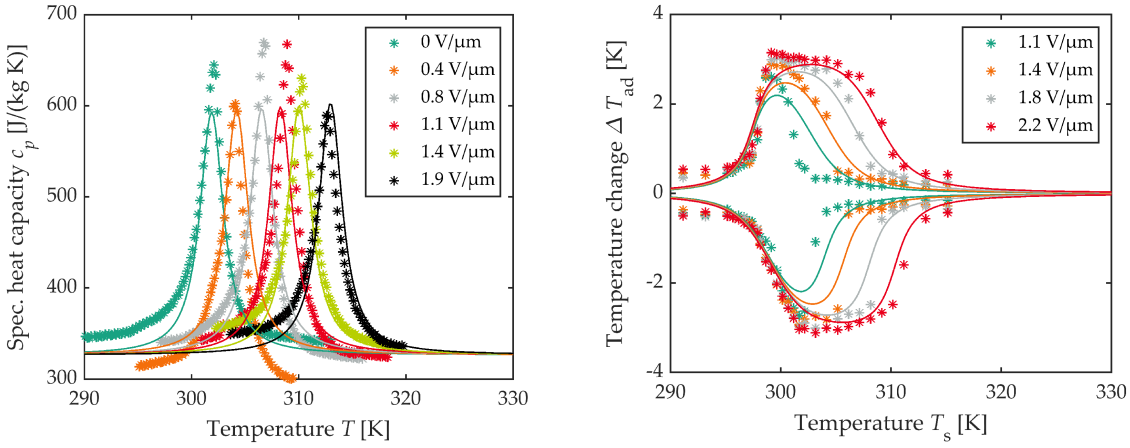

(**a**) (**b**)

Figure 45 The phenomenological model of an electrocaloric material shows very good agreement with (symbols) experimental data with respect to the (lines) calculated specific heat capacity and adiabatic temperature change (Figure is taken from [19])

On the efficiency of caloric materials in direct comparison with exergetic grades of compressors [20]. For most caloric materials, the phase transition results in a certain amount of power dissipation, which drastically affects the efficiency of a caloric cooling system. The effect on the efficiency can be expressed by an FOM, which can directly be deduced from material properties. This FOM has been derived for 36 different magneto-, elasto-, electro-, and barocaloric material classes based on literature data. This research found that the best materials can theoretically attain second law efficiencies of over 90%. The FOM is analogous to the isentropic efficiency of idealized compressors of VC systems. The isentropic efficiency can thus be directly linked to the theoretically achievable efficiency of a compressor-based VC refrigeration system for a given refrigerant. Figure 46 shows the main results of a theoretical comparison between the efficiency of caloric HPs and VC systems based on the material losses for the caloric HP and the efficiency of the compressor for VC systems. The effect of heat regeneration is considered in both cases. In VC systems, the effect of the working fluid on the efficiency is also studied.

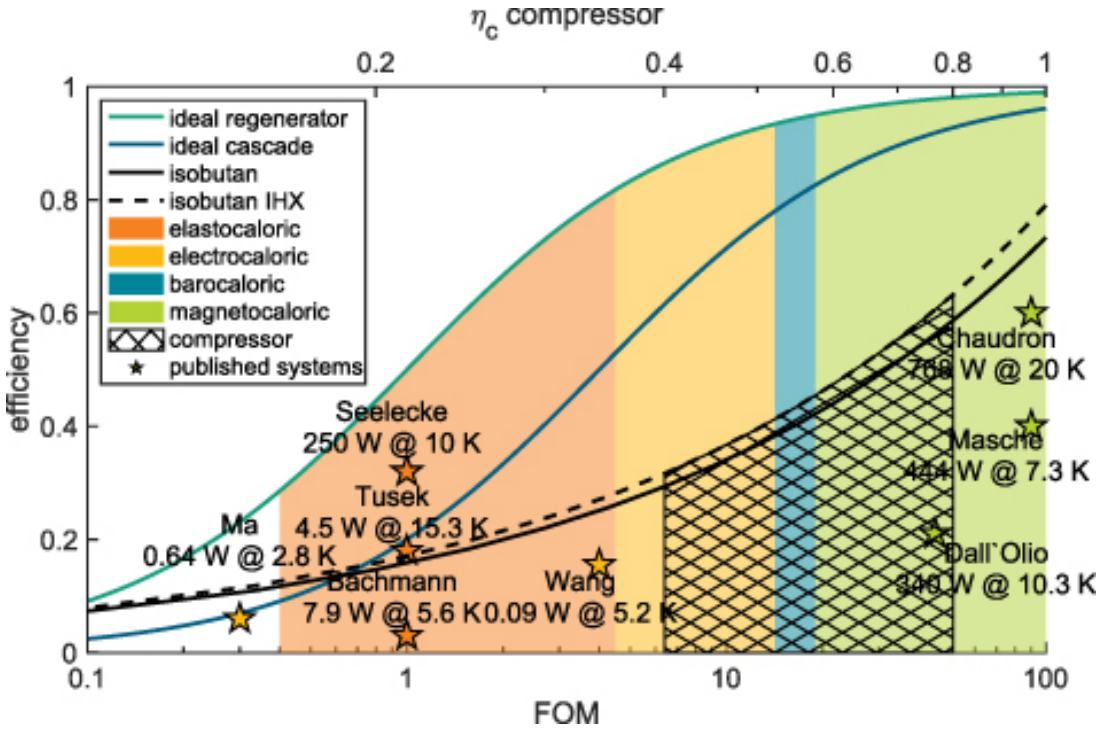

Figure 46 Efficiency potential of the different caloric technologies derived from a material's FOM in comparison with the efficiencies of current compressor systems derived from their isentropic efficiencies. Additionally, the best published efficiencies of caloric systems are shown (Figure is taken from [20]). NOTE: IHX = "internal heat exchanger" in this instance.

Spatiotemporal solid-state electrocaloric effect exceeding twice the adiabatic temperature change [21]. In an all-solid-state electrocaloric arrangement, an absolute temperature change that exceeds twice the electrocaloric adiabatic temperature change was locally realized using just the distributed thermal electrocaloric adiabatic temperature change for several implementations of all-solid-state distributed element configurations. An all-solid-state test assembly (Figure 47) was built from commercial electrocaloric capacitors with two independently controlled parts, and the surface temperature change was measured to be 223% of the adiabatic electrocaloric temperature change, which clearly exceeds twice the adiabatic temperature change and verifies the practical feasibility of the approach. This result allows a significant increase of the maximum temperature difference per stage in cascaded and thermal switch-based electrocaloric HPs, which was previously limited by the adiabatic electrocaloric temperature change (100%) under no-load conditions. Distributed thermal element simulations provide insight in the spatiotemporal temperatures within the all-solid-state electrocaloric element. Because only the distributed thermal capacitance and resistance is used to boost the temperature change, the maximum absolute temperature change occurs only in parts of the all-solid-state element—for example, close to the surfaces. A trade-off of the approach is that the required electrocaloric capacitance increases more than the gained boost of the absolute temperature change, reducing the power density and electrical efficiency in HP systems. Nevertheless, the proposed approach enables a simplification of electrocaloric HPs or an increase in the achievable temperature span and might also improve other electrocaloric applications.

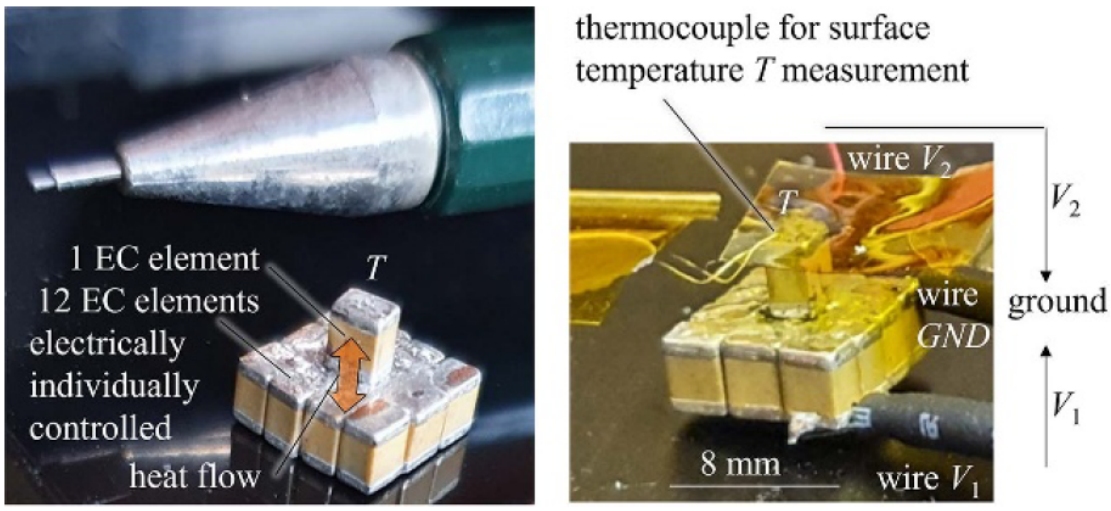

Figure 47 Experimental setup of a demonstrator mockup showing the potential of increasing the temperature lift by a spatiotemporal setup of the electrocaloric elements. EC is electrocaloric in this figure (Figure is taken from [21])

Latest Results

An electrocaloric device based on the heat pipe concept has been realized in the lab, showing a maximum cooling power of more than 2 W at a system frequency of 5 Hz using PST components. This device has a cooling power density of 1.5 W/g, which is the largest value shown in literature so far (publication is in preparation). This result demonstrates that electrocaloric components can be integrated into heat pipes to enhance heat transfer from the electrocaloric to heat sink and source. Further research will focus on the enhancement of the temperature lift by cascading the electrocaloric segments, as well as the experimental quantification of the system efficiency.

Most Significant Accomplishments

For all three technologies—magneto-, elasto-, and electrocaloric—the heat pipe system concept was successfully demonstrated. Thus, for each technology, high cooling power densities were attained (Table 3).

Table 3 Comparison of the experimental data for the magneto-, elasto-, and electrocaloric heat pipes

	MC heat pipe	EC heat pipe	Electrocaloric heat pipe
Maximum system frequency (Hz)	20	1.5	5
Maximum cooling power density (W/g)	12.5	6.27	1.5
Maximum cooling power (W)	30	7.9	2

NOTE: cooling power density is based on the caloric material mass

At this point, an increase in system frequency, and thereby in maximum cooling power density, was hindered by the structure size of the caloric material (magneto- and electrocalorics) or the self-heating owing to dissipative losses in the material (ECs). These aspects will be addressed in future work, as well as an increase in the temperature lift of the systems by cascading several segments.

Most Relevant End-Use Application Areas

The following end-use applications are most relevant for caloric systems.

- Cooling for medical and laboratory devices: For many medical and laboratory devices, only non- or low-flammable refrigerants are permitted. Furthermore, high energy efficiency becomes more crucial. At the same time, the cost pressure is not as strong as in other applications, making it a promising application for newly developed cooling technologies.
- AC in automotive: Existing refrigerants all show significant disadvantages, and the use of natural refrigerants is difficult because of their flammability. At the same time, for electromobility, the energy efficiency of the AC system becomes more crucial because it directly influences the range of the e-vehicle.
- Heat pumps for private homes: The annual performance number as an indicator for the energy efficiency of the HP is a very central selling argument for an HP. At the same time, the indoor usage of flammable refrigerants above a certain amount comes along with strong regulations. Thus, a new HP technology with potentially larger energy efficiency and nonflammable fluids would be highly favored.

Follow-On Work Priorities

An important task for a follow-on annex would be the standardization of caloric measurements (e.g., adiabatic temperature change, isothermal entropy change, hysteretic losses of materials, cooling power, temperature lift and efficiency of systems), as well as an establishment of a standardized nomenclature.

Relevant Publications

Mönch, Stefan, and Kilian Bartholomé. 2023. “Spatio-temporal solid-state electrocaloric effect exceeding twice the adiabatic temperature change.” *Journal of Physics: Energy* 5, no. 4: S. 45001.

Schipper, Jan, et al. 2023. “On the efficiency of caloric materials in direct comparison with exergetic grades of compressors.” *Journal of Physics: Energy* 5, no. 4: S. 45002.

Unmüßig, Sabrina, David Bach, Youri Nouchokgwe, Emmanuel Defay, and Kilian Bartholomé. 2023. “Phenomenological material model for first-order electrocaloric material.” *Energies* 16, no. 15: S. 5837.

Hess, T., L. M. Maier, P. Corhan, O. Schäfer-Welsen, J. Wöllenstein, and K. Bartholomé. 2019. “Modelling cascaded caloric refrigeration systems that are based on thermal diodes or switches.” *International Journal of Refrigeration* 103: 215–222.

Hess, T., C. Vogel, L. M. Maier, A. Barcza, H. P. Vieyra, O. Schäfer-Welsen, J. Wöllenstein, and K. Bartholomé. 2019. “Phenomenological model for a first-order magnetocaloric material.” *International Journal of Refrigeration*.

Hess, T., L. M. Maier, N. Bachmann, P. Corhan, O. Schäfer-Welsen, J. Wöllenstein, and K. Bartholomé. 2020. “Thermal hysteresis and its impact on the efficiency of first-order caloric materials.” *Journal of Applied Physics* 127: 75103.

Maier, L. M., P. Corhan, A. Barcza, H. A. Vieyra, C. Vogel, J. D. Koenig, O. Schäfer-Welsen, J. Wöllenstein, and K. Bartholomé. 2020. “Active magnetocaloric heat pipes provide enhanced specific power of caloric refrigeration.” *Communications Physics* 3: 1–6.

Bachmann, N., A. Fitger, L. M. Maier, A. Mahlke, O. Schäfer-Welsen, T. Koch, and K. Bartholomé. 2021. “Long-term stable compressive elastocaloric cooling system with latent heat transfer,” *Communications Physics* 4: 615.

Ianniciello, L., K. Bartholomé, A. Fitger, and K. Engelbrecht. 2022. “Long life elastocaloric regenerator operating under compression.” *Applied Thermal Engineering* 202: 117838.
Bachmann, N., A. Fitger, S. Unmüßig, D. Bach, O. Schäfer-Welsen, T. Koch, and K. Bartholomé. 2022. “Phenomenological model for first-order elastocaloric materials.” *International Journal of Refrigeration* 136: 245–253.
Bachmann, N., D. Schwarz, D. Bach, O. Schäfer-Welsen, T. Koch, and K. Bartholomé. 2022. “Modeling of an elastocaloric cooling system for determining efficiency.” *Energies* 15: 5089.
Moench, S., R. Reiner, K. Mansour, M. Basler, P. Waltereit, R. Quay, and K. Bartholomé. “GaN power converter applied to electrocaloric heat pump prototype and carnot cycle.” *2022 IEEE 9th Workshop on Wide Bandgap Power Devices & Applications (WiPDA)*, Redondo Beach, CA, USA, 2022 186–191, https://ieeexplore.ieee.org/document/9955287.
Mönch, S., R. Reiner, K. Mansour, P. Waltereit, M. Basler, R. Quay, C. Molin, S. Gebhardt, D. Bach, R. Binninger, and K. Bartholomé. 2023. “A 99.74% Efficient Capacitor-Charging Converter Using Partial Power Processing for Electrocalorics.” *IEEE Journal of Emerging and Selected Topics in Power Electronics* 11: 4491–4507.

3.2.5. USA, Ames Laboratory: High Power Density Magnetocaloric (MC) Systems

Lead PI: Dr. Julie Slaughter

Latest Results

The team at Ames National Laboratory for the project “High Power Density (HPD) Magnetocalorics” has demonstrated a gadolinium-based MC device that is projected to have similar power density as off-the-shelf compressors in the 50 W range (Figure 48, gold star). The power density data in Figure 48 is based on total magnetic material mass in the system (e.g., caloric material, permanent magnets, magnetic steel, etc.).

To evaluate the scalability and potential of MC devices, methods to improve the magnetic circuit were evaluated and demonstrated using models. Targeting magnetic fields in the range of 0.9 T, the volume of permanent magnet material, assumed to be NdFeB with an energy product of 50 MGOe, was minimized by controlling the air gap thickness-to-magnet ratio and reducing stray fields outside the active area. Magnetic steel components were reduced in size and placed only in areas of high flux density. They were also sized to carry more magnetic flux, thus increasing flux density. Maximum magnetic flux density in magnetic steel components was increased from 1.2 T to 1.5 T, which resulted in an approximately 25% reduction in the mass of steel while still being well below magnetic saturation. As larger-scale cooling devices were evaluated, increasing the diameter and the length-to-diameter ratio of the magnet reduced both the amount of permanent magnet and magnetic steel by improving stray magnetic flux. Another method shown to reduce system mass at larger scales was modifying the design from two magnetic poles to increasing numbers of poles that act in adjacent pairs. Implementing these changes and improvements for larger-scale designs results in the same or better device power density as compressors (gray circles) up to nearly 500 W (red squares) with gadolinium-packed particle beds.

All of the changes discussed so far have been demonstrated using gadolinium, which is a second-order MC material with a relatively low power density (550 W/kg was used for calculations). First-order MC materials have a much narrower operating temperature range but a potentially larger power density when used in layers to achieve the full temperature span. Devices have been demonstrated with as much as 1,650 W/kg using layers of packed particles of materials from the LaFeSi family. Assuming that this same power density can be achieved with the high–power density magnet designs, this study estimated larger-scale device power densities. These projections (green diamonds) show that MC devices can achieve similar power density as compressors up to nearly 3,000 W using first-order MC materials. Demonstrating power densities competitive with existing compressors is a step toward cost parity and commercial adoption of MC technology.

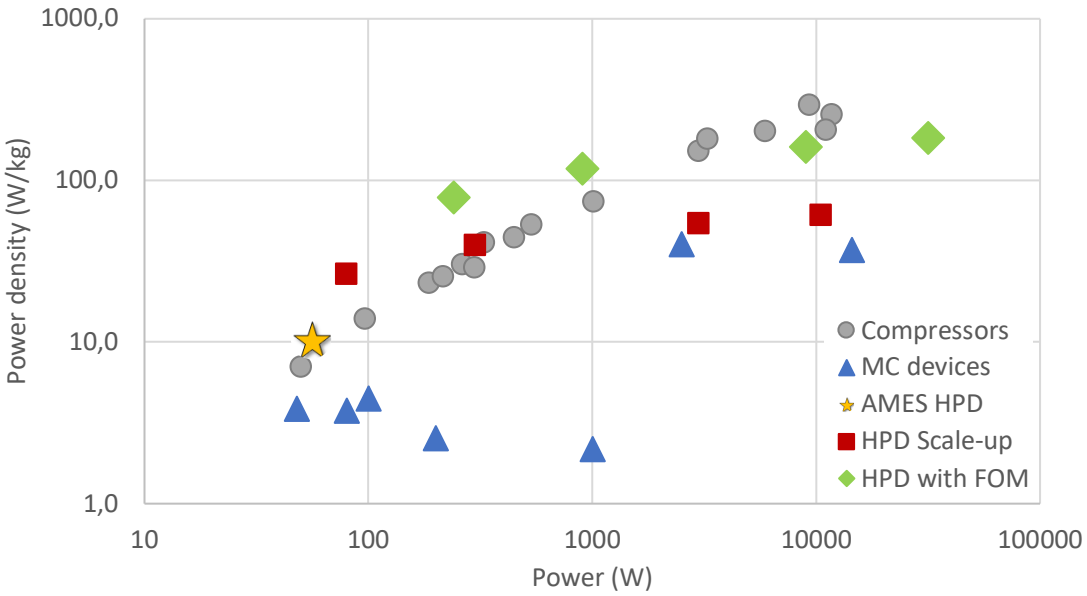

Figure 48 The new device developed at Ames National Laboratory exceeds the power density performance of (blue triangles) existing MC devices in the same power range (1–7) and meets or exceeds the power density of (gray circles) off-the-shelf compressors (8–10). (Red squares) Models using outlined scaling strategies show that HPD MC devices match compressors up to approximately 500 W using gadolinium-packed particle beds. (Green diamonds) Assuming the use of first-order MC materials, such as the LaFeSi family, models indicate power density parity with compressors up to approximately 3 kW [22–31]

Most Significant Accomplishments

- This work demonstrated an MC device that is projected to have approximately 10 W/kg power density at 50 W cooling power, which is higher than almost all MC devices in similar cooling power ranges.
- Estimates show that power density increases with size and can match that of compressors up to approximately 500 W using gadolinium MC material.
- The highest estimated power density for MC devices using first-order MC materials was approximately 170 W/kg at about 10 kW (based on total magnetic material mass in the system).
- Meeting or exceeding the power density of compressors in certain power ranges demonstrates that there is a viable path to cost parity and commercial adoption of the technology.

Most Relevant End Use Applications

The cooling power ranges and temperature spans demonstrated and projected are suitable for residential refrigeration and AC applications. MC devices with similar or better power density than compressors should be able to meet size and cost requirements for these applications.

Potential Tasks for a Follow-On Annex

- Demonstrate first-order MC materials and advanced regenerators to achieve power density parity with compressors above approximately 10 kW.
- Investigate additional materials and device concepts that can meet temperature spans and power (heating or cooling) of additional end-use applications.
- Investigate the potential for both cooling and heating in a single caloric (magneto-, elasto-, electro-, multicaloric) HP.

Relevant Publications

Czernuszewicz, A., L. Griffith, J. Slaughter, and V. Pecharsky. 2023. “Balancing performance of active magnetic regenerators: A comprehensive experimental study of aspect ratio, particle size, and operating conditions.” *Journal of Physics: Energy* 5, no. 2: 024008.

Griffith, L., A. Czernuszewicz, J. Slaughter, and V. Pecharsky. 2021. “Active magnetic regenerative cooling with smaller magnets.” *International Journal of Refrigeration* 125: 44–51.

Slaughter, J., A. Czernuszewicz, L. Griffith, and V. Pecharsky. 2020. “Compact and efficient elastocaloric heat pumps—Is there a path forward?” *Journal of Applied Physics* 127, no. 19: 194501.

Czernuszewicz, A., L. Griffith, J. Slaughter, and V. Pecharsky. 2020. “Low-force compressive and tensile actuation for elastocaloric heat pumps.” *Applied Materials Today* 19: 100557.

3.2.6. USA, ORNL: Alternative Cooling Technology Using MC Materials

Lead PI: Dr. Ayyoub Momen

Description

This project’s goal was to investigate the potential of applying the MC effect with a multistage regenerator to develop an MC refrigeration system with higher efficiency than conventional VC refrigeration technologies. Alternative approaches to MC regenerators (MCRs) include a multiple-stage MCR and a solid-state MCR. In the multiple-stage approach (e.g., the 16 stages in Figure 49), multiple MC materials with different Curie temperatures were combined to optimize the MC effect according to the temperature distribution along the axis, as shown in Figure 49(a) [32]. The solid-state MCR approach uses a high-conductivity material (e.g., copper) to transfer the cooling power between the MC material and the target [33].

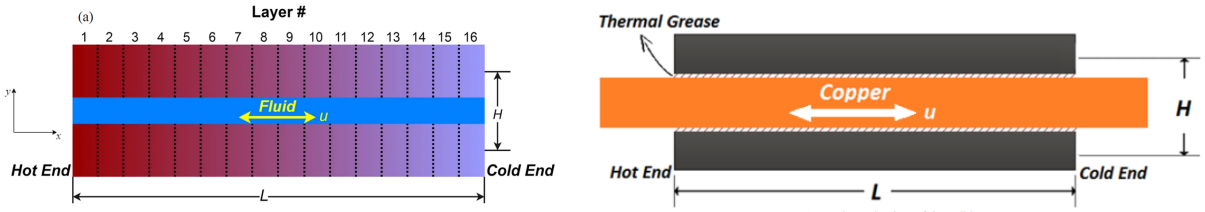

(a) **(b)**

Figure 49 (a) MC regenerator with 16 stages of MC materials and (b) solid-state MCR

Development Status and Plans

To guide MCR research, an analytical model of an MCR was derived to describe the heat transfer in the regenerator. Based on the analytical model, a numerical model was developed to reveal the system performance and act as a guide to approach an optimal design. The numerical model predicts that a 16-stage regenerator can provide a COP as high as 84% of the Carnot cycle COP, as shown in Figure 50 [32].

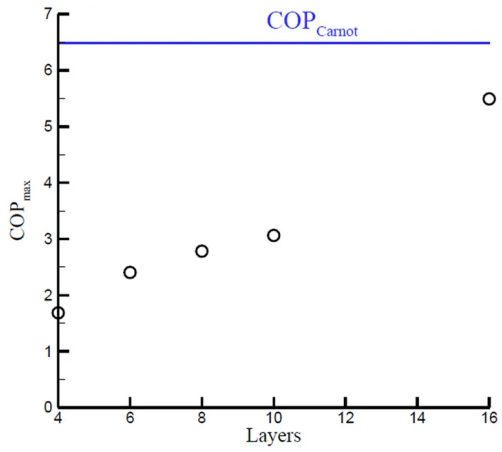

Figure 50 MC cycle COP vs. the number of regenerator stages

Most Significant Accomplishments

Model results indicate the potential for an MC refrigeration cycle with a 16-stage regenerator to reach 84% of the Carnot COP.

Most Relevant End Use Application Areas

- Refrigerators, residential, or specialty use

Relevant Publications

Zhang, M., O. Abdelaziz, A. M., Momen, and A. Abu-Heiba. 2017. “A numerical analysis of a magnetocaloric refrigerator with a 16-layer regenerator.” *Scientific Reports* 7: 13962.

Zhang M., A. Momen, and O. Abdelaziz. 2016. “Preliminary analysis of a fully solid state magnetocaloric refrigeration.” International Refrigeration and Air Conditioning Conference, paper 1758. http://docs.lib.purdue.edu/iracc/1758.

4. References

[1] Goetzler, W., M. Guernsey, J. Young, J. Fuhrman, and O. Abdelaziz. 2016. *The Future of Air Conditioning for Buildings*. DOE/EE-1394. Washington, DC: US Department of Energy, Office of Energy Efficiency and Renewable Energy, Building Technologies Office. https://www.energy.gov/eere/buildings/downloads/future-air-conditioning-buildings-report

[2] University of Birmingham. 2015. *Doing Cold Smarter*. Birmingham, United Kingdom: University of Birmingham, Birmingham Energy Institute. http://www.birmingham.ac.uk/Documents/college-eps/energy/policy/Doing-Cold-Smarter-Report.pdf

[3] The Business Research Company. 2023. *Cold Chain Global Market Report*. The Business Research Company. https://www.reportlinker.com/p06280930/Cold-Chain-Global-Market-Report.html

[4] Salin ,V. 2018. *2018 Global Cold Storage Capacity Report*. International Institute of Refrigeration.

[5] Sapienza, Alessio, Vincenza Brancato, Yuri Aristov, and Salvatore Vasta. 2021. "Plastic heat exchangers for adsorption cooling: Thermodynamic and dynamic performance." *Applied Thermal Engineering* 188: 116622.

[6] Qi, R., D. Li, and L.-Z. Zhang. 2017. "Performance investigation on polymeric electrolyte membrane-based electrochemical air dehumidification system." *Applied Energy* 208: 1174–1183.

[7] Qi, R., D. Li, L.-Z. Zhang, and Y. Huang. 2017. "Experimental study on electrolytic dehumidifier with polymer electrolyte membrane for air-conditioning systems." *Energy Procedia* 142: 1908–1913.

[8] Mischenko, A. S., Q. Zhang, J. F. Scott, R. W. Whatmore, and N. D. Mathur. 2006. "Giant electrocaloric effect in thin-film $PbZr_{0.95}Ti_{0.05}O_3$." *Science* 311: 1270–1271.

[9] Neese, B., et al. 2008. "Large electrocaloric effect in ferroelectric polymers near room temperature." *Science* 321: 821–823.

[10] Crossley, S. et al. 2016. "Direct electrocaloric measurement of $0.9Pb(Mg_{1/3}Nb_{2/3})O_3$-$0.1PbTiO_3$ films using scanning thermal microscopy." *Applied Physics Letters* 108, no. 5.

[11] Hou, Y., L. Yang, X. S. Qian, T. Zhang, and Q. M. Zhang. 2016. "Electrocaloric response near room temperature in Zr- and Sn-doped $BaTiO_3$ systems." *Philosophical Transactions of the Royal Society A: Mathematical Physical and Engineering Sciences* 374.

[12] Moya, X., et al. 2013. "Giant electrocaloric strength in single-crystal $BaTiO_3$." *Advanced Materials* 25: 1360–1365.

[13] Chen, X. Z., et al. 2013. "A nanocomposite approach to tailor electrocaloric effect in ferroelectric polymer." *Polymer* 54: 5299–5302.

[14] Qian, X.-S., et al. 2014. "Giant electrocaloric response over a broad temperature range in modified $BaTiO_3$ ceramics." *Advanced Functional Materials* 24: 1300–1305.

[15] Nair, B., et al. 2019. "Large electrocaloric effects in oxide multilayer capacitors over a wide temperature range." *Nature* 575: 468–472.

[16] Qian, X., et al. 2021. "High-entropy polymer produces a giant electrocaloric effect at low fields." *Nature* 600: 664–669.

[17] Gu, H., et al. 2013. "A chip scale electrocaloric effect based cooling device." *Applied*

Physics Letters 102: 122904.

[18] Han, D., et al. 2023. “Molecular interface regulation enables order-disorder synergy in electrocaloric nanocomposites.” *Joule* 7: 1–17.

[19] Unmüßig, Sabrina, David Bach, Youri Nouchokgwe, Emmanuel Defay, and Kilian Bartholomé. 2023. “Phenomenological material model for first-order electrocaloric material.” *Energies* 16, no. 15: S. 5837.

[20] Schipper, Jan, et al. 2023. “On the efficiency of caloric materials in direct comparison with exergetic grades of compressors.” *J. Phys. Energy* 5, no. 4: S. 45002.

[21] Mönch, Stefan, and Kilian Bartholomé. 2023. “Spatio-temporal solid-state electrocaloric effect exceeding twice the adiabatic temperature change.” *J. Phys. Energy* 5, no. 4: S. 45001.

[22] Arnold, D. S., A. Tura, A. Ruebsaat-Trott, and A. Rowe. 2014. “Design improvements of a permanent magnet active magnetic refrigerator.” *International Journal of Refrigeration* 37, no. 1: 99–105.

[23] Lozano, J. A., Matheus S. Capovilla, Paulo V. Trevizoli, Kurt Engelbrecht, Christian R. H. Bahl, and Jader R. Barbosa Jr. 2016. “Development of a novel rotary magnetic refrigerator.” *International Journal of Refrigeration* 68: 187–197.

[24] Aprea, C., Adriana Greco, Angelo Maiorino, Rita Mastrullo, and Armando Tura. 2014. “Initial experimental results from a rotary permanent magnet magnetic refrigerator.” *International Journal of Refrigeration* 43: 111–122.

[25] Engelbrecht, K., D. Eriksen, C. R. H. Bahl, R. Bjørk, J. Geyti, J. A. Lozano, K. K. Nielsen, F. Saxild, A. Smith, and N. Pryds. 2012. “Experimental results for a novel rotary active magnetic regenerator.” *International Journal of Refrigeration* 35, no. 6: 1498–1505.

[26] Masche, M., J. Liang, K. Engelbrecht, and C. R. H. Bahl. 2022. “Performance assessment of a rotary active magnetic regenerator prototype using gadolinium.” *Applied Thermal Engineering* 204: 117947.

[27] Jacobs, S., J. Auringer, A. Boeder, J. Chell, L. Komorowski, J. Leonard, S. Russek, and C. Zimm. 2014. “The performance of a large-scale rotary magnetic refrigerator.” *International Journal of Refrigeration* 37: 84–91.

[28] Lionte, S., Michel Risser, and Christian Muller. 2021. “A 15kW magnetocaloric proof-of-concept unit: Initial development and first experimental results.” *International Journal of Refrigeration* 122: 256–265.

[29] Tecumseh (models: AZA1332YXA, ALX435U-DS3A, AWG5520WXN, AWF5532EXN, AGB5553EKZ (TAG5553E)). From data sheets.

[30] Panasonic/Matsushita (models: QA110K27CAU6, QA125K29CAU6 (100µF Start Cap.), QA43K11GAU6, QA51K13GAU6, QA66K16GAU6). From data sheets.

[31] Embraco/Nidec (models: EMI40HNR, EGAS100CLP, EM2X1121U, NJ6220Z, NTU6222ZV, SE6067GS-O). From data sheets.

[32] Zhang, M., O. Abdelaziz, A. M., Momen, and A. Abu-Heiba. 2017. “A numerical analysis of a magnetocaloric refrigerator with a 16-layer regenerator.” *Scientific Reports* 7: 13962.

[33] Zhang M., A. Momen, and O. Abdelaziz. 2016. “Preliminary analysis of a fully solid state magnetocaloric refrigeration.” International Refrigeration and Air Conditioning Conference, paper 1758. http://docs.lib.purdue.edu/iracc/1758.

5. Appendices

Appendix A. Overview of Annex 53 Tasks

Task 1: Identify cooling/refrigeration focus areas for annex technical contributions

Participants will describe the current development status of their candidate technologies and target applications.

Task 2: Perform modeling/simulation and lab evaluations of advanced air-conditioning/refrigeration technologies

This task constitutes the main part of the annex. Country reports will describe the advances in the development of candidate technologies, including comparison with vapor compression technologies and realistic estimates of cost potential.

Task 3: Identify the next steps for developing and deploying advanced air-conditioning/ refrigeration systems

This task aims to evaluate design optimization and advancement on the life cycle climate performance reduction.

Task 4: Report and information dissemination

This task aims to report the works conducted and disseminate information developed in this annex.

Appendix B. Abbreviations

ABS	acrylonitrile butadiene styrene
AC	air-conditioning
AHT	adsorption heat transformation
ANL	Ames National Laboratory
ATB	absorption thermal battery
ATES	absorption thermal energy storage system
BNNS	boron nitride nanosheet
C-MVD	condenser-combined membrane-based vacuum dehumidification
CAU	Chung-Ang University
COP	coefficient of performance
CUHK	City University of Hong Kong
DES	deep eutectic solvent
DH	dehumidification
EC	elastocaloric
EC	electrochemical
ECC	electrochemical compression
ECE	electrocaloric effect
EHD	electrohydrodynamic
ERHX-REC	economizer and recuperator
ERI	Energy Recovery Inc.
ESD	energy storage density
ESE	energy storage efficiency
FAO	United Nations Food and Agriculture Organization
FOM	figure of merit
GCP	Global Cooling Prize
GWP	global warming potential
HEx	heat exchanger
HP	heat pump
HP	high pressure
HPD	high power density
HVAC	heating, ventilation, and air-conditioning
IEA	International Energy Agency
IIR	International Institute of Refrigeration
IPM	Fraunhofer Institute for Physical Measurement Techniques
ITAE	Institute for Advanced Energy Technologies
LCC	levelized cooling capacity cost
LP	low pressure
MC	magnetocaloric
MCR	magnetocaloric regenerator
MEA	membrane electrode assembly
MHP	membrane heat pump
MLCC	multilayer ceramic capacitor
MVD	membrane-based vacuum dehumidification
ORNL	Oak Ridge National Laboratory
OECD	Organisation for Economic Co-operation and Development
PEx	pressure exchanger
PLA	polylactic acid
PST	lead scandium tantalate
R&D	research and development
RD&D	research, development, and demonstration
SCP	specific cooling power
SE	superelastic
SJTU	Shanghai Jiao Tong University
SMA	shape memory alloy
SPTMS	3-sulfurouspropyltrimethoxysilane
TP	terpolymer
TRL	technology readiness level
TU	Tsinghua University
UoMD	University of Maryland
VC	vapor compression
W-MVD	water vapor–discharged membrane-based vacuum dehumidification
XJTU	Xi'an Jiao Tong University

Heat Pump Centre
c/o RISE - Research Institutes of Sweden
PO Box 857
SE-501 15 BORÅS
Sweden
Tel: +46 10 516 53 42
E-mail: hpc@heatpumpcentre.org

www.heatpumpingtechnologies.org

Report no. HPT-AN53-2